ARISTOTLE UNIVERSITY OF THESSALONIKI
SCHOOL OF GEOLOGY
DEPARTMENT OF METEOROLOGY AND CLIMATOLOGY



JUSTUS-LIEBIG-
UNIVERSITÄT
GIESSEN

TSOMPANIDOU AIKATERINA
ENVARIONMENTALIST

STUDY OF THE IMPACT OF A STRATOSPHERIC INTRUSION EVENT ON TROPOSPHERIC OZONE AND THE IMPLICATIONS IN FUTURE SCENARIOS OF CLIMATE CHANGE

MASTER THESIS

POSTGRADUATE STUDIES PROGRAMME
'Meteorology, Climatology and Atmospheric Environment'

THESSALONIKI-GIESSEN
2024

TSOMPANIDOU AIKATERINA
ΤΣΟΜΠΑΝΙΔΟΥ ΑΙΚΑΤΕΡΙΝΑ
Πτυχιούχος Περιβαλλοντολόγος

ΜΕΛΕΤΗ ΤΗΣ ΕΠΙΔΡΑΣΗΣ ΕΝΟΣ ΕΠΕΙΣΟΔΙΟΥ ΣΤΡΑΤΟΣΦΑΙΡΙΚΗΣ ΕΙΣΒΟΛΗΣ ΣΤΟ ΤΡΟΠΟΣΦΑΙΡΙΚΟ ΟΖΟΝ ΚΑΙ ΟΙ ΕΠΙΠΤΩΣΕΙΣ ΣΕ ΜΕΛΛΟΝΤΙΚΑ ΣΕΝΑΡΙΑ ΚΛΙΜΑΤΙΚΗΣ ΑΛΛΑΓΗΣ

Three-member Examining Board

Professor Zanis Prodromos, School of Geology, A.U.Th., Supervisor

Associate Professor Pytharoulis Ioannis, School of Geology, A.U.Th., member

Akademische Rätin, Xoplaki Eleni, School of Geographie, Justus-Liebig-University of Giessen, member

Τριμελής Εξεταστική Επιτροπή

Καθηγητής Ζάνης Πρόδρομος, Τμήμα Γεωλογίας, Α.Π.Θ., Επιβλέπων Καθηγητής

Αναπληρωτής Καθηγητής Πυθαρούλης Ιωάννης , Τμήμα Γεωλογίας, Α.Π.Θ., μέλος

Akademische Rätin, Ξοπλάκη Ελένη, Τμήμα Γεωγραφίας, JLU, μέλος

STUDY OF THE IMPACT OF A STRATOSPHERIC INTRUSION EVENT ON TROPOSPHERIC OZONE AND THE IMPLICATIONS IN FUTURE SCENARIOS OF CLIMATE CHANGE– Master Thesis

ΜΕΛΕΤΗ ΤΗΣ ΕΠΙΔΡΑΣΗΣ ΕΝΟΣ ΕΠΕΙΣΟΔΙΟΥ ΣΤΡΑΤΟΣΦΑΙΡΙΚΗΣ ΕΙΣΒΟΛΗΣ ΣΤΟ ΤΡΟΠΟΣΦΑΙΡΙΚΟ ΟΖΟΝ ΚΑΙ ΟΙ ΕΠΙΠΤΩΣΕΙΣ ΣΕ ΜΕΛΛΟΝΤΙΚΑ ΣΕΝΑΡΙΑ ΚΛΙΜΑΤΙΚΗΣ ΑΛΛΑΓΗΣ– Μεταπτυχιακή Διπλωματική Εργασία

Citation:
Tsompanidou A., 2024. – STUDY OF THE IMPACT OF A STRATOSPHERIC INTRUSION EVENT ON TROPOSPHERIC OZONE AND THE IMPLICATIONS IN FUTURE SCENARIOS OF CLIMATE CHANGE. Master Thesis, School of Geology, Aristotle University of Thessaloniki, 112 pp.
Τσομπανίδου Α., 2024. – ΜΕΛΕΤΗ ΤΗΣ ΕΠΙΔΡΑΣΗΣ ΕΝΟΣ ΕΠΕΙΣΟΔΙΟΥ ΣΤΡΑΤΟΣΦΑΙΡΙΚΗΣ ΕΙΣΒΟΛΗΣ ΣΤΟ ΤΡΟΠΟΣΦΑΙΡΙΚΟ ΟΖΟΝ ΚΑΙ ΟΙ ΕΠΙΠΤΩΣΕΙΣ ΣΕ ΜΕΛΛΟΝΤΙΚΑ ΣΕΝΑΡΙΑ ΚΛΙΜΑΤΙΚΗΣ ΑΛΛΑΓΗΣ.
Μεταπτυχιακή Διπλωματική Εργασία, Τμήμα Γεωλογίας Α.Π.Θ., 112 σελ.

PREFACE

In this thesis, the synoptic and dynamic aspects of stratosphere-troposphere interactions and the effects of climate change on tropospheric ozone levels are analysed using data from the CMIP6 models of the Earth system under the SSP3-7.0 scenario. The research was carried out within the framework of the postgraduate program "Meteorology, Climatology and Atmospheric Environment" of the Faculty of Geology of the Aristotle University of Thessaloniki (A.U.Th.).

The first chapter presents information on ozone, mechanisms of stratospheric penetration and climate change. The second chapter describes the simulations used in this thesis. In the third chapter, the results obtained are discussed and the fourth chapter contains a summary of the results and conclusions.

The successful completion of this thesis would not have been possible without the valuable guidance and support of my esteemed committee members. I express my deepest gratitude to Professor Zanis Prodromos, of the Department of Geology, Aristotle University of Thessaloniki (A.U.Th.), whose insight and support were instrumental in shaping the direction and quality of this thesis. His role as my supervisor provided the academic context necessary to carry out this complex study. I am equally grateful to Professor Ioannis Pytharoulis, from the School of Mathematics of the Aristotle University of Thessaloniki, for his significant contribution by providing valuable information during the postgraduate program, related to the topic of my thesis. Many thanks also to Akademische Rätin, Eleni Xoplaki, from the School of Geography at the Justus-Liebig-University of Giessen (JLU). During my studies at the university in Germany, her help in orienting our understanding of climate processes, combined with her constructive criticism, greatly enhanced the interdisciplinary character of this thesis. I would like to thank Dr. Dimitris Akritidis for his valuable and important help with the download of the data and their processing. Last but not least, I would like to thank my family and friends, for their support over the years.

Contents

Abstract (English)

In the present study, a synoptic and dynamic analysis of a stratospheric air intrusion episode into the troposphere in the Hohenpeissenberg region (47°48'N 11°0'E) on 26 January 2015 is initially conducted. A deep Stratosphere to Troposphere Transport (STT) event is presented, followed by an examination of its impact on tropospheric ozone levels in the study area. Of crucial importance is the reduction in the tropopause height, indicating the potential for a stratospheric intrusion to penetrate the troposphere, contributing to the downward transport of ozone. This intrusion results in the tropopause fold, leading to a continuous layer with discontinuities, termed dynamic tropopause, promoting the mixing of stratospheric and tropospheric air and consequently enhancing ozone levels in the troposphere, reducing water vapor, and increasing potential vorticity (PV) values. The synoptic analysis of this phenomenon describes an upper-level trough and a deep tropopause fold at 500 hPa. Disturbances in the upper troposphere, directly associated with positive PV anomalies, presuppose the use of PV for diagnosing synoptic processes. Tropopause folds are located at the entrance of subtropical jet streams and are determined by their intensity and position, mainly prevailing in subtropical zones based on the downward vertical extent of the stratospheric intrusion to a certain geopotential height. In the context of the development and implementation of the thesis, ozone measurements from the WOUDC ozonesonde and data from the Copernicus Atmosphere Monitoring Service (CAMS) were used, successfully reproducing the so-called “hook-shaped” streamer with ozone rich and dry air in the troposphere. In the second part of this study, an examination of the impact of climate change on tropospheric ozone and in the transport of stratospheric ozone to the troposphere is conducted using data from simulations by CMIP6 Earth system models under the SSP3-7.0 scenario. This takes into account global warming and the ozone impact near polluted areas according to future climate change scenarios. The role of anthropogenic emissions in the future is crucial, as an increase in ozone is observed in both polluted and unpolluted regions above the critical point in the coming decades. Climate change positively influences ozone in remote areas away from pollution sources but has negative effects only in regions close to polluted sources. Climate change due to intensified warming associated with jet stream activity

contributes to higher stratospheric ozone values due to the tropopause fold mechanism by the end of the 21st century in subtropical and polluted regions. The continuous and progressively increasing exposure to stratospheric ozone contributes to increased mortality attributable to ozone, owing to population growth and ageing.

Key words: stratospheric intrusion, tropospheric ozone, CAMS, CMIP6

ABSTRACT (GREEK)

Στην παρούσα διπλωματική εργασία πραγματοποιείται αρχικά συνοπτική και δυναμική ανάλυση ενός επεισοδίου εισβολής στρατοσφαιρικού αέρα στην τροπόσφαιρα στην περιοχή του Hohenpeissenberg (47°48'N 11°0'E), το οποίο συμβαίνει στις 26 Ιανουαρίου 2015. Παρουσιάζεται ένα γεγονός μεταφοράς αέρα από την στρατόσφαιρα προς την τροπόσφαιρα, ενώ στη συνέχεια μελετάται ποια ήταν η επίδραση του στα επίπεδα τροποσφαιρικού όζοντος στην περιοχή μελέτης. Καίριας σημασίας είναι η μείωση στο ύψος της τροπόπαυσης η οποία υποδηλώνει μια πιθανή στρατοσφαιρική εισβολή να διεισδύει στην τροπόσφαιρα συνεισφέροντας στην καθοδική μεταφορά όζοντος. Αυτή η εισβολή έχει ως συνέπεια την αναδίπλωση της τροπόπαυσης δηλαδή παρατηρείται ένα συνεχές στρώμα με ασυνέχειες στην τροπόπαυση, η οποία ορίζεται ως δυναμική τροπόπαυση, οδηγώντας σε ανάμειξη στρατοσφαιρικού και τροποσφαιρικού αέρα με αποτέλεσμα να προάγει την αύξηση στα επίπεδα όζοντος στην τροπόσφαιρα, την μείωση των υδρατμών και την αύξηση των τιμών δυναμικού στροβιλισμού (PV). Η συνοπτική ανάλυση αυτού του φαινομένου περιγράφεται από έναν αυλώνα (trough) και μια βαθιά αναδίπλωση της τροπόπαυσης στο ισοβαρικό επίπεδο των 500hpa. Οι διαταραχές στην ανώτερη τροπόσφαιρα οι οποίες είναι άμεσα συνυφασμένες με θετικές ανωμαλίες δυναμικού στροβιλισμού (PV) προϋποθέτουν τη χρήση του PV η οποία εφαρμόζεται για την διάγνωση συνοπτικών διεργασιών. Οι αναδιπλώσεις της τροπόπαυσης βρίσκονται στην είσοδο των υποτροπικών αεροχειμάρρων και καθορίζονται από την ένταση και τη θέση τους. Επικρατούν κυρίως στις υποτροπικές ζώνες σύμφωνα με την προς τα κάτω κατακόρυφη έκταση της στρατοσφαιρικής εισβολής έως κάποιο γεωδυναμικό ύψος. Στο πλαίσιο της εκπόνησης και της διεκπεραίωσης της διπλωματικής εργασίας χρησιμοποιήθηκαν μετρήσεις όζοντος από το WOUDC ozonesonde καθώς και δεδομένα από το Copernicus Atmosphere Monitoring Service (CAMS), τα οποία αναπαράγουν επιτυχώς την ονομαζόμενη “hook shaped” ροή πλούσιο σε όζον σε συνδυασμό με ξηρό αέρα στην τροπόσφαιρα.

Στο δεύτερο μέρος της διπλωματικής εργασίας διεξάγεται μελέτη της επίδρασης της κλιματικής αλλαγής στο τροποσφαιρικό όζον και στην μεταφορά στρατοσφαιρικού όζοντος προς την τροπόσφαιρα με δεδομένα προσομοιώσεων από το CMIP6 Earth

system models υπό το σενάριο SSP3-7.0, λαμβάνοντας υπόψη την υπερθέρμανση του πλανήτη και το αντίκτυπο του όζοντος κοντά σε ρυπασμένες περιοχές σύμφωνα με το μελλοντικό σενάριο κλιματικής αλλαγής. Σημαντικός θεωρείται ο ρόλος των ανθρωπογενών εκπομπών στο μέλλον διότι παρατηρείται αύξηση του όζοντος σε μολυσμένες και μη περιοχές πάνω από το κρίσιμο σημείο (κατώφλι) στις επόμενες δεκαετίες. Ωστόσο η κλιματική αλλαγή επιδρά θετικά στο όζον σε απομακρυσμένες περιοχές από ρυπασμένες πηγές, ενώ επιδρά αρνητικά μόνο σε περιοχές κοντά σε ρυπασμένες πηγές. Η κλιματική αλλαγή σχετίζεται με τη δραστηριότητα του jet stream λόγω της εντονότερης θέρμανσης, συμβάλλει στην αύξηση των επιπέδων στρατοσφαιρικού όζοντος εξαιτίας του μηχανισμού αναδιπλώσεων της τροπόπαυσης μέχρι το τέλος του 21ου αιώνα στις υποτροπικές και μολυσμένες περιοχές. Η συνεχής και ολοένα αυξανόμενη έκθεση στο τροποσφαιρικό όζον συμβάλλει στην αύξηση της θνησιμότητας που αποδίδεται στο όζον εξαιτίας της αύξησης του πληθυσμού και της γήρανσης.

Chapter 1. Introduction

In this study, we investigated the synoptic, dynamic and thermodynamic characteristics of a deep stratospheric intrusion into the troposphere, known as the tropopause fold. The ultimate goal was to analyze ozone concentrations in the study area of Hohenpeissenberg during the event that occurred at 00Z on 26 January 2015. The purpose of this study is to comprehensively analyze and depict the thermodynamic and synoptic features of the tropopause fold episode. It aims to explore all relevant meteorological parameters that interact and relate to each other, incorporating various observational and model data to determine the atmospheric conditions responsible for the development of such episode. The analysis period begins shortly before the clear appearance of the tropopause fold event and extends slightly beyond its dissipation.

1.1 Historical review

The discovery of ozone took place in 1840 by the German chemist Schönbein, who during a thunderstorm, detected an electrical smell in the air and named the gas responsible "ozone". Since then, ozone has become a significant chemical substance in atmospheric chemistry. By the 1850s, measurements of ozone were conducted at various stations, revealing concentrations approaching 15 ppb (Percy et al., 2003). In 1940, it was identified as a chemical compound in smog, particularly in Los Angeles and London, leading to adverse effects on the atmosphere and human health. Continuous ozone measurements indicated a subsequent global increase, reaching up to 40 ppb in recent studies. According to future scenarios, ozone levels are projected to rise by more than 60 ppb by 2100.

1.2 Tropospheric & Stratospheric Ozone- Mechanisms of Tropospheric O_3 Production

Ozone is considered a Near-Term Climate Forcer (NTCF), as it has a short atmospheric lifetime, lasting at most a few weeks. This practically means that it can directly influence the global radiation balance, exhibiting a positive radiative forcing of 0.40W/m^2, leading to an average global surface temperature increase of 0.23°C attributed to ozone. Other NTCFs include aerosols, precursor substances of O_3 and CH_4 (Turnock et al., 2023; Akritidis et al., 2022). Therefore, the reduction of these substances will be much more active than, for example, CO_2, which has a lifetime of 100 years. Atmospheric chemistry investigates the dynamic and photochemical processes that determine the rate of production and destruction of oxidative substances in the troposphere. The distribution of ozone in different layers of the atmosphere depends on its production, loss and transport. Tropospheric ozone is noteworthy because it originates either photochemically through reactions or is transported from the stratosphere. In the lower stratosphere, there is less ultraviolet radiation compared to the upper stratosphere, leading to ozone presence primarily due to stratospheric transport rather than production. Conversely, the upper stratosphere has sufficient ultraviolet radiation for photochemical reactions to occur, resulting in ozone observed

primarily due to production (Stratospheric Ozone-An Electronic Textbook). Photochemical oxidants such as ozone (O_3) holds significant importance in the atmosphere, affecting both the environment and human health. Ozone constitutes 90% of the stratosphere, with maximum values in the ozone layer (a part of the stratosphere) at an altitude of 15-30 km, while the remaining 10% exists in the troposphere. Stratospheric ozone absorbs ultraviolet radiation, consequently it protects the organism from diseases. For this reason, it is referred to as beneficial ozone. However, tropospheric ozone has both positive and negative impacts on the atmosphere. On the one hand, it is considered detrimental ozone (so called ¨bad ozone¨) as it absorbs infrared Earth radiation, contributing to its greenhouse gas effect in the upper atmosphere. Additionally, pollution issues arise because tropospheric ozone is considered a photochemical pollutant due to the creation of a photochemical smog, intensified under solar radiation. On the other hand, its contribution to the hydroxyl radical (OH) in the troposphere is crucial. Hydroxyl radical (OH) is generated from the photolysis of ozone at $\lambda < 315$ nm and oxidizes trace elements. Essentially, tropospheric ozone constitutes as a primary source of the most oxidizing agent in the troposphere, especially for OH. Consequently, essential reactions occur in the troposphere, oxidizing trace elements and reducing greenhouse gases. It is hence called atmospheric detergent, reducing the lifetime of organic (volatile organic compounds (VOCs)) and inorganic compounds (CO_2, CH_4), thereby mitigating the greenhouse effect. It functions as a strong phytodetoxification agent on the Earth's surface. In the stratosphere, O_3 (so called ¨good ozone¨) absorbs damaging UV-C radiation $\lambda<290$ nm (Zanis, 2014).

Ozone is secondary pollutant that not directly emitted but formed under the action of sunlight and oxidate other agents. Nitrogen oxides (NOx) and volatile organic compounds (VOCs) called ozone precursors. The origin of tropospheric ozone involves two distinct pathways. Firstly, the photochemical production of O_3 in the troposphere depends on the presence of primary pollutants such as nitrogen oxides (NOx: NO + NO_2) and volatile organic compounds (VOCs). This involves the photodissociation of NO_2 and VOCs with the contribution of light (Finlayson-Pitts & Pitts, 2000). At such low altitudes, only radiation with $\lambda > 280$ nm reaches and the significant production of atomic O occurs through the photodissociation of NO_2. The second pathway occurs due to the transport of stratospheric ozone to the troposphere. Furthermore, when the quantity of NOx is less than 20 pptv, atmospheric chemistry leads to ozone destruction,

while NOx values exceeding 50 pptv lead to ozone production. The chemistry of tropospheric ozone is defined as the balance between its production and destruction. Deviation from photochemical equilibrium refers to ozone production without destruction, according to ozone production reactions, as illustrated below. The accumulation of ozone occurs through these reactions eq.1.1 and eq.1.2, leading to deviation from photochemical equilibrium, ozone production without destruction.

Equation for Tropospheric Ozone Production:

$NO_2 + hv\ (280\ nm < \lambda < 424\ nm) \rightarrow NO + O$ (1.1)

$O + O_2 \rightarrow O_3$

$NO + O_3 \rightarrow NO_2 + O_2$

$NO + HO_2 \rightarrow OH + NO_2$ (1.2)

$NO + RO_2 \rightarrow RO + NO_2$ (1.3)

The origin of stratospheric ozone takes place through the photodissociation of O_2 at an altitude above 20 km. Atomic O is produced from the photodissociation of molecular O_2 by deep ultraviolet radiation. The difference in O_3 production in the troposphere and stratosphere is the source of atomic O. In the O_3 layer, there is a maximum vertical distribution of O_3 at 25 km, which acts as a filter for harmful solar ultraviolet radiation. Stability prevails in the stratosphere because air warms with increasing altitude. Stability in the stratosphere depends on potential temperature (K), where temperature consistently increases in the stratosphere, making it stable and unfavorable for vertical movements. An isentropic surface consists of a specific stable potential temperature (Stratospheric Ozone-An Electronic Textbook).

According to general atmospheric circulation, primary ozone production occurs in tropical regions. However, the Brewer-Dobson circulation leads to a higher concentration at the poles. In the Northern Hemisphere, the Brewer-Dobson circulation is stronger, resulting in a greater concentration at the North Pole. Essentially, ozone increases where it is not produced photochemically but is transported by the Brewer-Dobson circulation. During lunch hours, there is a maximum ozone concentration due to maximum solar radiation (hv). Conversely, ozone is destroyed during night time

hours due to NO_2. Thus, NO_3 is produced, acting as a significant oxidizing agent during the night. Ultimately, HNO_3 is produced, which is removed as acidic rain. According to the eq.1.4, oxygen (O_2) absorbs the destructive high energy short wavelength λ ultraviolet radiation. Figure 1.1 represents the chemical process of creating ozone.

Equation for Stratospheric Ozone Production:

O_2 + hv (deep ultraviolet) -> O + O (1.4)

O +O_2->O_3

Figure 1.1: Ozone formation processes (source: https://www.ozoneindustries.co.th/how-ozone-works/)

The concept of background ozone exists due to the transport of ozone through dispersion in remote areas. It is not influenced by nearby anthropogenic pollution emissions. Additionally, ozone is transported more rapidly to the free troposphere because it exhibits a longer lifetime, owing to more radiation and higher wind speeds compared to the lower troposphere. The lifetime of ozone is short, ranging from a few days to a few weeks, especially when it is located higher in the stratosphere, hence it can be transported over long distances.

1.3 Stratosphere -Troposphere Exchange (STE)

The exchange between the stratosphere and troposphere is of interest as these two layers differ in composition and thermodynamic properties related to stability and instability. Moreover, they contribute to the ozone budget in the troposphere through transport.

Stratosphere-Troposphere Exchange (STE) involves two types of transport: Stratosphere-to-Troposphere (STT), transferring rich stratospheric ozone to the troposphere and Troposphere-to-Stratosphere (TTS), involving the transport of substances produced by human activities, such as volatile organic compounds (VOCs), which are ozone-depleting in the stratosphere, impacting human health (Gray, 2006; Stohl et al., 2003b). In the ozone layer in the stratosphere, stability conditions prevail. When adiabatic changes dominate, there is no exchange of heat with the environment, resulting in downward and upward movements of air masses. This ozone transport is attributed to the Brewer-Dobson circulation (BDC), first used by Brewer and Dobson to understand ozone and water vapor distribution through circulation between the stratosphere and troposphere. In the tropics, upward movements dominate due to intense heating. However, due to the BDC, zonal circulation changes to meridional. This meridional circulation is due to dynamic processes resulting from the vertical propagation of planetary waves from the troposphere to the stratosphere, not due to upward movements in the tropics. Planetary waves are created due to large-scale topography and temperature contrasts between land and sea, more intense in the Northern Hemisphere. Consequently, these planetary waves move upward above the subtropical jet stream and in the stratosphere, they break. Below the wave breaking level, energy and momentum are released, causing meridional circulation in the stratosphere only in the Northern Hemisphere. Subsequently, due to descending motions over mid and high latitudes, ozone accumulates at the poles, explaining higher ozone concentrations at the poles despite ozone creation occurring in the tropics. Finally, owing to the ozone-rich air in the troposphere, stratospheric ozone is minimal (Bönisch et al., 2010). The significant ozone production occurs in the tropical stratosphere due to ultraviolet radiation, where solar radiation breaks molecular oxygen into atomic oxygen, which then reacts with molecular oxygen to produce ozone. According to the large-scale Brewer-Dobson circulation, ozone is transported to the poles. Therefore, polar air is richer in ozone compared to tropical air. In the lower stratosphere, due to lower absorption of ultraviolet radiation, there are fewer atomic oxygen molecules, leading to a longer ozone lifetime and more difficult destruction in this region (Stratospheric Ozone-An Electronic Textbook). The Stratosphere-Troposphere Exchange (STE) occurs through the mechanism of tropopause fold, which takes place in the subtropical regions at mid-latitudes due to the presence of jet streams

(Sprenger et al., 2007; Sprenger et al., 2003). In addition, Stratosphere-Troposphere Exchange (STE) is observed even at higher latitudes.

1.4 Dynamic Analysis - The Role of Potential Vorticity

Vorticity is a measure of the local rotation of the atmosphere and its quantity is not conserved as it changes with convergence and divergence. However, potential vorticity constitutes as a dynamic parameter occurring in an adiabatic atmosphere under frictionless conditions, where the air particles move along isentropic surfaces, generating vorticity in a gas mass. The analysis of potential vorticity is performed on isentropic levels, surfaces where the potential temperature remains constant, providing stability to these surfaces (Pytharoulis, 2022). The conservation of potential vorticity contributes to maintaining the stability of these surfaces. Isentropic analysis can be conducted on these surfaces, which are crucial for understanding and predicting atmospheric circulation and weather systems. The potential vorticity (PV) is represented by the sum of absolute vorticity and atmospheric stability, expressed as PV = (jr + f)/dp = constant.

$$PV = (\zeta_\theta + f) \cdot (-g \frac{\partial \theta}{\partial p}) \quad (1.5)$$

The eq.1.5 consists of absolute vorticity and atmospheric stability, visually depicted by the contours of Potential Vorticity Units (PVU). Potential vorticity plays a significant role in distinguishing between the troposphere and the stratosphere. Specifically, the surface with a value of 2 PVU separates tropospheric from stratospheric air and is known as the dynamic tropopause. Stratospheric air is identified by higher values of potential vorticity exceeding 2 PVU due to substantial static stability, indicating a strong PV with low relative humidity (Miglietta et al., 2017). Moreover, potential vorticity is useful in identifying stratospheric air penetration into the troposphere. The troposphere typically has PV values ranging from 0.5 to 1 PVU, signifying weak vorticity. It is also employed to determine the height of the dynamic tropopause based on the predefined value of potential vorticity at 1.5-2 PVU (Feidas and Kartalis, 2003). Potential vorticity increases with geographical latitude and it holds dual importance due to its dynamic property (absolute vorticity) and thermodynamic property (potential temperature) (Ertel, 1942). A positive anomaly of PV in the upper atmosphere in the

northern hemisphere contributes to the intensification of cyclonic circulation, particularly in the genesis of a cyclone near the surface, amplifying latent heat flux (Pytharoulis, 2022). When there is a significant slope of potential vorticity, it generally implies that air changes its direction and speed with height over a large extent. This can lead to the slope of isentropic surfaces.

1.5 Dynamic Analysis - Dynamic Tropopause Anomaly

The dynamic tropopause anomaly refers to the low region of the tropopause where a decrease in tropopause height is observed, with the tropopause positioned at lower altitudes. This indicates that stratospheric air with high values of potential vorticity has penetrated into the upper troposphere, resulting in intense vertical motions and severe weather conditions at the Earth's surface. Essentially, a pronounced gradient in the geopotential height of the tropopause is created, attributed to the intrusion of potential vorticity from the upper stratosphere into the upper troposphere. This distortion of the tropopause signifies the minimum height of the tropopause, caused by a very dry stratospheric intrusion into the upper troposphere. In dynamic tropopause anomalies, due to the persistent nature of potential vorticity, there is distortion of isentropic surfaces and the vorticity of the surrounding air. Vertical motions prevail in this distortion, induced by the intrusion of potential vorticity in baroclinic flow. Consequently, ascent occurs in the front, leading to stretching and an increase in vorticity and circulation, resulting in cyclonic circulation in the lower troposphere, known as the local maximum height. Behind, descent dominates, creating a local minimum height (Georgiev et al., 2016). The dynamic tropopause takes the value of 1.5 PVU or 2 PVU (1 PVU = 10^{-6} K m^2 kg^{-1} s^{-1}) (Holton et al., 1995; Hoskins et al., 1985), remaining stable due to the continuity of potential vorticity and its inherent property of persistence. The continuous surface of 1.5 or 2 PVU, known as the dynamic tropopause, delineates the troposphere from the stratosphere with the assistance of potential vorticity. Low potential vorticity values are found in the troposphere, while high potential vorticity values in the stratosphere, owing to significant static stability.

1.5.1 Tropopause Fold - Stratospheric Intrusion

The positive anomaly of potential vorticity enhances dynamic instability in the atmosphere just below the tropopause, leading to downward transport (Škerlak et al., 2015; Russell et al., 2012). This is particularly intensified when situated in a baroclinic region, where density varies with height, resulting in tropopause fold (Abdel Basset & Gahein, 2003; McWilliams, 1980; Reed et al., 1992). At the tropopause at 11 km (16 km in the tropical zone with a potential temperature of 380 K), a stable temperature prevails, indicating static stability in the layer of temperature inversion. Therefore, there is no mixing in this continuous layer (Makrogiannis, 2007). However, when a continuous layer has discontinuities, the tropopause at these discontinuities can fold, meaning that one part is situated above the other in an altitude difference of a few kilometers. In these discontinuities, stratified stable stratospheric air mixes with well-mixed tropospheric air (Kunz, 2011; Holton et al., 1995). Tropopause folds are associated with the positions of jet streams, which are located at mid-latitudes. There, a strong vertical wind shear prevails. Tropopause folds are created only at mid-latitudes through large-scale cyclonic and anticyclonic disturbances at the entrance of the jet stream (Akritidis et al., 2010; Danielsen and Mohnen, 1977), where significant vertical wind shear and strong mid-latitude temperature gradients are observed. The positive anomaly of potential vorticity penetrates into the upper troposphere due to upper-level disturbances. This tropopause anomaly modifies the temperature field and induces cyclonic circulation, known as positive vorticity anomaly. In combination with jet stream interaction, it contributes to the strengthening and intensification of surface weather phenomena, as well as a reduction in the height of the dynamic tropopause (Andrei et al., 2019). This distortion results in high static stability at the center, where isentropes converge, while static stability above and below decreases and absolute vorticity increases (Georgiev et al., 2016). Very high values of potential vorticity above the tropopause can generate cyclogenesis if it penetrates downward into the troposphere. Tropopause folds are one of the main mechanisms for mass exchange between the stratosphere and troposphere, where stratospheric intrusions into the upper troposphere occur due to ageostrophic flow at the entrance of the jet stream (Hoskins et al., 1985; Holton et al., 1995). Tropopause folds can contribute to cyclogenesis at the surface or to cutoff lows in the 500 hPa isobaric surface (Danielsen, 1968). The

tropopause folds are classified into shallow, medium and deep, depending on the altitude difference. The vertical extent (dp) of the tropopause fold is defined as the distance between the highest and lowest dynamic tropopause. Therefore, a tropopause fold is associated with the intrusion of stratospheric air into the troposphere, resulting in an increase in ozone levels in the troposphere. This mass air transport from the stratosphere to the troposphere exhibits the following characteristics: high values of potential vorticity greater than 2PVU, increased ozone levels, low water vapor content and high stability. Essentially, these are the prevailing characteristics in the stratosphere (Akritidis et al., 2018). A stratospheric intrusion that descends into a baroclinic zone beneath the subtropical jet stream is termed a tropopause fold, formed by a tropopause and isentropic slope. This mechanism is common in mid-latitudes and occurs on the western side of cutoff lows. Abrupt slopes in isentropic surfaces imply enhanced baroclinicity, favoring tropopause folds that intensify surface cyclogenesis (Wandishin, 2000; Uccellini et al., 1985). Tropopause folds are meteorologically significant as they are linked to changes in weather and climate conditions, as well as the development and intensification of weather systems such as cyclones and anticyclones. Tropopause fold is observed in regions with significant vertical wind shear, involving sudden changes in wind speed. However, it is difficult to accurately detect and correctly represent this phenomenon in these abrupt slopes in dynamic tropopause from the models (Roelofs et al., 2003). This influences and intensifies the jet stream, particularly when there is a strong meridional temperature gradient, further enhancing the jet stream by inducing disturbances that eventually lead to the formation of tropopause folds. The mixing observed during stratospheric intrusion is initially nonreversible. The transport of stratospheric air occurs along isentropic surfaces towards the troposphere (WMO, 1985) and secondly, it happens due to the instability prevailing at the tropopause fold, attributed to the low Richardson number (Price & Vaughan, 1993; Shapiro 1978, 1980). Tropopause folds and cutoff lows, as discussed below, contribute to the transport of stratospheric air from the stratosphere to the troposphere in mid-latitudes (Ancellet et al., 1994; Keyser and Shapiro, 1986). During summer, high ozone values are recorded, especially in hot spot regions, due to tropopause folds and the contribution of dynamic processes (Dafka et al., 2020; Zanis et al., 2014), as well as photochemical production and reactions influenced by high pollution levels and intense solar radiation (Dafka et al., 2020; Kanakidou et al., 2011). Tropopause fold was first introduced by Reed (1959) due to the higher values of potential vorticity observed during tropopause distortion.

This stratospheric intrusion impacts ozone equilibrium (Holton et al., 1995; Hoskins, 1985). Tropopause fold is indicated by the abrupt temperature gradient (Wimmers, 2003) and the presence of dry stratospheric air in the troposphere (Bithell et al., 2000). Noteworthy stratospheric intrusions into the troposphere are the deepest intrusions that can reach very low isobaric levels, leading to a permanent state of stratospheric-tropospheric air mixing, resulting in the alteration of the troposphere's composition (Zanis et al., 2003). In Figure 1.2, it is observed that the isentropic surfaces at 380K intersect the tropopause. Additionally, dynamic tropopause fold occurs at the isobaric level of 400hPa, while a clear descent of the tropopause is evident at lower isobaric levels, specifically in the mid-latitudes to the polar zone, falling below 300hPa. The exchange of masses between the troposphere and the stratosphere is thus observed due to various contributing factors. In this transport, aircraft emissions play a role as they release gases into the atmosphere, which are subsequently transported. Furthermore, industrial activities emit greenhouse gases into the atmosphere, modifying its chemical composition, thereby resulting in a significant impact on climate change. Noteworthy is the contribution of the tropopause fold, where this mechanism presents a downward slope, hence termed dynamic tropopause fold, leading to the transport of masses, such as ozone, from the stratosphere to the troposphere. In the same figure, ascending motions are observed in the tropical zone, giving rise to precipitation formations due to convergence. However, the Brewer-Dobson process plays a key role in the transport of ozone from the tropical zone to the polar zone, where descending motions occur.

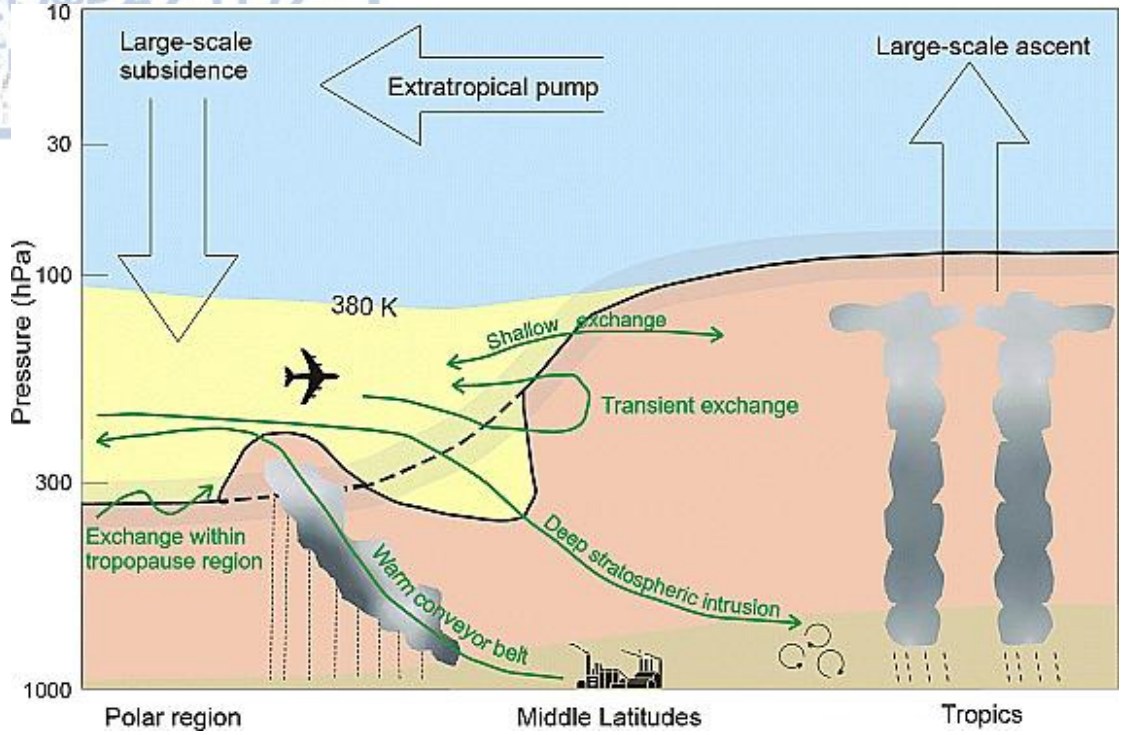

Figure 1.2: Global scale circulation: Tropopause is shown by the black line, the yellow area is the lowermost stratosphere, the pink area is the free troposphere, and the bottom layer is the atmospheric boundary layer. The isentropic surfaces (at 380K) intersect the tropopause. (source: https://agupubs.onlinelibrary.wiley.com/doi/full/10.1029/2002JD002490).

1.6 Jet Streams- Climatology of the jet stream

The jet stream moves horizontally between high pressure and low pressure systems, primarily observed in mid-latitudes, 8-13 km below the tropopause, forming on the warm side. It is generated by temperature and pressure differences among air masses. Jet streams form in regions with significant horizontal temperature gradients (in the transitional zone between subtropical and temperate geographical zone). The jet stream is a narrow air current that attains high speeds in the upper atmosphere, typically near the 300hPa isobaric level and is associated with a strong vertical wind gradient near the tropopause. The axis of the jet stream aligns precisely with the moisture boundary to the right of the tropopause fold, where wind speeds reach maximum values exceeding 100 knots (51,44 m/s), moving from west to east. It is characterized by high vertical velocities (on the order of a few centimeters per second) and horizontal wind speed shears. However, the vertical wind component is quite small near the surface and near the tropopause, where only the horizontal wind component prevails. At approximately

500 hPa, the vertical wind component is maximal and the horizontal winds are minimal, constituting what is referred to as the zero-divergence layer. Additionally, it may exhibit one or more maxima in wind speed. Jet streaks or jet maxima, refer to the maximum wind speed region and can be considered a disturbance of the jet stream caused by the interaction between the jet stream and the dynamic tropopause anomaly. Changes in horizontal wind are linked to jet streaks and there is interaction with the dynamic tropopause anomaly as the jet stream approaches, resulting in an increase in jet stream speed and, consequently, vertical movements in the entrance and exit regions of the jet stream. This strengthens the dynamic tropopause anomaly and deepens it further. Tropopause fold is considered the minimum height of the tropopause, situated below the jet streak (Georgiev et al., 2016). According to the figure 1.3, the subtropical jet stream is located at 30°, where the upper-level wind enters from the equator due to the Hadley cell and begins to flow zonally from west to east, influenced by the Coriolis force. The Polar jet stream is situated at 60°, where the upper-level wind flowing toward the pole is deflected from west to east.

Figure 1.3: Jet stream circulation (source: www.srh.noaa.gov/jetstream/global/jet.htm).

Large variations in air mass speed occur at the entrance and exit of the jet stream and thus, the geostrophic balance is not valid. Instead, the ageostrophic wind prevails. This leads to vertical movements at the jet stream maxima and ultimately enhances surface systems due to convergence and divergence. As a result of the acceleration at the entrance of the jet stream, the ageostrophic wind is vertical to the acceleration, causing divergence to the left and downward motions at the surface. Conversely, at the exit, due to deceleration, the ageostrophic flow is directed upward. Therefore, a closed circulation is observed (fig.1.4) due to the ageostrophic wind, creating intense vertical motions and reinforcing surface systems and cyclogenesis. Along the axis of the jet stream, cyclonic development is observed to the left of the exit and to the right of the

entrance. Specifically, surface convergence occurs on the left side, leading to upward motions, surface cyclogenesis and upper-level divergence with downward motions. Conversely, on the right side of the exit and the left side of the entrance, anticyclonic development is noted. More precisely, surface divergence results in downward motions, while upper-level convergence occurs. When the jet stream weakens, air masses move more slowly in the atmosphere, winds decelerate, potentially leading to prolonged stable conditions in an area. Consequently, due to the jet stream, atmospheric disturbances may persist in a region for an extended period. This situation can favor the north to south meridional flow, diverging from the zonal flow, resulting in extreme weather phenomena such as heatwaves and floods. The meridional flow may cause significant temperature contrasts due to the movement of colder air masses from higher latitudes towards lower ones. During winter months, the temperature difference between the warm equator and the cold pole intensifies, enhancing the jet stream's strength and southward movement. This results in the transport of colder air masses from higher to lower latitudes, significantly impacting atmospheric circulation and weather patterns (Makrogiannis and Sahsamanoglou, 2004). The intense thermal gradient leads to a strong pressure gradient, influencing air mass movement. This intensified jet stream is a consequence of the substantial temperature difference between the tropics and the poles, a difference predicted to increase in the future according to climate models (Stohl et al., 2003; Rind et al., 1998).

The curved jet stream, as proposed by Bjerknes and Holmboe (1944), differs from the horizontal jet stream as it forms troughs or ridges. Essentially, it depends directly on pressure systems. During the intrusion of stratospheric air into the troposphere, during tropopause folds, the jet stream follows these slopes-oscillations and becomes curved. Rossby waves, considered large-scale waves of pressure systems, contribute to the formation and evolution of the jet stream, which tends to curve and develop due to the Coriolis effect. The temperature difference between tropical and polar regions, due to the predicted temperature increase according to climate models, results in an increased air pressure difference called pressure gradient. This creates high-pressure systems in polar areas and low-pressure systems in tropical regions. Consequently, air moves from high-pressure (polar) to low-pressure (tropical) regions, resulting in westerly winds, which are stronger the more intense the pressure gradient. Thus, the curvature of the jet stream in the upper troposphere intensifies due to the Coriolis force. Studying jet stream is crucial for predicting severe weather phenomena. However, due to the intense variability of the wind, accurate prediction is challenging. Therefore, an essential meteorological parameter for detecting disturbances in the atmosphere is potential vorticity.

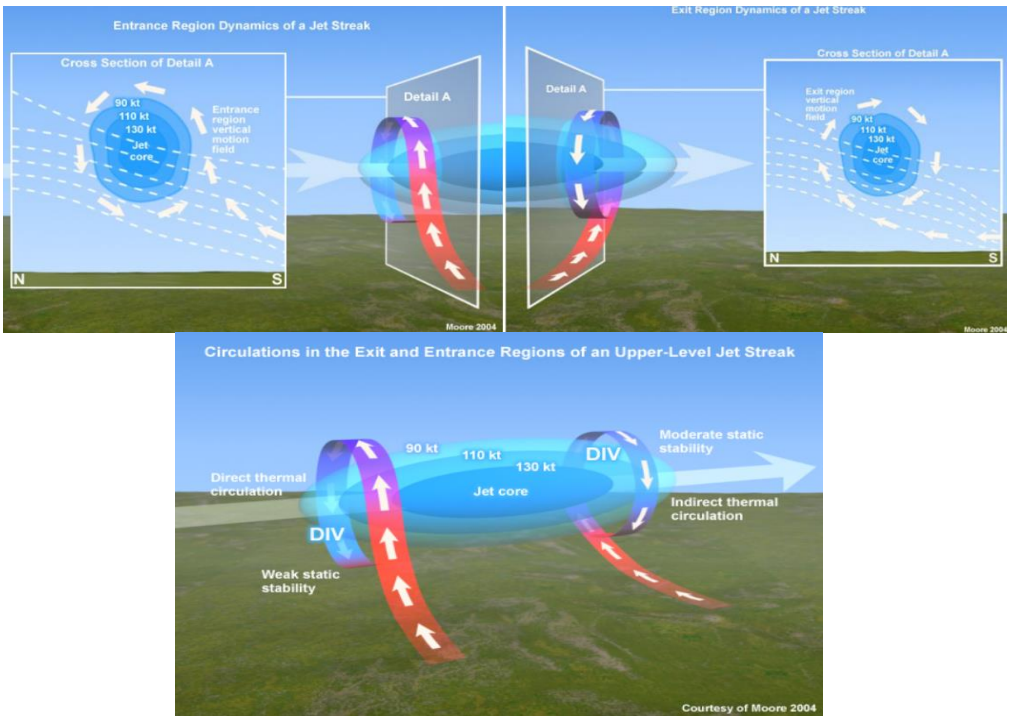

Figure 1.4: Cross sections of isotachs of ageostrophic circulation in isentropic surfaces (source: https://www.meted.ucar.edu/labs/synoptic/jets_ageo_circ/print.php).

The climatology of the jet stream exhibits seasonality, meaning its position and intensity vary according to geographical and seasonal distributions. The average climatology of ozone is depends on the average climatology of tropopause folds, which, in turn, relies on the average climatology of the jet stream. Therefore, the average climatology of tropopause fold is observed in winter, near the equator, in the subtropical zone and is more pronounced compared to summer months when it shifts northward and weakens. Hence, a higher frequency of jet stream occurrences is noted from January to April in mid-latitudes (20-40°N), mainly in the subtropical zone. During summer months, the jet stream weakens and shifts northward, moving above the Balkans at 40°N. Consequently, during summer, tropopause folds exhibit lower frequency and weaker intensity due to the weakened jet stream. According to the figure 1.5, shallow tropopause folds are observed in winter, primarily in Asia. In spring, there is a tendency for jet stream strengthening in North India, while during summer, the strengthening trend is observed in the eastern Mediterranean, the Middle East, the North Indian Ocean, and Australia. Medium scale tropopause folds are identified in polar regions such as the Arctic Ocean and Antarctica in both hemispheres. In winter, the deepest folds (below 700 hPa) are observed in extratropical and polar regions, specifically in the North Atlantic Ocean and North America. However, during summer, high ozone values are observed in the eastern Mediterranean due to tropopause folds and subsidence in this region, combined with the northerly winds - Etesian winds resulting from the pressure gradient. The eastern Mediterranean is a hot spot for tropopause fold events. As a result, shallow tropopause folds in the subtropical zone exhibit higher frequency. Consequently, shallow folds determine the average climatology of tropopause folds (Akritidis et al., 2021; Škerlak et al., 2015; Sprenger et al., 2003). Shallow tropopause folds are located at the mean climatological tropopause height, while medium and deep tropopause folds approach lower isobaric levels, below the mean climatological tropopause height.

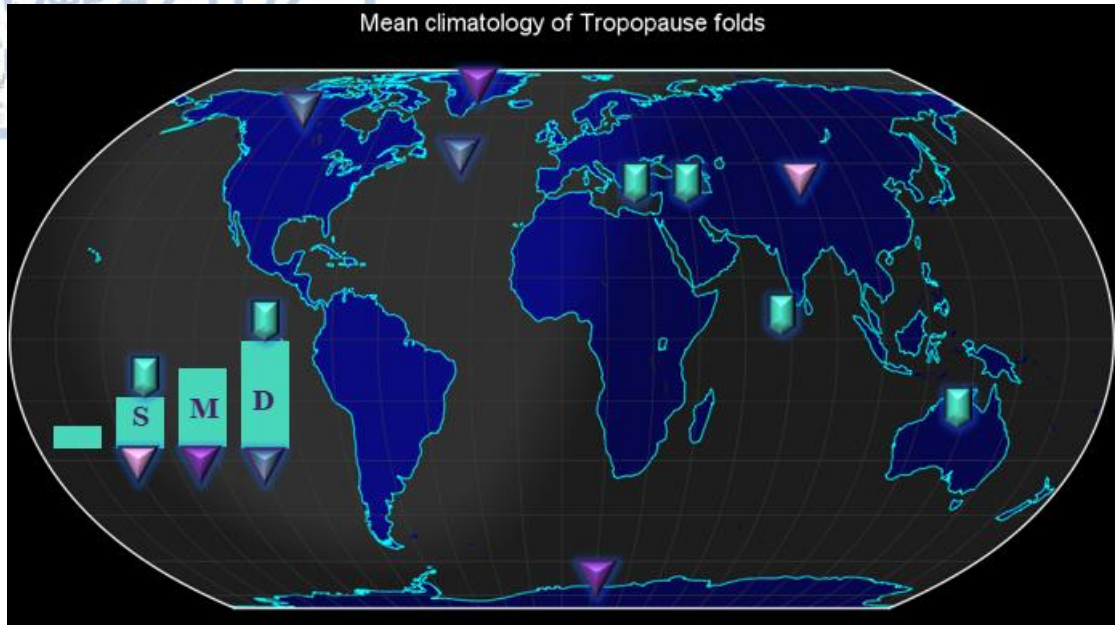

Figure 1.5: Spatial distribution of the average climatology of tropopause folds (Shallow=S, Medium=M, Deep=D; the rhombus represents the winter months, while the rectangle represents the summer months). (The figure was based on results from Akritidis et al., 2021)

1.7 Role of ageostrophic Wind & baroclinic theory-cutoff lows

According to the figure 1.6, the Coriolis force creates a geostrophic balance. The geostrophic wind *Vg* is a stable, non-accelerating, horizontal wind with straight and uniform motion. It results from the balance between the horizontal component of the pressure gradient force and the Coriolis force.

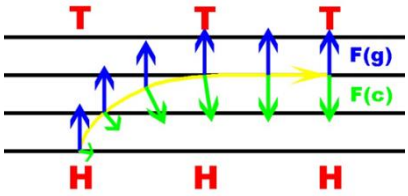

Figure 1.6: Geostrophic equilibrium (wind direction: yellow color, geopotential height: blue color and Coriolis force: green color) (source: http://de.wikipedia.org/wiki/Geostrophischer_Wind).

For geostrophic flow to exist, isobars (on horizontal surfaces) or isohypses (on isobaric surfaces) must be straight and parallel to each other and to the geostrophic wind (Karakostas, 2021). In geostrophic wind, there is no vertical motion and the stronger the geostrophic wind, the denser the isobars. However, when isobars are not parallel, the geostrophic wind *Vg* changes resulting in the ageostrophic wind (*Vag*). The vector *Vag* represents the vector difference between the actual wind and the geostrophic wind. *Vag* is perpendicular to the acceleration vector and is located to its left. Through the study of *Vag*, a crucial meteorological system, the jet stream, is analyzed. Regarding its correlation with the jet stream, convergence occurs at the entrance, while divergence occurs at the exit and the non-geostrophic wind is perpendicular to the geostrophic wind. These non-geostrophic movements at the entrance and exit of the jet stream result in changes in surface systems. According to Karakostas (2021), the geostrophic wind in an isobaric coordinate system is calculated using the following relationships (eq.1.6):

$$\upsilon_g = \frac{g}{f}\left(\frac{\partial z}{\partial x}\right)_P$$
$$u_g = -\frac{g}{f}\left(\frac{\partial z}{\partial y}\right)_P \qquad (1.6)$$

The ageostrophic wind in a local coordinate system is calculated from the following equations (eq.1.7):

$$\left.\begin{aligned} f\upsilon_g &= \frac{1}{\rho}\frac{\partial P}{\partial x} \\ fu_g &= -\frac{1}{\rho}\frac{\partial P}{\partial y} \end{aligned}\right\} \Rightarrow \boxed{\begin{aligned} \upsilon_g &= \frac{1}{\rho f}\frac{\partial P}{\partial x} \\ u_g &= -\frac{1}{\rho f}\frac{\partial P}{\partial y} \end{aligned}}$$
$$\boxed{f\left(\vec{V}_g \times \vec{k}\right) = \frac{1}{\rho}\vec{\nabla}_2 P} \qquad (1.7)$$

In a barotropic atmosphere, where density ρ=ρ(P) is a function of pressure (*P*), vertical motion is significantly weakened because equilibrium is hardly disturbed (Georgiev et al., 2016). Consequently, there is no vertical variation of the geostrophic wind. In baroclinic regions, which refer to a baroclinic atmosphere, isobaric surfaces (surfaces of constant density) intersect with isopycnic surfaces. Density depends on both pressure and temperature (Holton, 1995), expressed by the relationship $\rho=\rho$ (*P*, *T*). Practically, systems in mid-latitude regions, such as low surfaces pressure, are linked to upper-level troughs and owe their formation and development to the mechanism of baroclinic instability. The development of these systems results from non-geostrophic motion since winds intersect isobars or isohypses. The concept of baroclinicity is associated with the temperature gradient, leading to a vertical change in the geostrophic wind. (Pytharoulis, 2022). Within the context of cyclogenesis, there is an enhancement of warm advection, consequently increasing the transported energy, which, in turn, feeds back into the system.

Cut-off lows consist of a closed upper-level low at the 500 hPa isobaric level, which becomes separated or fully detached from the westerly flow, influencing surface weather conditions due to their slow movement. The majority of cut-off lows form during the summer months and can persist for several days. Generally, they form as the jet stream distorts and an upper tropospheric trough elongates southward, favoring the meridional flow. This phenomenon is particularly prevalent in summer when air masses weaken and the meridional flow is favored due to heating (Kentarchos and Davies, 1998). As this detachment from the main flow occurs, air with characteristics of the polar source region becomes isolated. This contains cold air with high potential vorticity and low relative humidity (Nieto et al., 2008). These systems can contribute as a mechanism for transporting ozone between the troposphere and stratosphere through convection (Li et al., 2015). Their role in stratospheric ozone is significant as they constitute a transport path and mixing of stratospheric and tropospheric ozone (Godoy et al., 2011; Rondanelli et al., 2002; Gimeno et al., 2007; World Meteorological Organization, 1986).

1.8 Vertical Velocity & Water vapor Satellite Analysis

According to the continuity equation $\omega=-\rho g w$, the vertical motion is referred to as vertical velocity, where $\omega=dz/dt$ (Pa/s) in the isobaric coordinate system. When $\omega<0$ for vertical velocity, it indicates convergence at the surface, favoring upward motions (adiabatic lifting) with the direction of cold air masses towards warm air masses (fig.1.7). Conversely, when $\omega>0$, it signifies divergence at the surface, favoring downward motions (adiabatic compression) with the direction from warm air masses to colder ones.

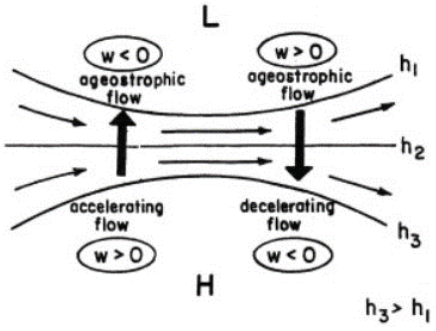

Figure 1.7: Ageostrophic flow and vertical velocity (source: https://www.sciencedirect.com/topics/earth-and-planetary-sciences/ageostrophic-flow).

In the Northern Hemisphere, circulation is always cyclonic, thus the potential vorticity is usually positive due to the Earth's cyclonic rotation. In the case of a low surface pressure and an upper-level trough, convergence occurs ($\omega<0$), resulting in upward motions at the surface and divergence in the upper atmosphere. This condition (fig. 1.8) promotes warm advection and positive vorticity advection (PVA), contributing to surface cyclogenesis due to cyclonic vorticity. Conversely, in the case of a high surface pressure, divergence occurs ($\omega>0$), leading to downward motions at the surface and convergence in the upper atmosphere. This situation favors cold advection and negative vorticity advection (NVA), contributing to subsidence and anticyclogenesis due to anticyclonic vorticity (Pytharoulis, 2022).

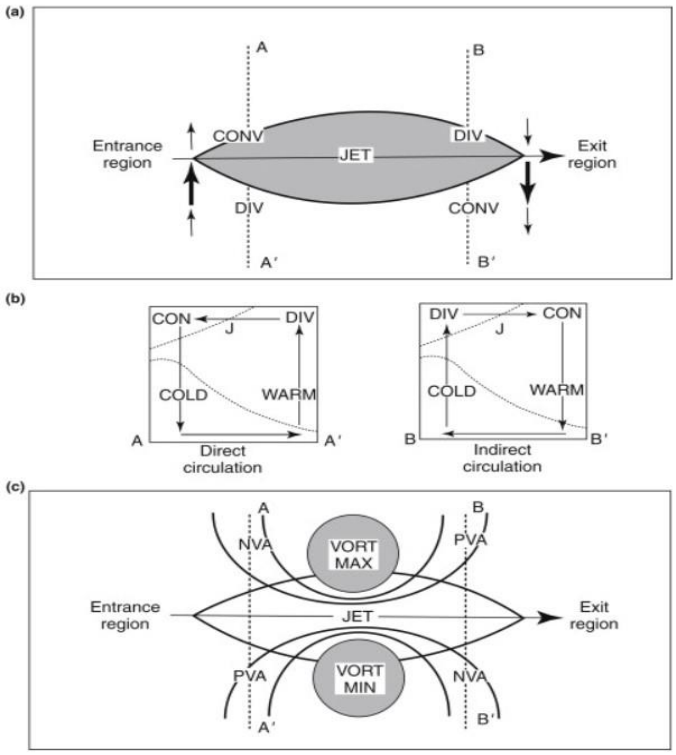

Figure 1.8: Ageostrophic wind and patterns of divergence and convergence at jet stream level (source:https://www.sciencedirect.com/topics/earth-and-planetary-sciences/ageostrophic-flow).

At the humidity boundary, the jet stream is observed with maximum speed and its axis precisely over the humidity boundary, at the alternation of high and low water vapors. The water vapor (WV) channel presents the wind shear, the jet stream. Satellite images aid in monitoring and detecting dry air intrusions (dark gray to black in water vapor images) (Pytharoulis, 2022).

B. The contribution of climate change

1.1 Climate Change Impact of STT on Tropospheric Ozone

The tropopause folds are located in regions characterized by significant temperature gradients along the tropopause. This pronounced temperature difference favors the formation of tropopause folds with the ultimate aim of vertically transporting ozone from the stratosphere to the troposphere. It is worth assessing the impact of climate change on this ozone transport (O_3s). Tropopause folds are typically formed in areas near jet streams, which are located in the subtropical zone. Therefore, an increase in O_3s is expected where these tropopause folds are formed (Akritidis et al., 2019). Thus, according to a future temperature increase, there will be an enhanced temperature difference along the folds, leading to strengthened tropopause folds and intensified O_3s transport. Additionally, climate change may also influence atmospheric circulation patterns, namely the intensity of jet streams, which in turn affect the formation of tropopause folds. In addition, the response of climate change to jet stream has been studied, where in a warmer climate due to an increase in the rate of water vapor can intensify the release of latent heat and thus the intensity of the jet stream (Harvey et al., 2020). The response to future climate change in the 21st century, up to 2100, is predicted to enhance the Stratosphere-Troposphere Exchange (STE) (Tang et al., 2011). Ozone is controlled by the Stratosphere-Troposphere Exchange (STE), which plays a crucial role in global climate change. However, stratospheric Brewer–Dobson circulation (BDC) affects the stratospheric STE flow and consequently the quantity of ozone in the lower stratosphere (Akritidis et al., 2019; Oberländer-Hayn et al., 2016; Morgenstern et al., 2018).

1.2 Climate Change Impact on Tropospheric Ozone

Climate change plays a significant role in tropospheric ozone with both positive and negative impacts depending on polluted regions. However, substance emissions into the atmosphere have a greater negative impact on tropospheric ozone. Under warmer climates, such as a potential temperature increase during climate change, enhanced ozone destruction prevails due to the high abundance of water vapor. Water vapors can

enhance OH production, leading to ozone destruction. Remote areas from polluted sources exhibit a strong reduction in surface ozone, except for the Arctic region, indicating a positive climate change impact on surface ozone (Zanis et al., 2022). In the Arctic region, an increase in ozone is observed due to the exchange of ozone from the stratosphere to the troposphere. However, areas near polluted sources, either anthropogenic or due to emissions, result in ozone increase, with the climate change impact being negative. Key factors expected to control ozone concentrations until 2100 include ozone-depleting substances (ODSs) and emissions of ozone precursor species (NOx) (Fiore et al., 2015; Revell et al., 2015; Zanis et al., 2022). Temperature change indicates the warming trend and serves as an indicator of global warming. According to Akritidis et al. (2019), the climate change impact due to temperature increase is the future reduction of ozone levels in the stratosphere, attributed to the abundance of water vapor leading to ozone destruction. The upward movement of the extratropical tropopause height and the poleward shift of the jet stream are associated with increased greenhouse gas abundance, resulting in stratosphere overheating and extending the tropopause to higher altitudes (Santer et al., 2003). Ozone-depleting substances (ODSs), such as chlorofluorocarbons and halons, can lead to a reduction in stratospheric ozone concentration (fig.1.9), preventing UV absorption and resulting in stratospheric cooling. As a consequence, a significant temperature difference between the cold stratosphere and the warm troposphere is created. In the stratosphere, the temperature increases with altitude. However, in the lower parts of the stratosphere, the air is colder than in the upper parts of the troposphere. For this reason, cold air descends from the stratosphere into the troposphere. Consequently, this temperature difference leads to instability and enhances the development of cyclonic disturbances. When this difference weakens, it results in the poleward movement of the jet stream due to its more wavelike form (Akritidis et al., 2019; Lorenz and DeWeaver, 2007). Therefore, future tropospheric ozone changes depend on a combination of factors, including human activities affecting precursor emissions, chemical processes governing ozone production and loss, the exchange of air masses between the stratosphere and troposphere (STE) and deposition processes (Akritidis et al., 2019; Young et al., 2013). However, the most significant factors expected to govern ozone quantities in their spatial distribution in the stratosphere and troposphere on a global scale (Table 2) are emissions of ozone precursor species, ozone-depleting substances (ODSs) such as chlorofluorocarbons (CFCs), contributing to ozone depletion in the stratosphere and

long-lived greenhouse gases (GHGs) such as carbon dioxide (CO_2) and short-lived greenhouse gases (GHGs) such as methane (CH_4), including temperature changes and lightning NOx emissions, biogenic volatile organic compound (BVOC) emissions and water vapor (Fiore et al., 2015; Revell et al., 2015; Zanis et al., 2022). The increase in concentrations of CO_2 can induce temperature rise due to its ability to absorb and re-emit radiation. Natural climate variability, such as volcanic eruptions, has the potential to reduce ozone quantities (Shepherd et al., 2005). According to the Montreal Protocol, a gradual reduction of ozone depleting substances (ODSs) is expected by 2050 (Europe's, M. E. Europe's Environment. The Third Assessment. A summary). The CFCs (chlorofluorocarbons) and halons are now controlled under the Montreal Protocol. The Kyoto Protocol deals with the greenhouse gases such as sulphur hexafluoride (SF6), hydrofluorocarbons (HFCs), perfluorocarbons (PFCs), CO_2, N_2O and CH_4. The investigation and future analysis of tropospheric ozone variation according to possible scenarios, such as Representative Concentration Pathways scenarios (RCPs), considering different emission values, aim to estimate the magnitude of global tropospheric ozone change. RCP scenarios represent different greenhouse gas concentration trajectories used in climate modeling and are useful to provide a view of the implications of developments. This essentially includes the impact of land use change on climate and the future climate is represented. The scenarios of climate change are based on specific greenhouse gas values in relation to the current observed climate. Consequently, this difference is estimated with the ultimate goal of researching the climate in the future. The RCPs produced by the integrated assessment models are used in the IPCC (Intergovernmental Panel on Climate Change) assessment, Fifth Assessment Report (AR5), as the basis for climate projections with the aim of analyzing and assessing climate change, presenting alternative gas emissions. The IPCC publishes credible reports and data concerning climate change, climate and socioeconomic impacts. The Sixth Assessment Report (AR6), completed in 2021, is based on the Coupled Model Intercomparison Project (CMIP6) and executed according to the Shared Socioeconomic Pathways (SSPs) climate scenario framework. These reports encompass existing knowledge on climate change and analyze the consequences of anthropogenic emissions, aiming to address them effectively. Essentially, future climate projections involve simulations based on different scenarios from various global climate models (GCM), allowing for an estimation of the range of change.

Significant is the study of ozone precursor substances such as NOx over time, as they partly influence the trajectory of tropospheric ozone. More specifically, according to CMIP6 models, particularly the SSP3-7.0 scenario representing weak mitigation actions for atmospheric pollutants, there is an increase in tropospheric ozone up to 10 ppb by 2050 primarily due to increased emissions of ozone precursor substances. Consequently, the ozone production rate exceeds the destruction rate and then there is a stabilization until 2100. However, despite the reduction in ozone precursor substances, the increase in tropospheric ozone continues to 16 ppb by 2100. Other contributing factors to this trend include potentially increased methane abundance, BVOCs, CO_2, an increase in tropopause height, downward transport of stratospheric ozone to the troposphere (STT) and climate change, particularly in Southeast Asia, Europe and North America (Turnock et al., 2020; Wild et al., 2012). This downward ozone transport is favored by the Brewer-Dobson circulation due to increased greenhouse gases, as projected in the pessimistic SSP3-7.0 scenario (Griffiths et al., 2021).

In an assessment report (Fifth Assessment Report (AR5)), which is published by IPCC, represented in Figure 1.10, scientists are divided into groups for this evaluation. Therefore, for the composition of the report, there is the Working Group 1 (WG1) <<The Physical Science Basis>>, which links current climate change conditions to human factors. The second group is WG2 <<Impacts, Adaptation and Vulnerability>> which deals with the implications of climate change. The third group is WG3 <<Mitigation of Climate Change>> which harmonizes the reduction or stabilization of climate change according to specific strategies, taking into account economic losses. Thus, a comprehensive assessment report is compiled with the ultimate goal of mitigating climate change in the future. Additionally, the interdependence between human activities and climate is ascertained. Essentially, the assessment of climate change is subject to an evaluation of future emissions, considering uncertainties due to the natural variability of the climate and the models.

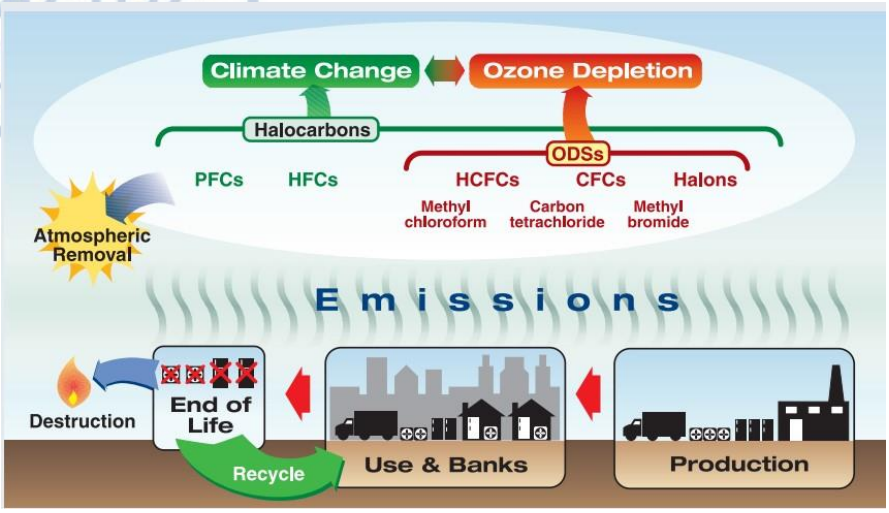

Figure 1.9: Interaction of climate change with anthropogenic emissions (source: https://www.ipcc.ch/site/assets/uploads/2018/03/sroc_full-1.pdf).

Ozone concentrations in the Northern Hemisphere have seen a doubled increase compared to pre-industrial period with an annual mean ranging from 11 to 23 ppb, due to the emission of precursor compounds resulting from industrial activities (Conte et al., 2021; Hartmann et al., 2013). According to a study assessing the potential risk of ozone levels for the year 2050, it was determined that the critical maximum daily 8h mean ozone threshold for risk assessment lies around 60 ppb (De Marco et al., 2022). Consequently, concentrations exceeding this threshold signify an escalation in anthropogenic emissions beyond normal limits, resulting in profound implications for both human health and vegetation (Lei et al., 2012). The regression coefficient $\Delta O_3/\Delta T$ reveals the spatial distribution of ozone in conjunction with the impact of climate change. When positive, it indicates that a slight increase in temperature leads to a significantly greater ozone change. This is observed in regions near polluted sources, such as North China and India, where the increase in ozone change may be attributed to NOx emissions (Zanis et al., 2022). However, with a sufficiently large increase in temperature change, the ozone change decreases. This is observed near the equator, indicating the strong signal of climate change in oceanic and remote regions away from polluted sources, as well as in North America. Essentially, the surface ozone decreases due to significant climate change resulting from global warming attributed to abundant water vapor. The future changes in global tropospheric ozone are based on different future scenarios according to simulations. Changes in human activities modify radiative

forcing proportional to the greenhouse gas, which acts either positively, leading to the warming of the atmosphere, or negatively, resulting in atmospheric cooling. Therefore, they have a direct impact on temperature and act as a cause of climate change, measured in Wm^{-2}. Consequently, tropospheric ozone contributes to anthropogenic radiative forcing, as it increases atmospheric temperature levels. The impact of tropospheric ozone on radiative forcing is +0.40 Wm^{-2}, is identified as the third most substantial contributor to global mean radiative forcing, is behind carbon dioxide and methane (Percy et al., 2003). Radiative forcing in the IPCC used as an indicator in energy balance changes. Analyses of historical records reveal a rapid increase in average surface ozone levels in developing countries due to anthropogenic emissions, while a gradual decline is observed in developed countries attributable to the control of high emission levels (Lei et al., 2012; Streets et al., 2004). Nevertheless, it undeniably constitutes a significant challenge in developed nations owing to climate change and the persistence of ozone background, which is transported over substantial distances for extended periods. Anticipated future increases in emissions resulting from anthropogenic activities are expected to be decisive factors contributing to elevated ozone levels, particularly in industrialized regions (Lei et al., 2012; Lin et al., 2008a).

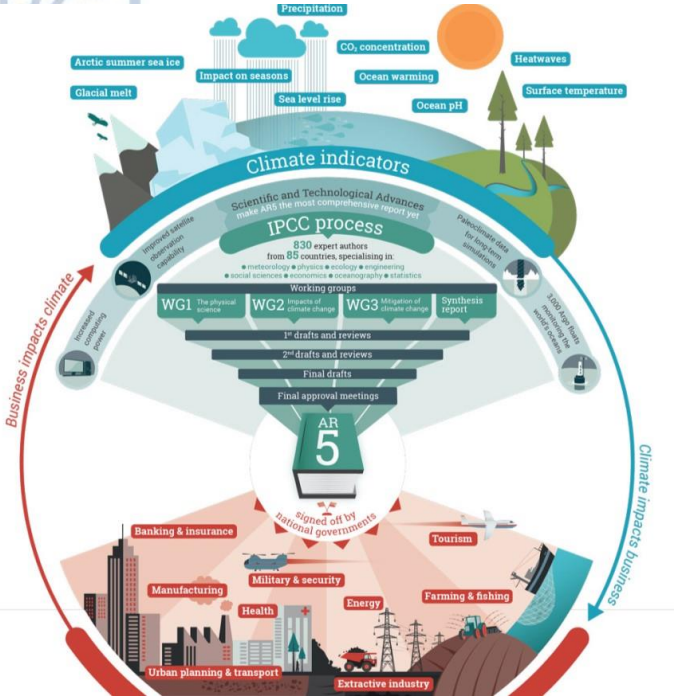

Figure 1.10: IPCC process (source: https://www.wwf.org.uk/updates?unewsid=6807).

1.3 The impact of demographic and climate factors on human health

According to the SSP3-7.0 scenario (<<regional rivalry>> with high challenges to mitigation and adaptation and weak air pollution controls), future increases in ozone concentrations are observed in studies until 2100 due to various factors by the end of the 21st century (Turnock et al., 2023; Rao et al., 2017). This long-term exposure to ozone results in significant impacts on human health, such as inflammatory lung effects and respiratory diseases (Turnock et al., 2023; Chen & Hoek, 2020). However, a more significant cause studied and identified as the strongest factor resulting in health burdens is the increase in population and ageing. This health burden often leads to premature mortality, at ages under 25 years, derived from either atmospheric pollutants or in combination with sociodemographic factors.

According to estimates, there will be an increase of approximately 3.5 million deaths annually by 2100 (Turnock et al., 2023), with premature deaths due to ozone expected to multiply ninefold, despite the projected reduction in ozone precursor substances (Akritidis et al., 2024). However, mortality is also driven by population ageing, making older age groups more vulnerable to atmospheric pollutants, resulting in higher

mortality rates, while younger individuals are less susceptible. This increased mortality is primarily observed in South and East Asia, where the population is ageing, leading to increased life expectancy and a larger proportion of the population exposed to atmospheric pollutants. Future mortality appears to be primarily attributable to population growth and ageing, observed particularly in South Asia and secondarily to anthropogenic emissions and climate change, as seen in China. Climate change, thus, contributes to this mortality to a very small extent. However, it is crucial to limit climate change as mortality is observed due to this factor by 2100, despite the benefits of reducing ozone precursor substances.

According to the table 1.1, the World Health Organization (WHO) provides air quality ozone guidelines based on experimental-clinical studies. In the case of tropospheric ozone, the WHO guideline estimates a 1-2% increase in mortality during periods when the average ozone concentration approaches 100 μg/m³ over an 8-hour period, as compared to the fundamental limit of 70 μg/m³ over the same time frame, equivalent to 35 ppb. Considering the conversion factor of 1 μg/m³ to 0.5 ppb for ozone, the 100 μg/m³ limit corresponds to 50 ppb. For the annual average exposure, the WHO recommends a guideline of 40 μg/m³, equivalent to 20 ppb for ozone (World Health Organization, 2006). These guidelines, which establish the critical threshold of ozone risk, are informed by both anthropogenic and natural emissions, accounting for stratospheric intrusion in surface concentrations. As depicted in the table 1.1, the standard threshold is set at 100 μg/m³ over an 8-hour period. The intermediate threshold is defined at 160 μg/m³ over an 8-hour period, that guarantees particular attention to respiratory implications. Concentrations exceeding 240 μg/m³ over an 8-hour period result in significant health impacts. However, it is important to note that specific threshold values for risk assessment related to tropospheric ozone may exhibit regional variations in accordance with air quality standards (Díaz et al., 2018). Projections indicate that, by the year 2100, a significant portion of the population is anticipated to be exposed to ozone concentrations exceeding 60 ppb. It is observed that future ozone concentrations continue to increase in certain areas exceeding the WHO guidelines, despite mitigation measures (Turnock et al., 2023; Shaddick et al., 2020).

Table1.1: Classification of the ozone threshold (source: https://iris.who.int/bitstream/handle/10665/69477/WHO_SDE_PHE_OEH_06.02_eng.pdf?sequence=1).

	Daily maximum 8-hour mean ($\mu g/m^3$)	**Basis for selected level**
High levels	240	Significant health effects; substantial proportion of vulnerable populations affected.
Interim target-1 (IT-1)	160	Important health effects; does not provide adequate protection of public health. Exposure to this level of ozone is associated with: • physiological and inflammatory lung effects in healthy exercising young adults exposed for periods of 6.6 hours; • health effects in children (based on various summer camp studies in which children were exposed to ambient ozone levels). • an estimated 3–5% increase in daily mortality[a] (based on findings of daily time-series studies).
Air quality guideline (AQG)	**100**	Provides adequate protection of public health, though some health effects may occur below this level. Exposure to this level of ozone is associated with: • an estimated 1–2% increase in daily mortality[a] (based on findings of daily time-series studies). • Extrapolation from chamber and field studies based on the likelihood that real-life exposure tends to be repetitive and chamber studies exclude highly sensitive or clinically compromised subjects, or children. • Likelihood that ambient ozone is a marker for related oxidants.

Table 1.2: Impact of changes in the major variables in tropospheric ozone.

Variables	**Change**	**Impact on O_3t**
BDC	↑	negative
Halocarbons ODS (CFCs, HCFCs, Halons)	↑	positive
Anthropogenic emissions GHGs [CO2, CH4, Halocarbons (PFCs, HFCs)]	↑	negative
Natural Precursor Emissions (NOx, BVOC, lightning activity during thunderstorms)	↑	negative
STT	↑	negative
ΔT (Temperature changes)	↑	Positive (unpolluted regions) Negative (polluted regions)

Chapter 2. Data and methodology

2.1 Data

The data used in this thesis includes ozone concentrations and various meteorological parameters such as geopotential height, horizontal wind speed components (u, v) vertical velocity (ω), relative and specific humidity and potential vorticity from the CAMS global reanalysis (EAC4) (https://atmosphere.copernicus.eu/data). The dataset has a temporal resolution of 3 hours. The European Copernicus Atmosphere Monitoring Service (CAMS), monitors the atmospheric composition and provide information related to air pollution and greenhouse gases. The CAMS Reanalysis encompasses model results in conjunction with data assimilation, it integrates meteorological observations and incorporates data from radiosonde, ozonesonde, air quality measurements and satellite data for ozone measurements. Additionally, observational ozonesonde data (Vertical ozone profile) containing radiosonde data for the Hohenpeissenberg station were obtained from the WOUDC data (World Ozone and Ultraviolet Radiation Data Centre) (https://woudc.org/data/dataset_info.php?id=ozonesonde). Furthermore, data from the CMIP6 project (Coupled Model Intercomparison Project Phase 6) Earth System Model (https://esgf-node.llnl.gov/search/cmip6/) were utilized. Coupled Model Intercomparison Project phase 6 (CMIP6) data based on shared socioeconomic pathways SSPs according to table 2.1 and the GCM in general for the purpose of future climate projections. There are four distinct scenarios ranging from the most optimistic, considering greenhouse gases with the least emissions, which is considered the best scenario, to the most pessimistic scenario with the highest emissions, considered the worst scenario. The scenario under investigation in this study is SSP3-7.0, which represents the pessimistic scenario, is noteworthy to explore the limits of risk, namely the threshold considered critical. So that appropriate strategies can be put in place to deal with them effectively.

The CAMS Reanalysis is a product utilizing data from observations and models with high spatiotemporal resolution. The horizontal resolution is 0.75°x0.75° (lat/lon), vertical resolution includes 60 model levels, temporal resolution is every 3 hours and

spatial resolution is 80 km. Therefore, with data assimilation, there is an overestimation relative to observations rather than underestimation. CMIP6 models are global climate model data and serve as the foundation for the 6th Assessment Report on climate change. Shared Socioeconomic Pathways (SSPs) are scenarios describing different trajectories of greenhouse gas emissions and socioeconomic development predictions (Turnock et al., 2020; O'Neill et al., 2014). They are used as input data to analyze and project changes in atmospheric pollutants and climate simulated by Earth System Models (ESMs). Essentially, experiments are conducted, followed by an evaluation of future changes in atmospheric gases by Earth System Models. Earth System Models are coupled climate models that integrate and simulate interactions between the atmosphere, ocean and land, incorporating chemistry along with physical processes according to equations, known as parameterizations. They are particularly utilized in CMIP6 due to their consideration of changes in emissions and climate change.

The most optimistic scenario SSP1-1.9 (sustainability) involves a climate forcing of 1.9 Wm^{-2}, corresponding to an increase in global temperature of less than 2 degrees Celsius by 2100 compared to the pre-industrial period. The scenario studied in the present analysis is SSP3-7.0 (regional rivalries), which has a climate forcing of 7 Wm^{-2}, corresponding to an increase in temperature up to 2.5 degrees Celsius by 2050 and up to 4.2 degrees Celsius by 2100. The SSP3-lowNTCF scenario has a climate forcing of 6.3 Wm^{-2}, corresponding to a temperature increase of 3.7 degrees Celsius by 2100. The most pessimistic scenario SSP5-8.5 (fossil fuel development) involves a climate forcing of 8.5 Wm^{-2}, corresponding to an increase in global temperature up to 5 degrees Celsius by 2100 (Katragkou, 2022).

Table 2.1: Classification of climate scenarios.

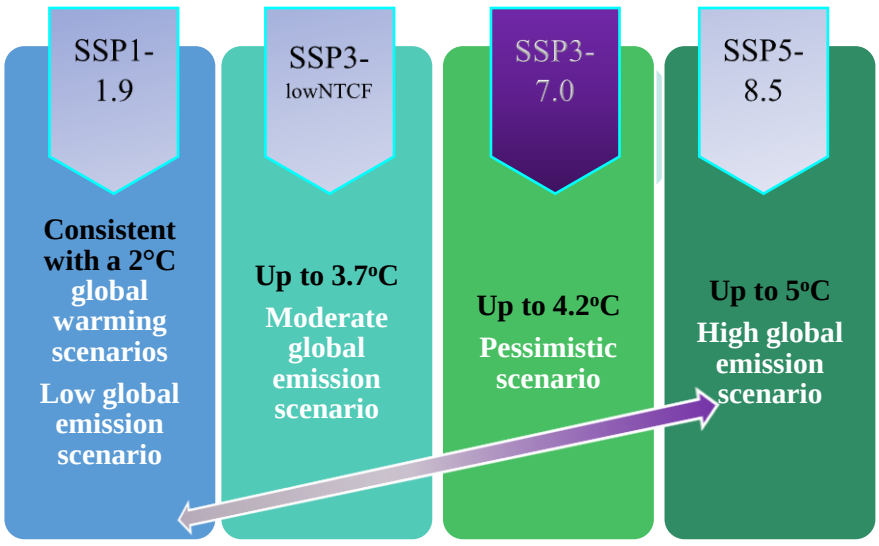

2.2 Methodology

The global model aims to assess the future impact of climate change on stratospheric ozone based on simulations on a global scale. Specifically, data from the AerChemMIP (Aerosol Chemistry Model Intercomparison Project) were employed and simulation experiments considered future climate (ssp370SST) and present-day climate (ssp370pdSST) under the same future anthropogenic emissions trajectory (SSP3-7.0 scenario). The experiment time period is from 2015 to 2100. The ssp370SST experiment account for the temporal variations in sea surface temperature (SST) and future anthropogenic emissions. In contrast, the ssp370pdSST experiment considers only changes in emissions, because sea surface temperature remains constant. Thus, the difference between the two experiments (eq.2.1) provides insight into the impact of climate change on ozone concentrations.

ssp370SST-ssp370pdSST= sign of climate change on ozone concentrations (2.1)

Table 2.2: Information on the simulations and the EC-Earth3-AerChem model output prepared for CMIP6 AerChemMIP ssp370SST and ssp370pdSST.

Model	**Experiment name/scenario**	**Model type**	**Variable**	**Resolution**	**Vertical level**	**References/ DOI**
CMIP6 (EC-Earth3-AerChem)	ssp370pdSST ssp370SST/ SSP3-7.0	ESM interactive chemistry	O3(mol mol-1)	3 ◦ × 2 ◦ 250km 120x90 lon/lat	34levels/ top level 0.1 hPa	EC-Earth Consortium (2020a, 2020b)

Analyses of specific meteorological parameters related to the stratospheric ozone intrusion event are presented at a specific isobaric level of 300 hPa and of 500 hpa for longitude and latitude maps and across all isobaric levels in cross-section. The analyzed parameters include geopotential height, potential vorticity fields, specific humidity, vertical and horizontal wind speed and ozone. The objective is a synoptic

thermodynamic analysis of a stratospheric intrusion. All analyses were conducted using statistical tools in Rstudio, Python and Excel.

2.3 Study area

The study area selected for the assessment and synoptic analysis of the stratospheric intrusion event is Hohenpeissenberg (47°48'N 11°0'E). This analysis aims to understand the increased ozone concentrations resulting from the stratospheric intrusion. Data were collected for the broader European region from -40°W to 40°E and from 30°N to 70°N. The CAMS data cover the time period from 00Z on 25 January 2015 to 18Z on 27 January 2015. The stratospheric ozone intrusion event occurred at 00Z on 26 January 2015. Observational ozonesonde data from WOUDC is available for 23, 26 and 28 January 2015 at 06Z.

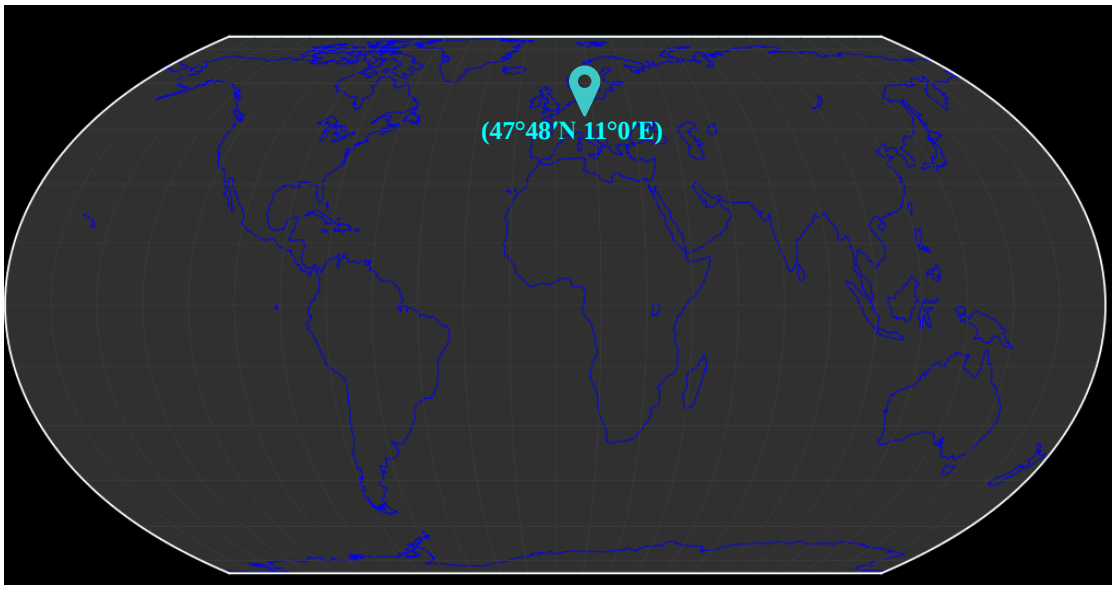

Figure 2.1: Study area of a world map (Hohenpeissenberg, Germany).

Chapter 3. Results

A synoptic and thermodynamic analysis of a stratospheric intrusion and the associated tropopause fold event during the period from 25 January to 27 January 2015 over Hohenpeissenberg is presented. Distributions of geopotential height, potential vorticity (PV), specific humidity, horizontal and vertical wind speeds and ozone were diagnosed. The analysis reveals a clear correlation between the increase in ozone concentration and tropopause fold.

A. Synoptic analysis

3.1 Ozone synoptic analysis

To investigate the stratospheric intrusion, several meteorological parameters are examined. Potential vorticity is depicted with contours (fig.3.1), while ozone concentrations are observed according to the color scale. From 25 January at 00Z, a distinctive flow with high ozone concentrations so-called “hook shaped” over the study area is noted. The synoptic situation on 25 January at 00Z is characterized by a deep upper-level trough at 300 hPa with a 4PVU isentropic surface, extending from Scandinavia to central Europe. This system moves eastward. Specifically, ozone concentrations exceed 100 ppb in the study area from 25 January at 00Z to 26 January at 00Z, coinciding with low relative humidity values and high PV values. On 25 January at 12Z, ozone concentrations approach 200 ppb, while on 26 January at 00Z, ozone concentrations approach 230 ppb. On 26 January at 12Z, ozone concentrations exceed 100 ppb, while on 27 January and later, the system has dissipated, moving southeastward. Consequently, over the study area, reduced ozone concentrations approaching 50 ppb are observed. In the region of high ozone concentrations approaching 200 ppb, potential vorticity values exceeding 2PVU are depicted. Therefore, the combination of both parameters demonstrates that dry air signifies stratospheric origin. High ozone values are mainly observed over southeastern Germany and appear at the ridge exit (east) and trough entrance (west), where convergence and divergence occur. Due to intense vertical motions, the transport of dry and stable stratospheric air rich in ozone is favored towards the troposphere. The system moves southward and eastward of Europe, specifically, the flow with high ozone values follows the jet stream path. However, on 26 January, a second flow with high ozone

values approaching Europe is observed. Nevertheless, it weakens as it moves eastward and gradually dissipates after 27 January.

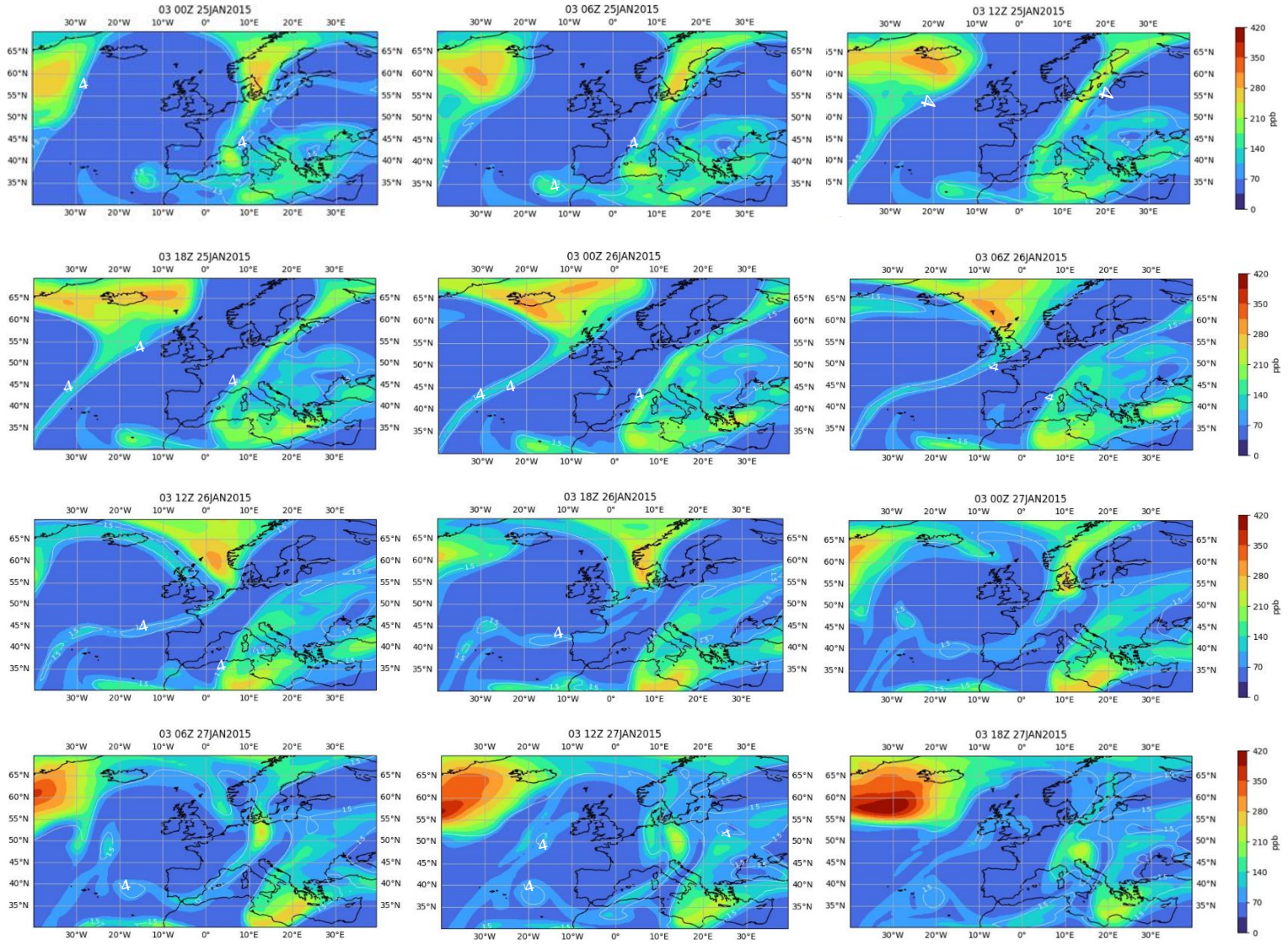

Figure 3.1: Ozone mixing ratio (color shaded in ppb), Potential Vorticity (white contours in pvu) at 300 hPa during the period from 00Z on 25 January 2015 to 18Z on 27 January 2015 (6h interval).

The monthly mean ozone values for January are observed over the time period from 2003 to 2022 at the 300 hPa isobaric level (fig.3.2). According to the color scale, over the European region and specifically above the study area, average monthly ozone values of 90 to 100 ppb are observed for the month of January. The highest monthly ozone values are discerned over the North Atlantic, exceeding 110 ppb, while the lowest monthly ozone values are located over the South Atlantic with values less than 70 ppb. This observation represent good agreement with the mean climatology of tropopause folds as mentioned earlier. Specifically, in the North Atlantic, the highest frequency of tropopause folds is observed, leading to elevated ozone concentrations in this region. Consequently, the highest ozone concentrations prevail in this area.

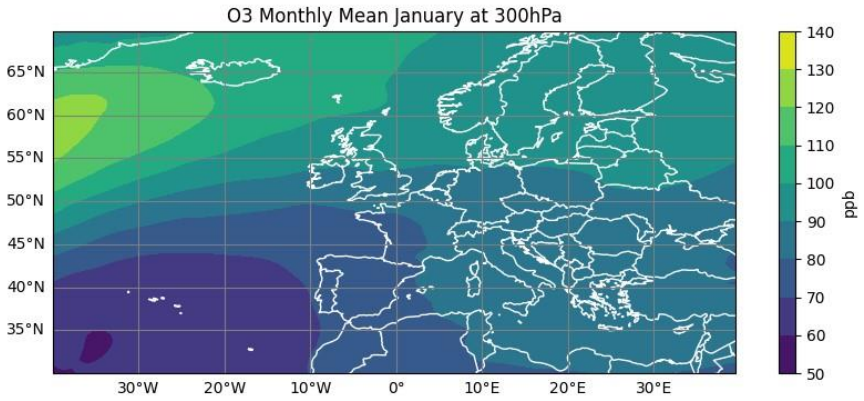

Figure 3.2: Average monthly January ozone value (in ppb) for the period from 2003 to 2022 at 300 hPa.

By comparing daily ozone values to the mean climatology of ozone, insights can be derived regarding whether daily values exceed the climatological average. This can be achieved through the representation of deviation patterns. The deviation indicates the extent to which the observed variable exceeds or falls below the mean value for a specific time period. Specifically, on 25 January at 00Z in the study area of Hohenpeissenberg (fig.3.3), where the so-called ¨hook-shaped¨ structure is present, the observed ozone value, highlighted in green, exceeds the mean value, namely the average monthly value for January from 2003 to 2022, by 10 units. As a result, the

occurrence of this tropopause fold mechanism is confirmed, justifying the higher ozone concentrations. In more detail, on 25 January 2015 at 00Z, ozone concentrations in the study area approach values around 100 ppb, whereas in the study area's climatology, average ozone values are observed at 90 ppb. Therefore, from the difference between the two, it is inferred that on 25 January at 00Z, there is an increase in ozone by 10 units Subsequently, on the following two dates on 25 January at 12Z and on 26 January at 00Z, there is again an increase in ozone levels. Specifically, on 25 January at 12Z, ozone values are at 200 ppb, indicating an increase in ozone by 110 units from the climatological average. While on 26 January at 00Z, an even greater increase in ozone is observed, by 140 units, as ozone values on that specific date approach 230 ppb. This practically demonstrates the stratospheric intrusion due to elevated ozone values above the normal mean values.

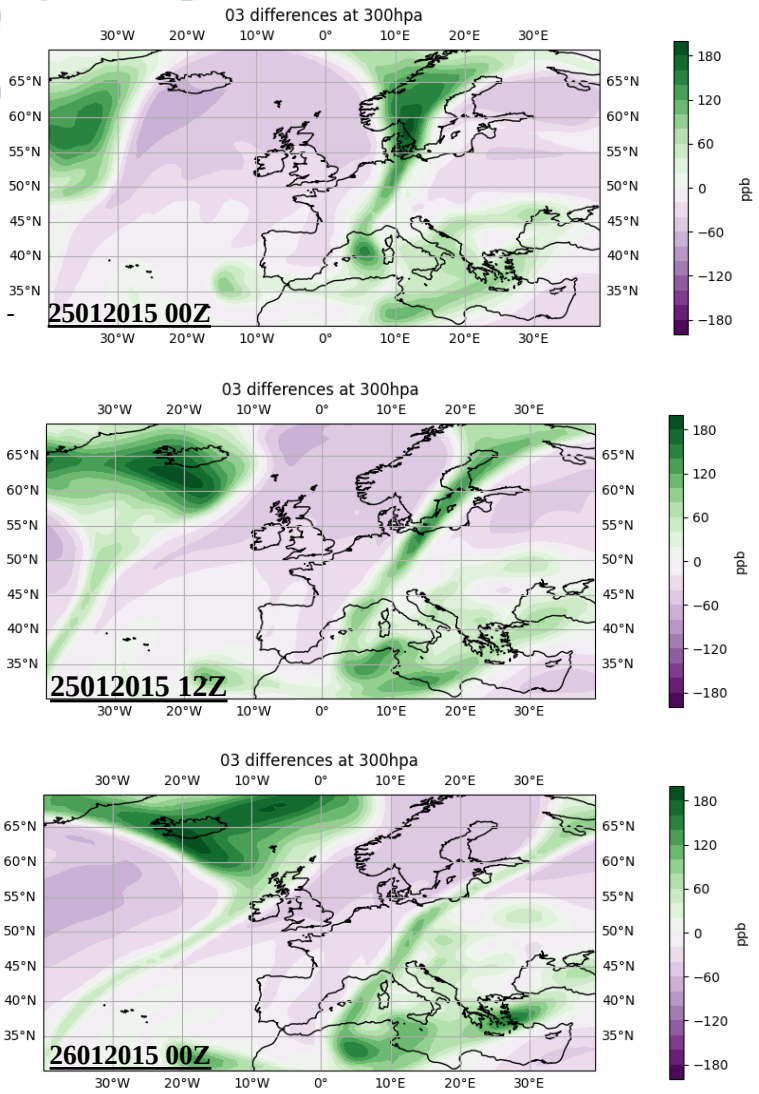

Figure 3.3: Differences of ozone between average monthly January ozone value during 2003-2022 and a) at 00Z on 25 January 2015, b) at 12Z on 25 January 2015 and c) at 00Z on 26 January 2015 at 00Z at 300 hPa.

Ozone constitutes the most significant parameter in the present study. Hence, a three-dimensional analysis is undertaken with the primary objective of investigating the evolution of the phenomenon over the broader region of Hohenpeissenberg. The three-dimensional field of ozone concentrations exceeding 200ppb at 00Z on 26 January 2015 is presented in Fig.3.4a, depicting the stratospheric ozone intrusion into the troposphere over Hohenpeissenberg (47.48N, 11E) region. The three-dimensional field illustrates the highest concentrations of ozone in the study area on 26 January 2015 at 00Z.

Correspondingly, Figure 3.5 depicts the elevated ozone concentration in a three-dimensional representation over Hohenpeissenberg, reaching values greater than 100 ppb, as observed in the longitude-latitude figures at the 300hPa level above. Essentially, the three-dimensional fields represent the longitude-latitude figures with the same ozone values.

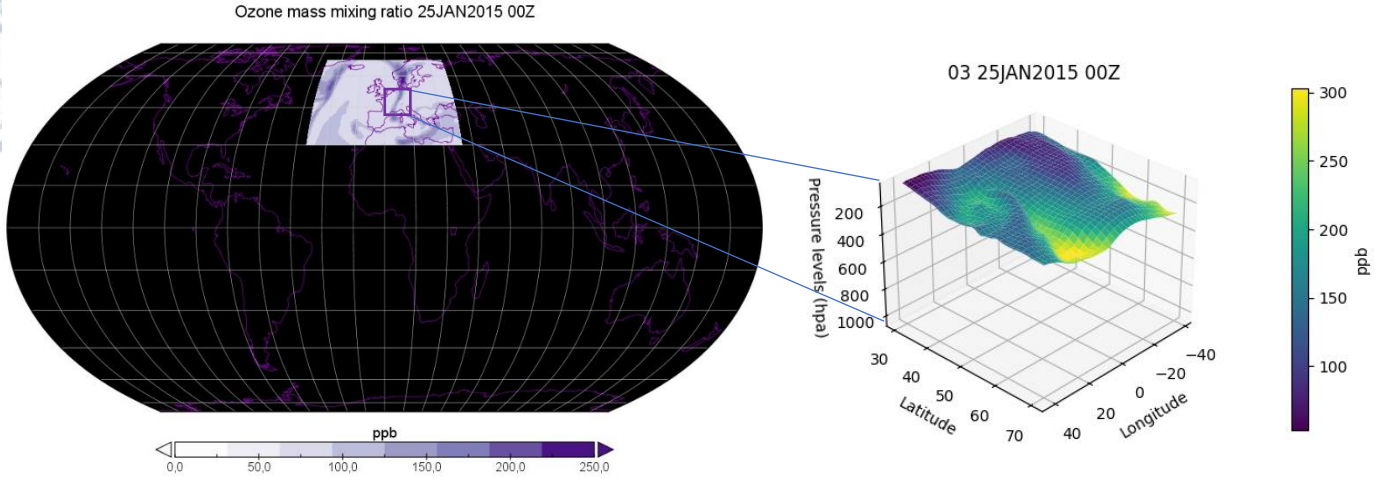

a)

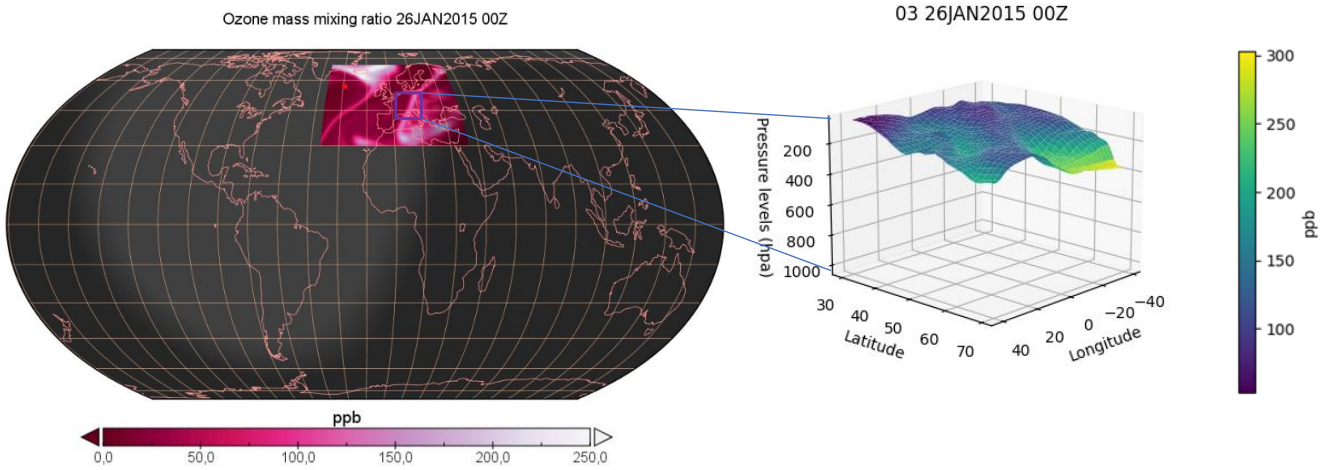

b)

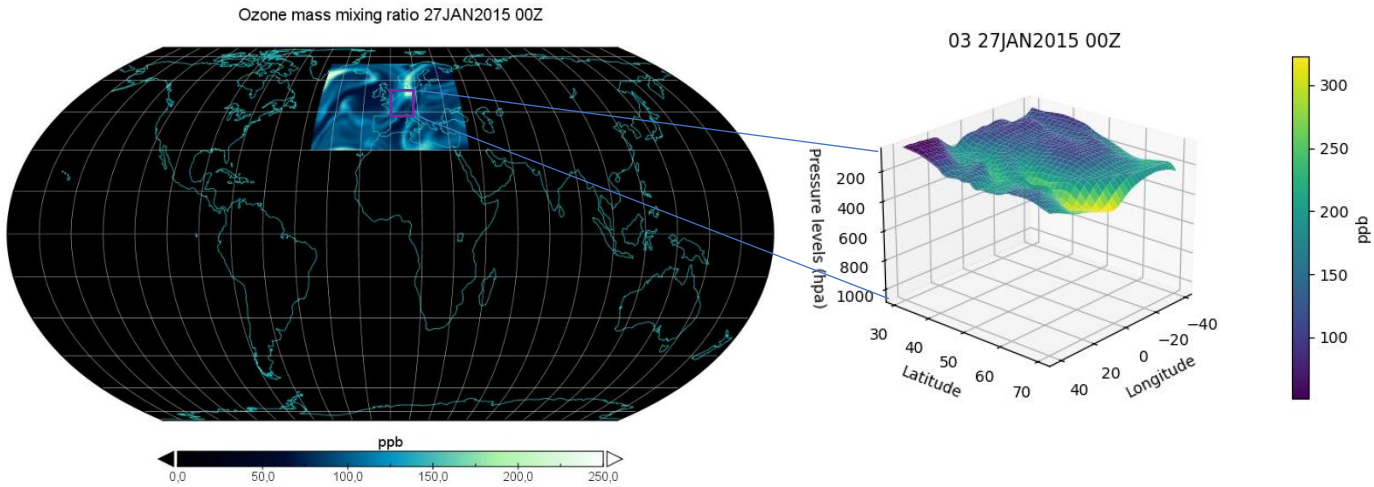

c)

Figure 3.4: Three-dimensional (longitude, latitude, Pressure (hPa)) spatial distribution of ozone concentrations in ppb a) at 00Z on 25 January 2015, b) at 00Z on 26 January 2015, c) at 00Z on 27 January 2015.

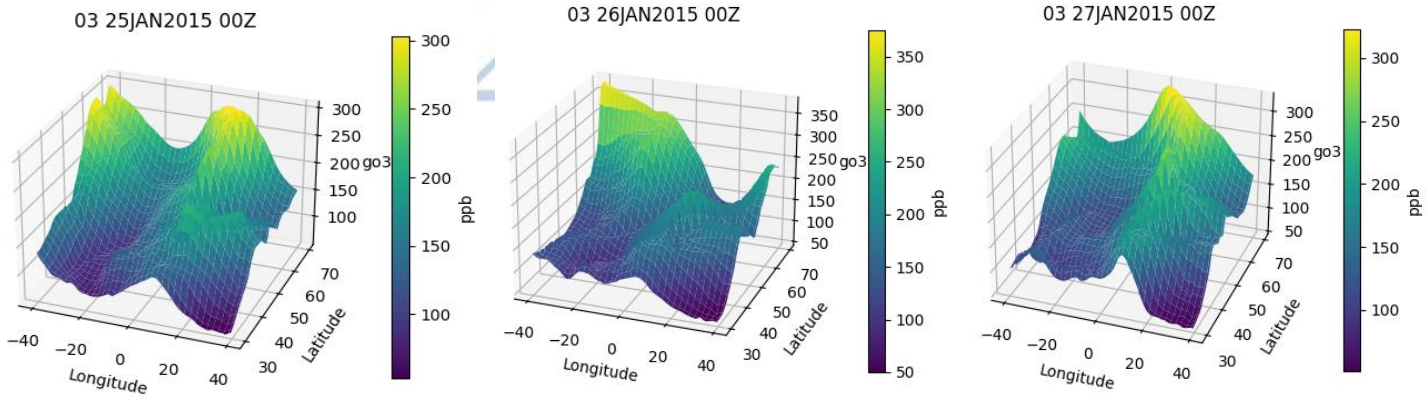

a) b) c)

Figure 3.5: Three-dimensional (longitude, latitude, ozone (ppb)) spatial distribution of ozone concentrations in ppb a) at 00 Z on 25 January 2015, b) at 00 Z on 26 January 2015, c) at 00 Z on 27 January 2015.

3.2 Potential vorticity synoptic analysis

The evolution of meteorological conditions can also be illustrated by the appearance of a sequence of potential vorticity (PV) maps at the 300 hPa isobaric surface from 00 UTC on 25 January to 18 UTC on 27 January (fig.3.6). The analysis of potential vorticity on isentropic surfaces reveals a flow with high PV values, extending southeastward and exhibiting cyclonic curvature. The figure 3.6 depicts the geopotential height field at the 300hPa isobaric level and the potential vorticity according to the color scale. A highly intense penetration of potential vorticity, with values exceeding 2PVU, was observed from 00Z on 25 January to 06Z on 26 January over the study area. However, at 12Z on 26 January, the values of potential vorticity are above 2PVU and the flow moves southeastward with cyclonic curvature. Specifically, from 25 January at 06Z to 26 January at 06Z, potential vorticity (PV) equal to 4 PVU is observed over Hohenpeissenberg. In comparison to surrounding regions, a notable difference in the value of potential vorticity is observed, consequently influencing the extension of the dynamic tropopause to lower isobaric levels. The intrusion of stratospheric air with high stability is observed to penetrate into the troposphere. On 27 January, the flow appears to be cut off from the main flow, indicating that the upper-level system has practically disconnected and the baroclinicity of the lower level has weakened. However, there is no apparent development of a cutoff low at the 300hpa isobaric level.

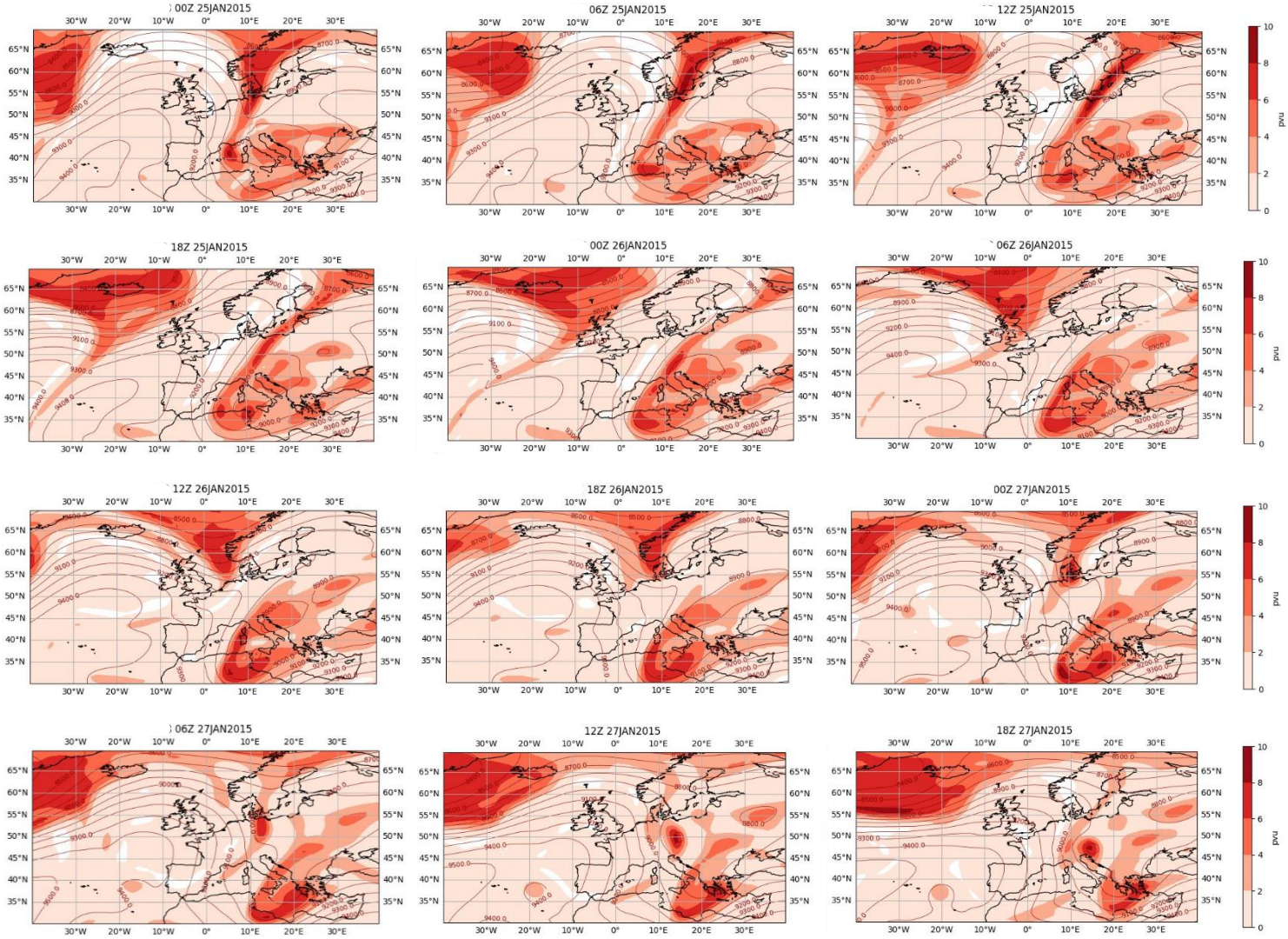

Figure 3.6: Potential Vorticity (color shaded in pvu) and geopotential height (red contours in gpm) at 300 hPa, during the period from 00Z on 25 January 2015 to 18Z on 27 January 2015 (6h interval).

3.3 Specific humidity synoptic analysis - satellite water vapor images & Jet stream

Regarding specific humidity (fig.3.7), a characteristic flow is observed over the study area with very low specific humidity values below 0.05. According to the previous parameters depicted in the figures, the low humidity values coincide with the presence of a dry intrusion into the troposphere. Contours represent the potential vorticity surface greater than 2PVU precisely over the study area with very low humidity, indicating the presence of dry air that has entered the troposphere from the stratosphere. The lowest humidity values below 0.05 are observed from 00Z on 25 January to 12Z on 26 January over Hohenpeissenberg, representing typical values of the corresponding high ozone and potential vorticity values. While on 27 January at 00Z, as the system begins to move away, it exhibits higher values approaching 0.15, which can be justified due to the absence of stratospheric intrusion. In other circumstances, stratospheric intrusion could result in lower relative humidity percentages.

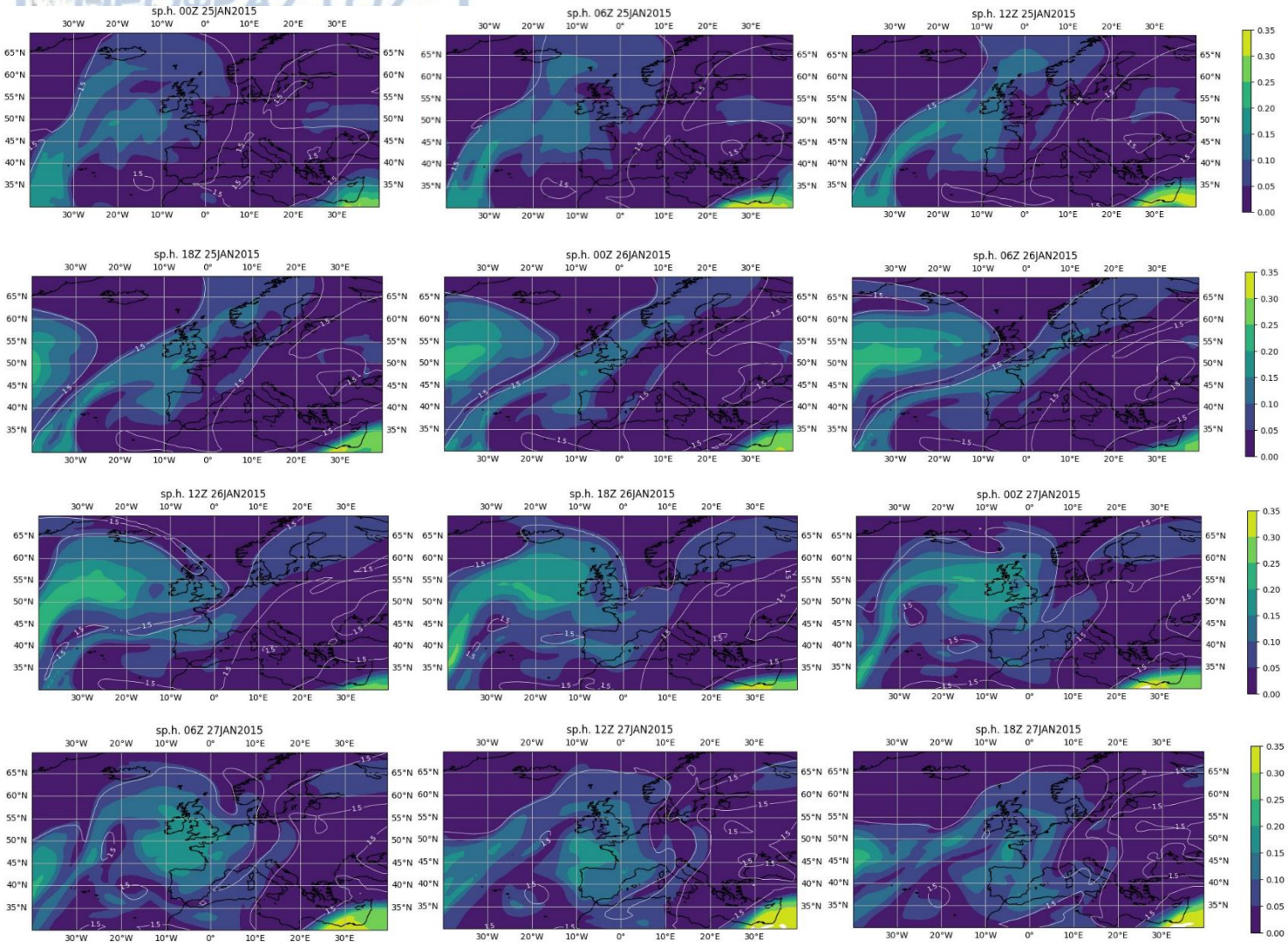

Figure 3.7: Specific humidity (color shaded in kg of dry air) and Potential Vorticity (white contours in pvu) at 300 hPa, during the period from 00:00 Z on 25 January 2015 to 18:00 Z on 27 January 2015 (6 h interval).

Meteorological satellites constitute a significant tool for analyzing a synoptic situation. The water vapor channel 6.2μm correspond to 300 to 500hpa. It is used for identifying jet streams, dry stratospheric intrusion and estimating upper level moisture. The water vapor satellite images (fig. 3.8) at 18:00 UTC on 25 January 2015, b) at 00:00 UTC on 26 January 2015 and c) at 06:00 UTC on 26 January 2015, presented in Fig. 3.8 and 3.9 respectively, display a “hook-shaped” streamer of dry air with dark color. The "hook-shaped" streamer extends over Hohenpeissenberg. Therefore, the water vapor content in channel 6.2 at the 300hPa level is observed. Water vapor images are valuable for the

dynamic analysis of the upper atmosphere. The dynamic interpretation of water vapor images occurs at humidity boundaries, in regions with strong contrasts between shades of gray. At these humidity boundaries, the jet stream is identified, where wind speeds exceeding 50m/s are observed at the 300hPa isobaric level. Additionally, dry stratospheric intrusion is identified by darker shades of gray, indicating the low altitude of the dynamic tropopause. In the figure 3.8, the potential vorticity with a 1.5PVU is located precisely at the humidity boundary, on the axis of the jet stream, where descent motions occur at the entrance of the trough over Hohenpeissenberg. The lighter shades of gray correspond to higher altitudes of the dynamic tropopause, as evident in western Germany. In this channel, only the highest white, cold clouds are observed, as only radiation from the upper layers of the troposphere reaches the satellite, because satellite images result from the recorded emission of radiant energy towards the satellite. In Figure 3.9, satellite images are presented, not in the infrared but in the visible spectrum. Clouds are visible and it serves as a surface pressure analysis map. Consequently, the atmospheric high pressure system is depicted. In the visible spectrum, light shades of gray or white correspond to areas with high reflectivity, while dark shades of gray represent regions with low reflectivity.

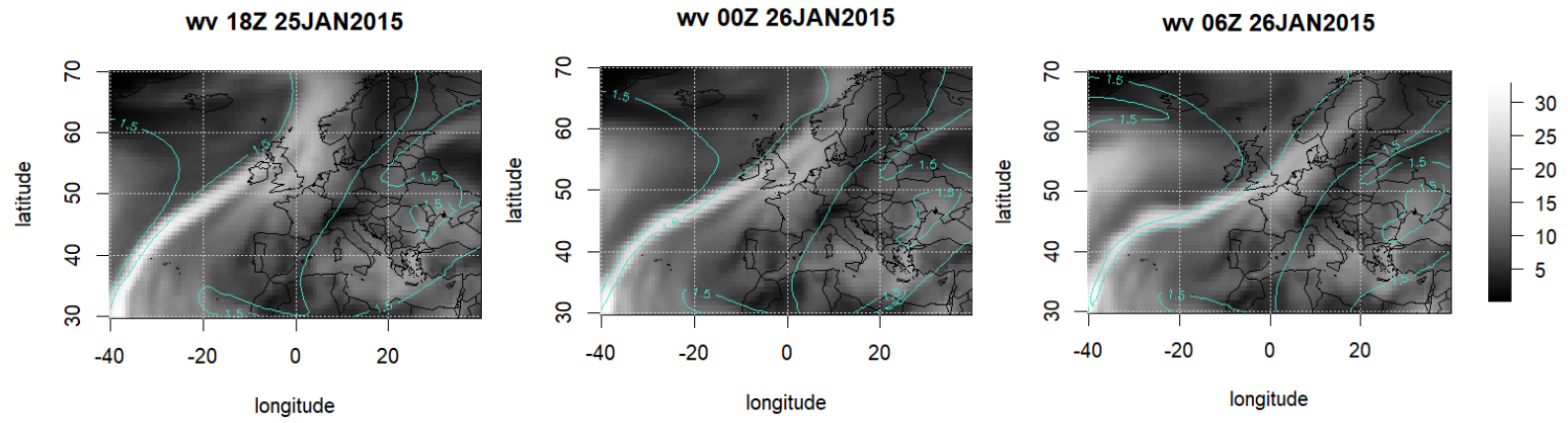

a) b) c)

Figure 3.8: Water vapor (6.2 μm; 300hpa) satellite images. The tirquoise contours represent the potential vorticity at 1.5PVU during the period from 18Z on 25 January 2015 to 06Z on 26 January 2015 (6 h interval).

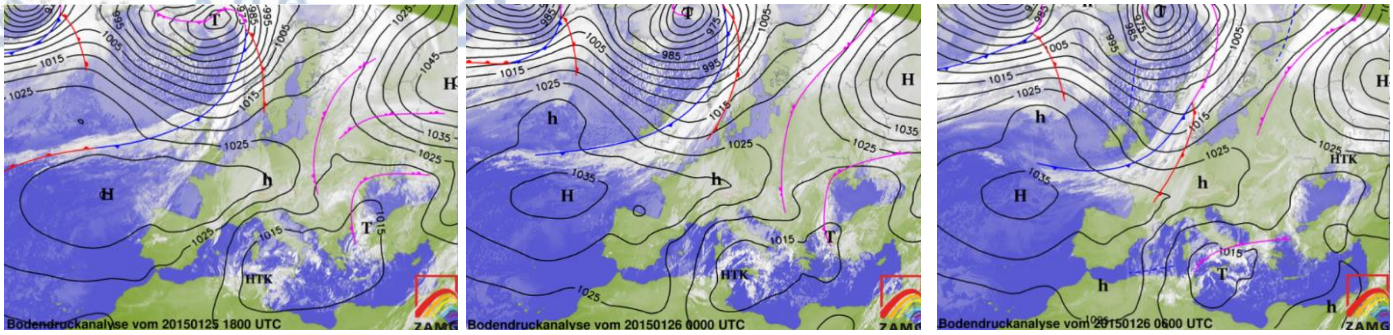

a) b) c)

Figure 3.9: Satellite images with synoptic surface pressure analysis. The black lines represent the isobars and the red, pink, blue lines indicates the fronts a) at 18:00 UTC on 25 January 2015, b) at 00:00 UTC on 26 January 2015, c) at 06:00 UTC on 26 January 2015. Satellite images (source: GeoSphereAustria: https://www.zamg.ac.at/cms/de/wetter/wetterkarte?tag=26&monat=01&jahr=2015&utc=06) (last access: 4 December 2023).

The synoptic situation is represented in figure 3.10, illustrating the horizontal velocity (x, y) and the geopotential height field at the 300 hPa isobaric surface with a temporal evolution every 6 hours for the period from 25 January to 27 January 2015. Observing the geopotential height field, a distinct upper-level ridge is clearly visible from 00Z on 25 January over the eastern Atlantic, which moves towards Eastern Europe in conjunction with a trough over Eastern and Central Europe. The jet stream exhibits its highest values on the western side of the upper-level trough with maximum wind speeds mainly exceeding 60 m/s during 00Z-12Z on 25 January. On 26 January at 00Z, the western side of the jet stream is directly over the study area with wind speed exceeding 40 m/s. Essentially, in the area with the maximum wind speeds, the so-called jet streak, intense updrafts and downdrafts occur due to the creation of an ageostrophic flow. This synoptic situation favors the formation of a tropopause fold along the jet stream and consequently the transport of flow from the stratosphere to the troposphere. This formation indicates the transport of cold air masses towards Central Europe and Southern Europe. On 27 January at 00Z, there is a southeastward movement of the geopotential heights and weakening of the jet stream.

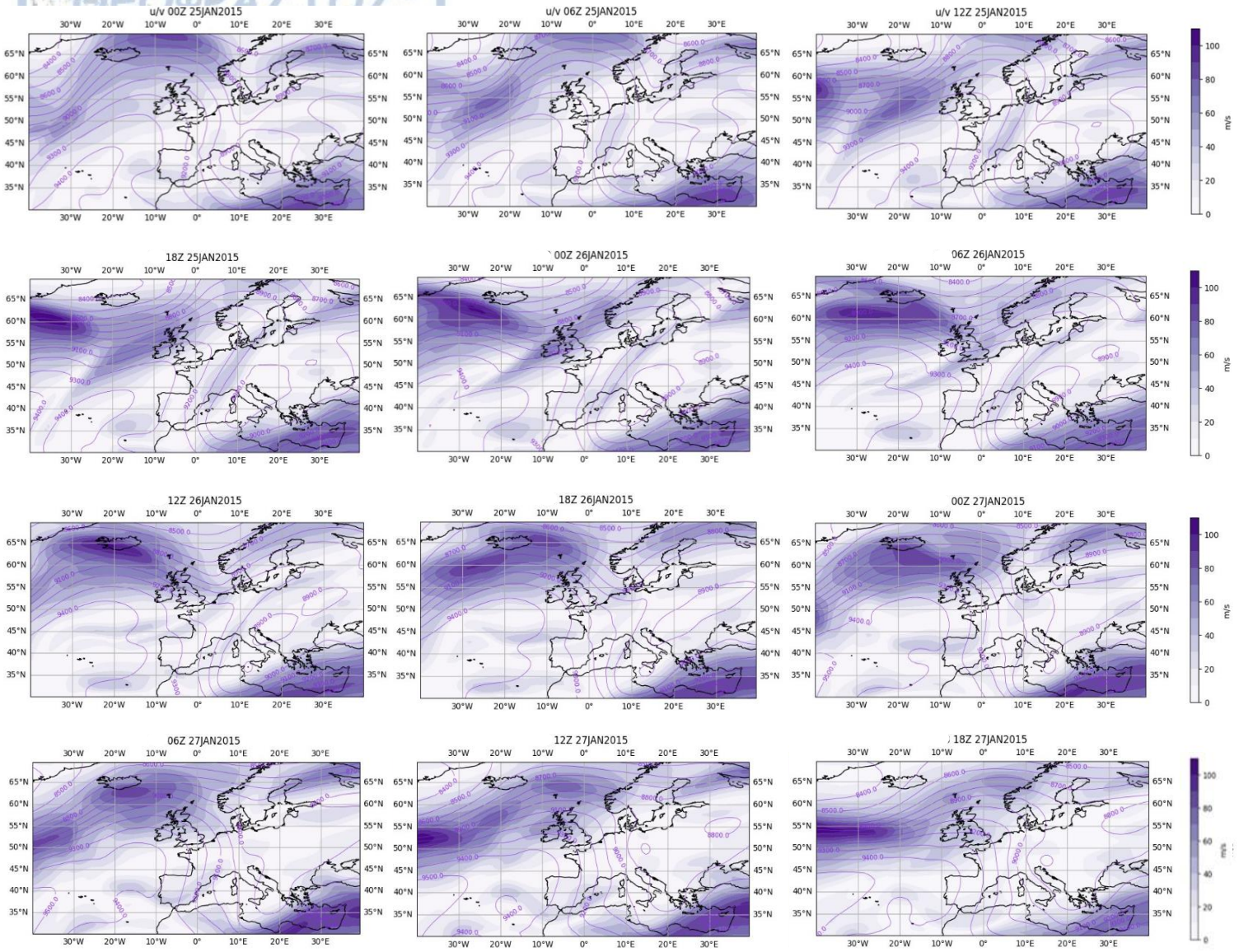

Figure 3.10: Wind speed (color shaded in m s^{-1}) and geopotential height (white contours in gpm) at 300 hPa, during the period from 00Z on 25 January 2015 to 18Z on 27 January 2015 (6 h interval).

In contrast to Figure 3.10, which depicts the wind magnitude as the speed of the wind using the components u and v, Figure 3.11 represents wind velocity, which refers to the vector quantity including both speed and direction. Comparatively, on 25 January at 18Z, Figure 3.11 shows high wind speed values averaging 45 m/s over Germany on the right side of the jet stream. As the jet stream moves on 26 January at 06Z, it is observed above Hohenpeißenberg with wind speed values exceeding 40 m/s.

a)

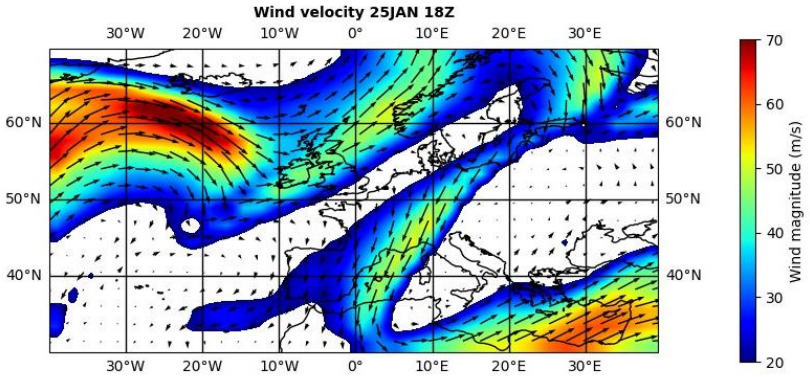

b1)

b2)

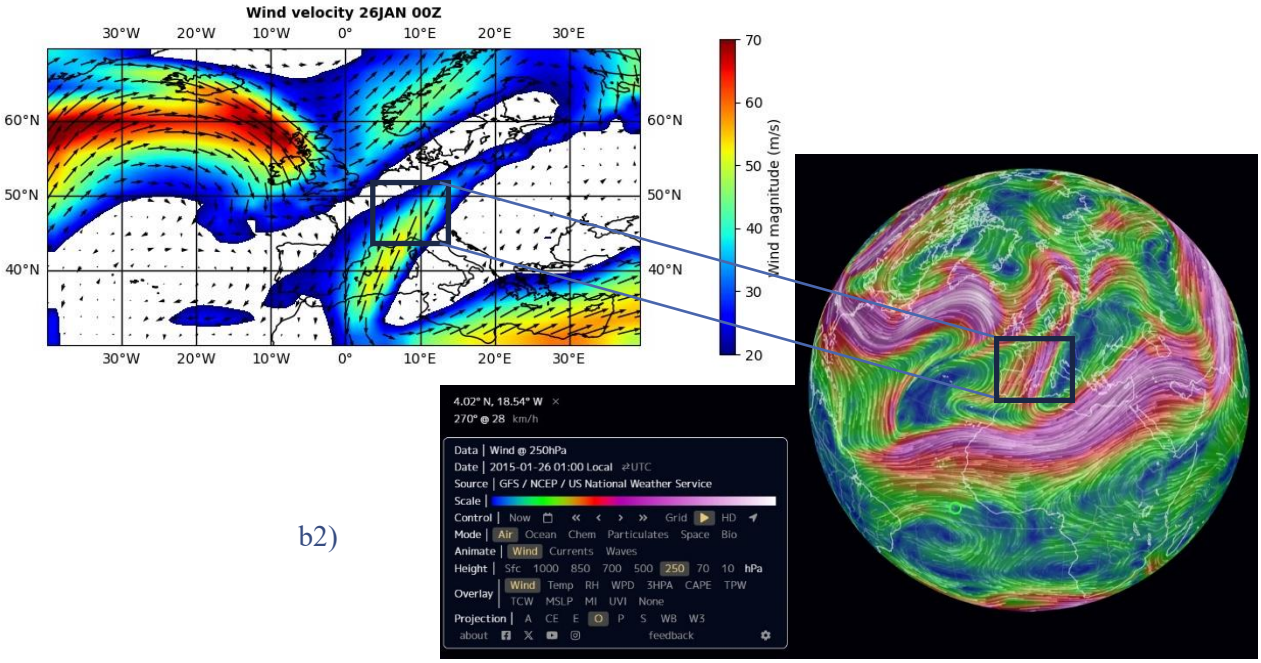

c)

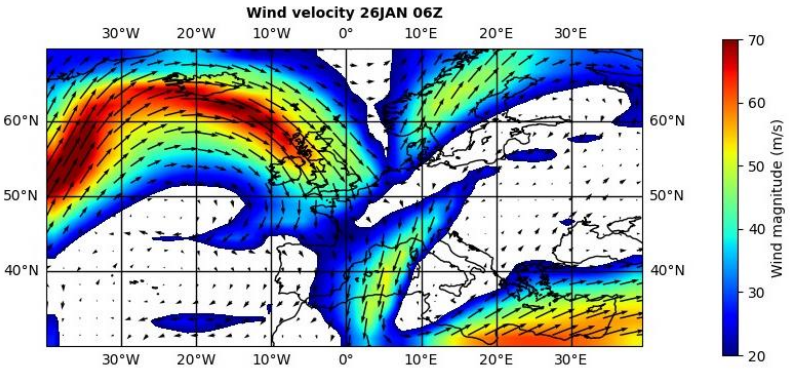

Figure 3.11: Wind velocity (color shaded in m s^{-1}) at 300 hPa, a) at 18Z 25 January 2015, b) at 00Z 26 January 2015, c) at 06Z 26 January 2015 (b2-source: https://earth.nullschool.net/).

3.4 Cross section synoptic analysis

The vertical distribution of relative humidity is depicted by the vertical cross-section of pressure-latitude (fig.3.12) at a specific longitude of 11E for relative humidity over Hohenpeissenberg (47.48N, 11E). On 26 January at 00 UTC (fig.3.12b) above the dynamic tropopause PV=2pvu, below 500hPa, low relative humidity percentages below 20% prevail, in the region where ozone concentrations are at high levels and the potential vorticity takes values greater than 2pvu. This occurs because stratospheric air contains small percentages of relative humidity, penetrating into the troposphere through the tropopause fold. Meanwhile, below the 500hPa isobaric surface down to the lower troposphere, relative humidity percentages are higher, approaching values above 80% near the surface. On 26 January at 00 UTC, at the latitude of 48N, encompassing the study area, the so-called “hook shaped” with humidity percentages below 25% is observed to penetrate up to the 500hPa isobaric level. The figures for 25 and 27 January at 00Z are also presented, where no stratospheric intrusion is observed at the latitude 48N, highlighting the contrast between them.

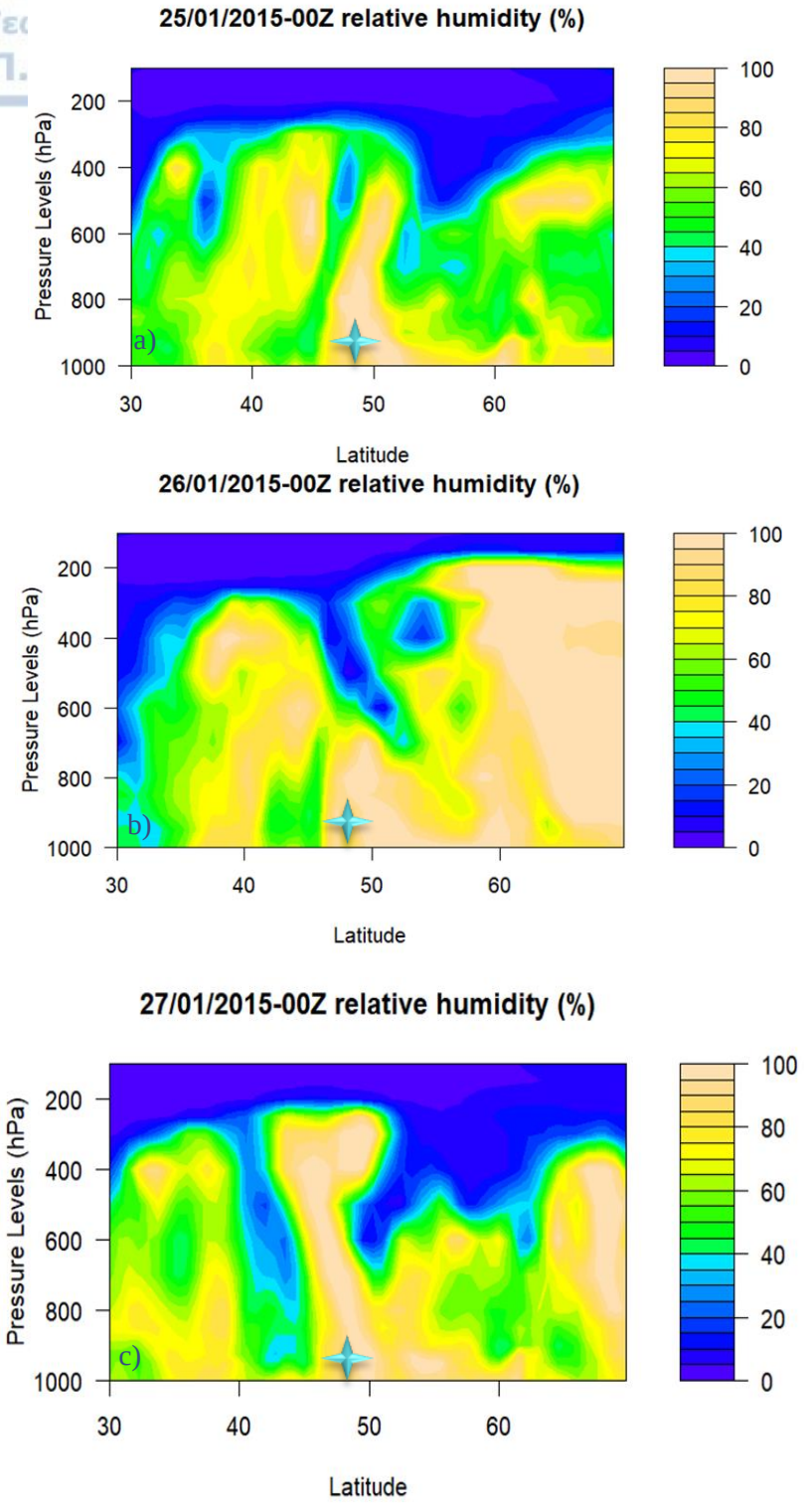

Figure 3.12: Latitude-Pressure vertical cross section at the longitude of Hohenpeissenberg (11.0° E) of relative humidity RH (shadings in %) a) at 00:00Z 25 January 2015, b) at 00:00Z 26 January 2015, c) at 00:00Z 27 January 2015. The asterisk indicates the latitude of Hohenpeissenberg (47.48° N).

The vertical distribution of ozone concentration is represented by the vertical cross-section of pressure - latitude (fig. 3.13) at a specific longitude of 11E for ozone over Hohenpeissenberg (47.48N, 11E) on 26 January at 00 UTC. Specifically, the color scale represents ozone concentration values, while red contours represent potential vorticity. On 25 January (fig.3.13a), no distinct stratospheric air intrusion has yet been formed. However, on 26 January at 00 UTC (fig.3.13b), an impressive intrusion of stratospheric air rich in ozone is observed in the lower free troposphere over Hohenpeissenberg at the latitude of 47.48N. The dynamic tropopause with PV=2pvu reaches the 500 hPa isobaric level. Therefore, stratospheric air rich in ozone has penetrated down to the 500 hPa isobaric surface, with ozone values exceeding 90 ppb and potential vorticity values equal to 2pvu. As the stratospheric air penetrates into the lower troposphere, ozone concentration decreases. At the 600 hPa isobaric level, ozone values approach 70 ppb, while ozone values approach 50 ppb up to the 900 hPa isobaric level, very close to the surface. On 27 January at 00 UTC (fig.3.13c), a clear eastward movement is observed.

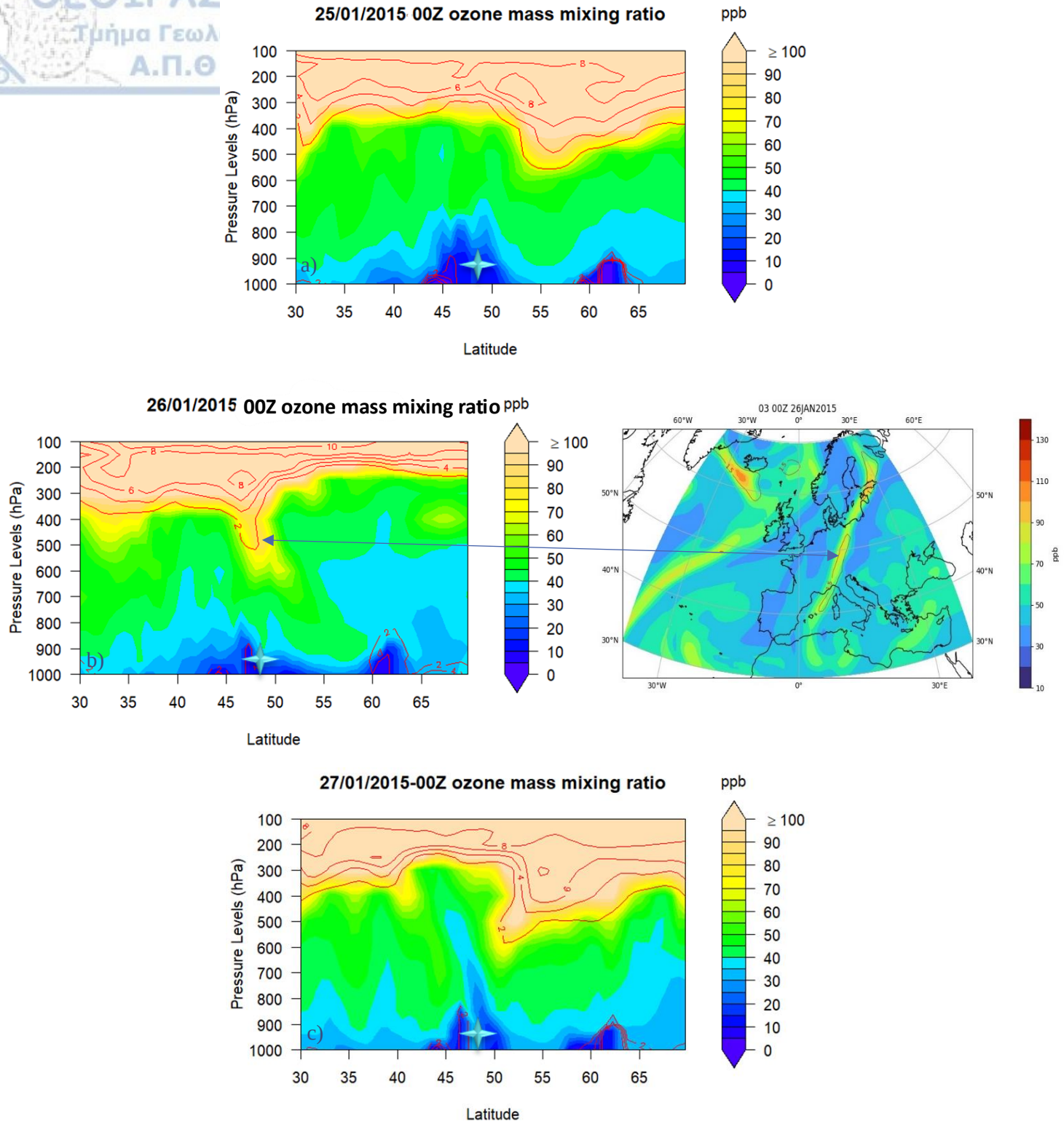

Figure 3.13: Latitude-Pressure vertical cross section at the longitude of Hohenpeissenberg (11.0 ° E) of ozone mass mixing ratio (shadings in ppb) a) at 00Z 25 January 2015, b) at 00Z 26 January 2015, c) at 00Z 27 January 2015. The red solid line indicates the contour of dynamical tropopause equal to 2 pvu, while the asterisk indicates the latitude of Hohenpeissenberg (47.48 ° N). Latitude-longitude at 500 hpa at 00Z 26 January 2015.

The vertical distribution of potential vorticity is represented according to the vertical cross-section of pressure-latitude (fig.3.14) at a specific longitude of 11E over Hohenpeissenberg (47.48N, 11E). The color scale depicts the potential vorticity and the contours illustrate the potential vorticity isosurface. This outlines the evolution of the tropopause fold. Thus, a high potential vorticity tongue begins to form on 26 January (fig.3.14b) with the tropopause reaching potential vorticity values equal to 2pvu, the so-called dynamic tropopause. This feature is clearly observed to have penetrated into the troposphere up to the 500hPa isobaric level on 26 January at 00 UTC, precisely over Hohenpeissenberg. Subsequently, a shift eastwards is observed on 27 January (fig.3.14c). Dry stratospheric air penetrates through this fold and approaches the lower troposphere, influencing the surface. Within the range of 0.5 to 1.5pvu, mixing of high potential vorticity stratospheric air (above 2pvu) with tropospheric air occurs.

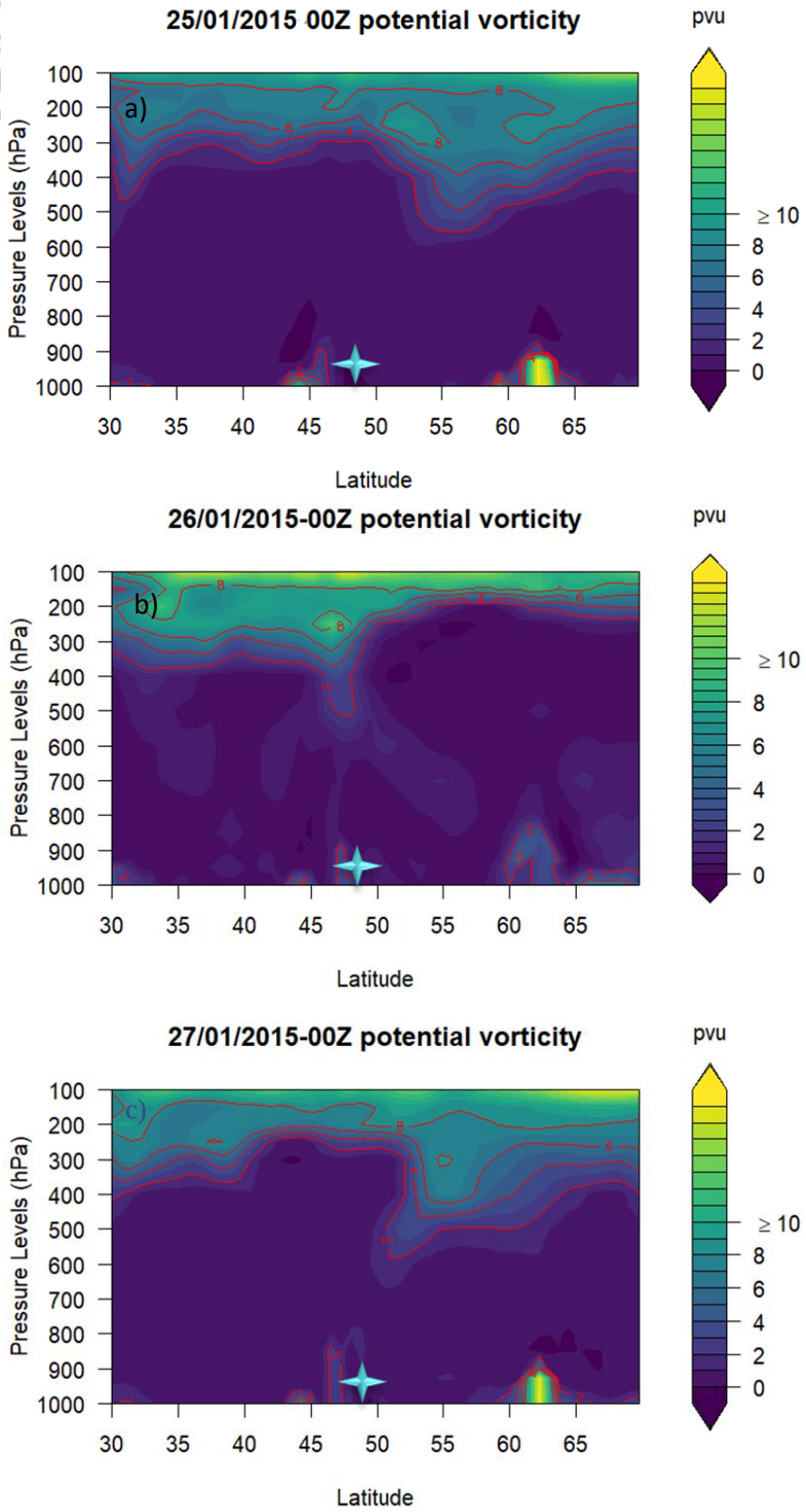

Figure 3.14: Latitude-Pressure vertical cross section at the longitude of Hohenpeissenberg (11.0 ° E) of potential vorticity PV (shadings in pvu) a) at 00Z 25 January 2015, b) at 00Z 26 January 2015, c) at 00Z 27 January 2015. The red solid line indicates the contour of dynamical tropopause equal to 2PVU, while the asterisk indicates the latitude of Hohenpeissenberg (47.48 ° N).

The vertical velocity (ω) is depicted according to the vertical cross-section of pressure-latitude (fig.3.15) at a specific longitude of 11E over Hohenpeissenberg (47.48N, 11E). On 25 January (fig.3.15a), positive values of vertical velocity are not yet observed at this particular longitude. However, the vertical distribution of vertical velocity (ω) is identified, indicating the transport of stratospheric air into the troposphere on 26 January at 00 UTC (fig.3.15b), where the dynamic tropopause has reached up to the 500hPa isobaric level. Under the tropopause fold, downward motions occur due to the positive values of vertical velocity (ω). Under the tropopause fold, vertical velocity takes positive values and at the isobaric level of 500 hPa, vertical velocity reaches its maximum positive value, indicating the strongest downward motions of the air towards the surface. Conversely, above the point of zero divergence, at lower isobaric levels, the vertical velocity begins to decrease. Specifically, over Hohenpeissenberg at the latitude of 47.48N, vertical velocity (ω) takes values greater than 0.1 Pa/s. It is clearly evident that to the right and left of the tropopause fold, the vertical velocity takes negative values, resulting in upward motions. Thus, it is correctly demonstrated that dry convection prevails ahead of the tropopause fold due to convergence at the surface and divergence in the upper troposphere. Downward motions signify convergence in the upper troposphere, near the tropopause fold and divergence in the lower troposphere. On 27 January (fig.3.15c), a movement towards the north of the potential vorticity is observed.

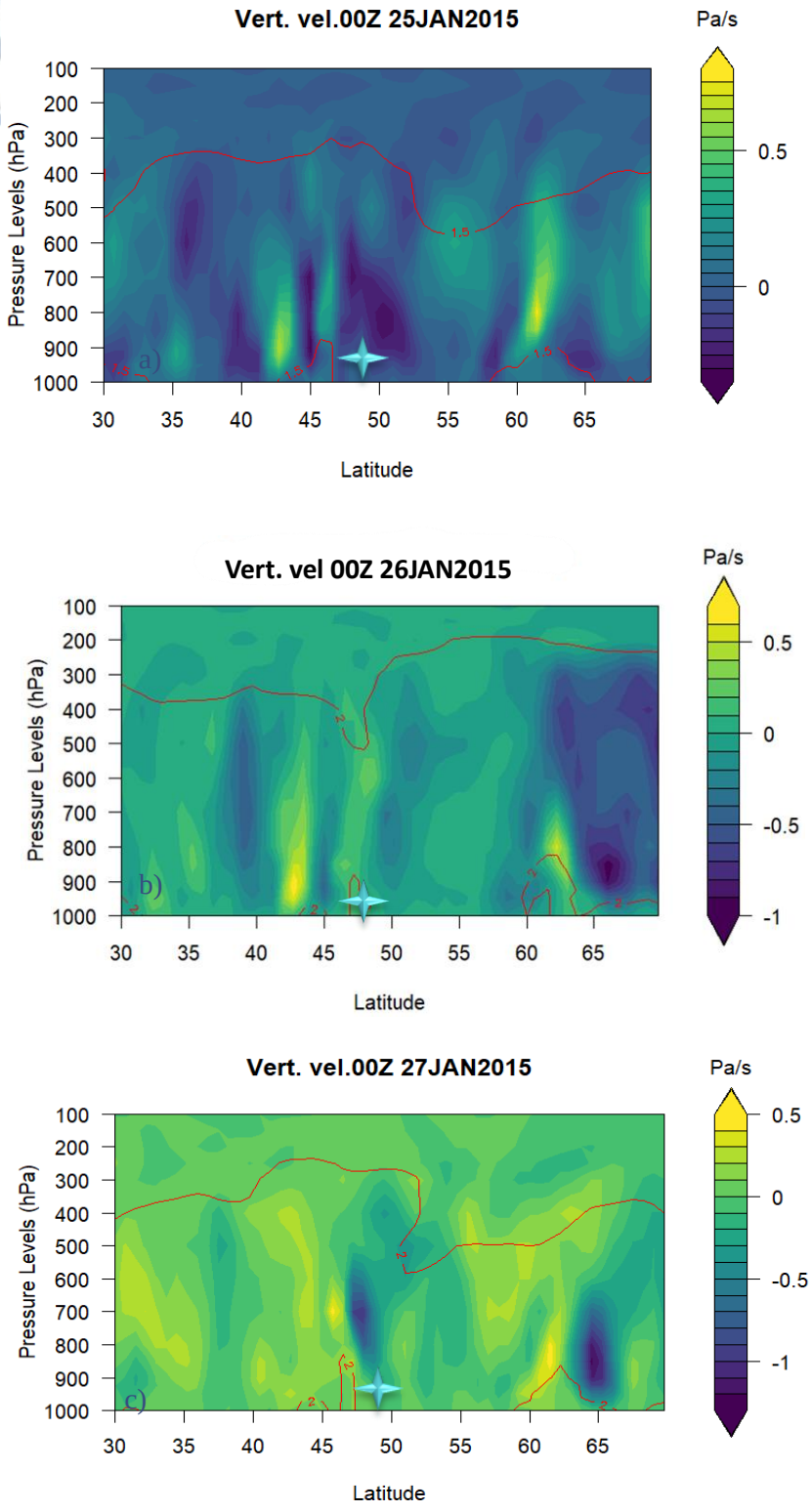

Figure 3.15: Latitude-Pressure vertical cross section at the longitude of Hohenpeissenberg (11.0° E) of vertical velocity (shadings in Pa/s) a) at 00Z 25 January 2015, b) at 00Z 26 January 2015, c) at 00Z 27 January 2015. The red solid line indicates the contour of dynamical tropopause (a) at 1.5pvu and (b, c) at 2 pvu, while the asterisk indicates the latitude of Hohenpeissenberg (47.48°N).

The ozone measurements for the Hohenpeissenberg station (47.48N, 11E) include ozonesonde data for the time period of 23, 26 and 28 January at 06 UTC. The diagram (fig.3.16) presents the vertical profile of observed ozone from WOUDC and ozone from the CAMS, indicating the discrepancies between the observed and modeled concentrations. It is acknowledged that models always exhibit errors and uncertainties, hence the divergences and underestimations or overestimations. On the specific dates of 23, 26 and 28 January according to the diagrams, there is a deviation between the observed ozone and ozone from the CAMS concentrations, mainly in the tropopause. The tropopause is an area where transport processes dominate. Therefore, it is observed that the CAMS underestimates the observations. However, during the event of the dry stratospheric intrusion on 26 January (fig.3.16b), the largest deviation is observed at the 500hPa isobaric level, indicating that the CAMS significantly underestimates the observations in the dynamic tropopause. Consequently, the ozone appears weaker than observed in reality. In general, the CAMS shows good agreement with observations. However, it exhibits errors when abrupt changes occur in the vertical profile of ozone concentrations. Possible causes of model error appear to be the coarse resolution and the fact that models do not account for all the physical processes present in the climate system. The discrepancies between the models and observations are attributed to multiple factors such as inadequate simulation of ozone precursor emissions due to uncertainties in NO_X and BVOCs and inaccurate parameterization. Additionally, due to the comparison of point data from observations at a specific station with a coarser resolution of the model, such as in the present case with CAMS having a resolution of 80 km, it results in differences in the spatial resolution of the models (Griffiths et al., 2021). In this particular case, there is also an overestimation of the model compared to observations due to running with data assimilation, which introduces biases in the middle and upper troposphere. Whereas without data assimilation, it exhibits underestimation (Akritidis et al., 2022). Furthermore, due to the coarse resolution of the model, there is an overproduction of ozone, whereas with finer vertical resolution, the ozone simulation is more improved (Turnock et al., 2020; Neal et al., 2017).

Clear observation is evident in Figure 3.16b, similar to Figure 3.1**,** indicating that at the 300 hPa isobaric level, ozone values approach 50 ppb according to the reanalyses from the ozone CAMS. Very good agreement is demonstrated with ozone observations, where at the same 300 hPa isobaric level, ozone values approach 100 ppb. At the 500

hPa isobaric level, ozone approaches a value of 110 ppb according to observations, while according to CAMS, it approaches a value of 50 ppb. However, the difference is observed in ozone concentrations at the 500 hPa isobaric level, but on 26 January at 06Z, shortly after stratospheric penetration. Therefore, according to observations, on 23 January, ozone takes a value of 50 ppb, while on 26 January, it increases abruptly to a value of 110 ppb. On 27 January, it takes a value of 60 ppb because the phenomenon has already started to move away from Hohenpeissenberg. On 23 and 28 January, a very good agreement is observed between ozone observations and ozone values from CAMS.

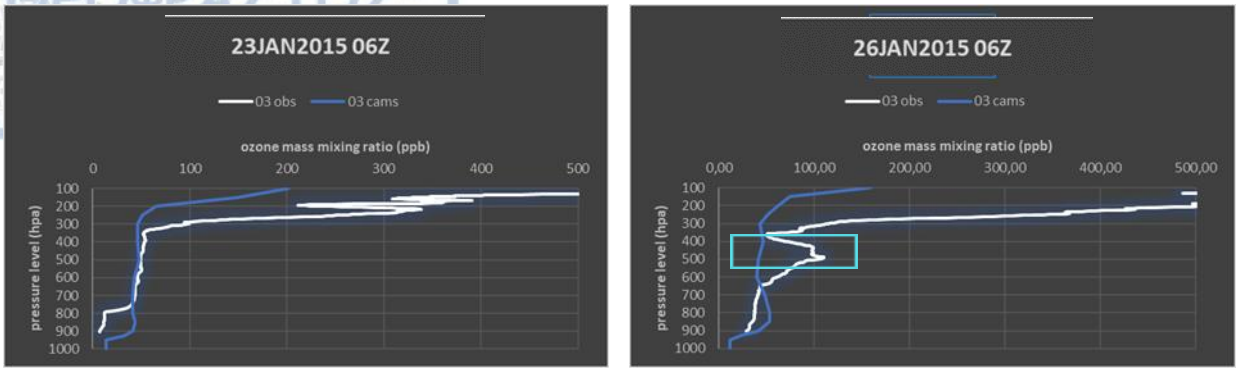

a)

b)

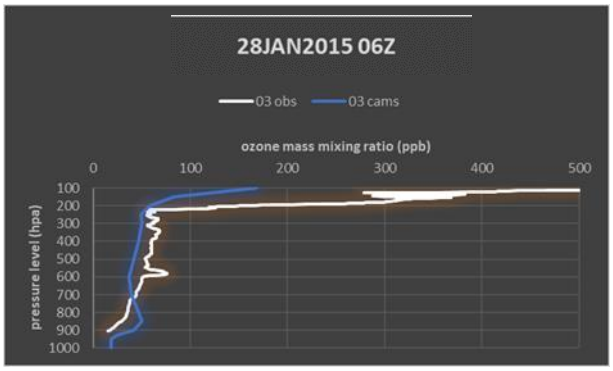

c)

Figure 3.16: Profile measurements of observational ozone (ppb) based on ozonesonde launches (white line) and ozone based on CAMS Model (blue line) a) at 06 UTC on 23 January 2015, b) at 06 UTC on 26 January 2015, c) at 06 UTC on 28 January 2015 over Hohenpeissenberg.

The ozonesonde for the Hohenpeissenberg station (47.48N, 11E) encompass radio-sonde data for the temporal duration of 23, 26 and 28 January at 06 UTC, providing the vertical distribution of ozone and relative humidity (fig.3.17), revealing the dry stratospheric intrusion. The diagram illustrates the vertical profile of ozone and relative humidity based on observations at the Hohenpeissenberg station, where the stratospheric air intrusion is clearly discernible deep into the troposphere. On 23 January at 06 UTC (fig.3.17a) at the 300hPa isobaric level, ozone values exceed 100ppb, while relative humidity at the same isobaric level drops below 40%. The dry intrusion is further confirmed by the vertical profile on 26 January (fig.3.17b) at the 500hPa isobaric level, where a sudden increase in ozone concentration occurs with values exceeding 100 ppb and relative humidity values lower than 10%. This substantiates the so-called stratospheric intrusion. On 28 January (fig.3.17c), a relative change is observed at the 600hPa isobaric level, with ozone values greater than 90ppb,

while relative humidity takes values lower than 10%. These low relative humidity percentages indicate the presence of very dry air entering from the stratosphere into the troposphere.

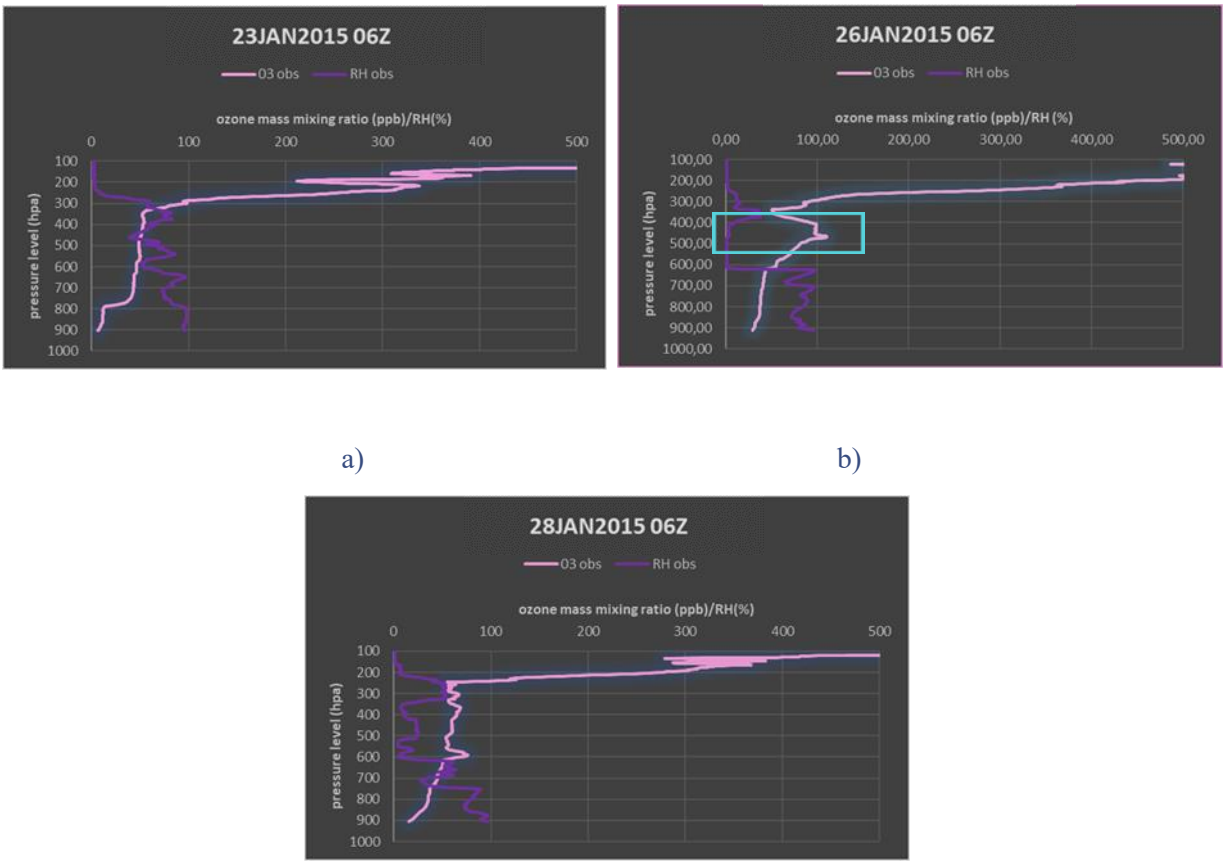

a) b)

c)

Figure 3.17: Profile measurements of observational ozone (ppb) based on ozonesonde launches (pink line) and observational relative humidity (%) RH (purple line) a) at 06:00 UTC on 23 January 2015, b) at 06:00 UTC on 26 January 2015, c) at 06:00 UTC on 28 January 2015 over Hohenpeissenberg.

B. Analysis of climate change on tropospheric and stratospheric ozone

3.1 Future projected changes on stratospheric ozone tracer

In Figure 3.18, the first column illustrates the future changes of O_3s according to the ssp370SST experiment for the periods 2020-2039, 2040-2059 and 2080-2099. Similarly, the second column depicts the future changes of O_3s according to the ssp370pdSST simulation for the corresponding time period. The comparison between the two simulations during the same time period and across different temporal phases does not exhibit significant variation. Specifically, in the ssp370SST experiment, it is demonstrated that emissions, in conjunction with climate change, impact stratospheric ozone. While the ssp370pdSST experiment refers to how emissions alone affect the quantity of ozone originating from the stratosphere (O_3s). In both experiments, it is observed that anthropogenic emissions, combined with the contribution of climate change, increase ozone levels mainly towards the end of the 21st century due to transport. It is noted that from 2020 to 2039, the subtropical regions of the northern hemisphere exhibit the highest ozone concentrations, up to 10-18 ppb, originating from the stratosphere. Meanwhile, in the southern hemisphere, from 2050 onwards, there is an increase in O_3s by 10 ppb, confirmed by the presence of jet streams in subtropical regions and thus the formation of tropopause folds favoring STT transport. Furthermore, during the time period from 2080 to 2099, higher ozone values originating from the stratosphere in the Arctic up to 8 ppb are observed, confirmed by existing literature. Additionally, during this time frame, elevated O3s levels in Asia are noted due to increased emissions, up to 20 ppb. In both simulations, from 2020 to 2099, high ozone concentrations up to 18 ppb originating from the stratosphere are observed in the Atlantic Ocean, confirmed by the increased frequency of tropopause fold formations in this region, which favor transport. It is noteworthy that very low O_3s values prevail in tropical regions during all three time periods due to the absence of jet streams, thus preventing the formation of tropopause folds necessary for ozone transport.

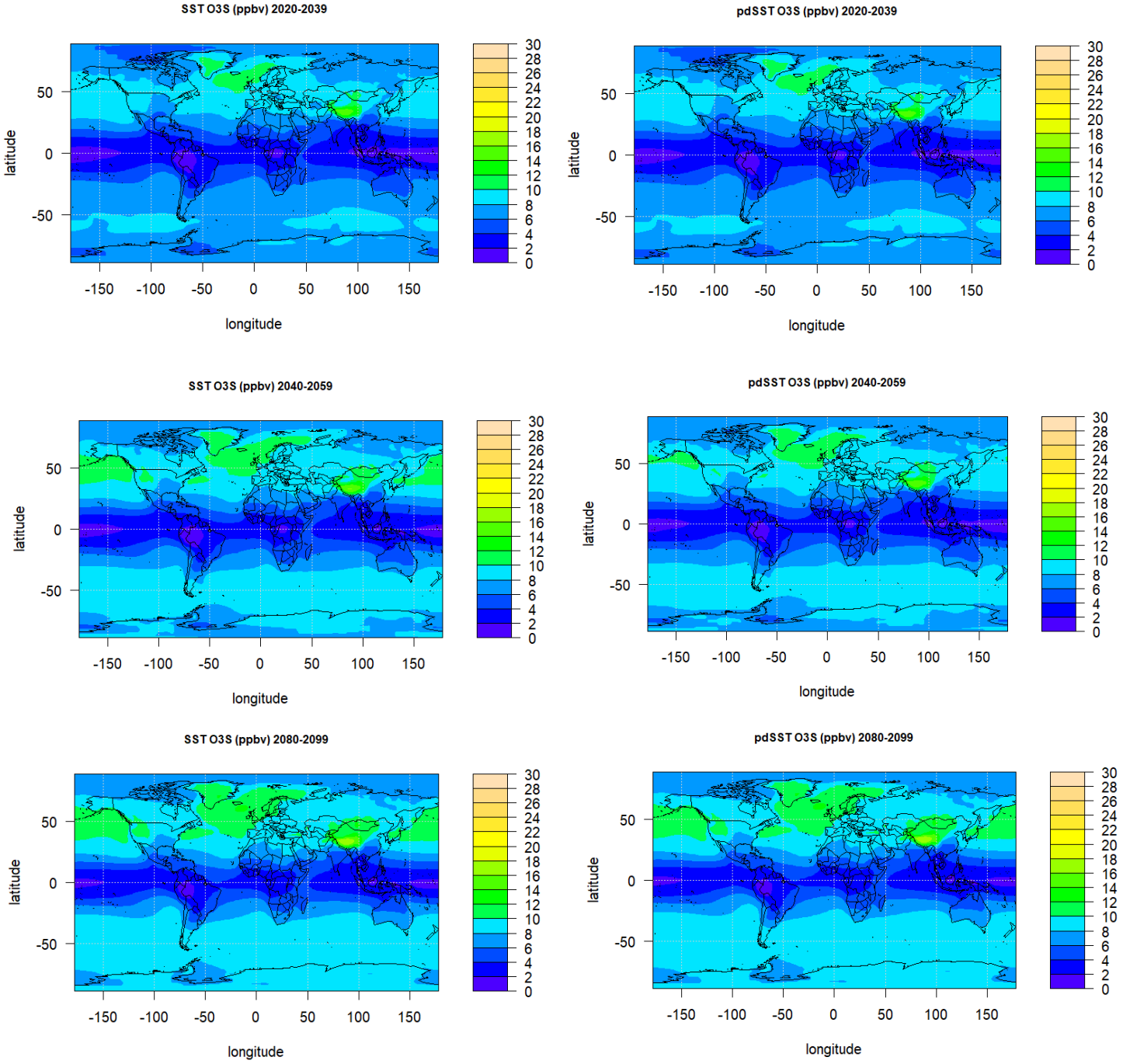

Figure 3.18: Ozone concentrations O_3s (shaded in ppbv) from CMIP6 model (EC-Earth3-AerChem) from two experiments a) ssp370SST and b) ssp370pdSST for the future period 2020-2039, 2040-2059,2080-2099, respectively.

In this particular case, simulations are conducted, according to the SSP3-7.0 scenario, to study the impact of climate change on the transport of ozone from the stratosphere to the troposphere (O_3s). Specifically, it assesses the extent to which this transport is enhanced by climate change during the 21st century, depending on temperature magnitude. The difference between the two experiments illustrates the effect of climate change on ozone transport from the stratosphere to the troposphere. Fundamentally, tropopause folds are favored in areas near jet streams, which occur in the subtropical regions of both the northern and southern hemispheres and vary in location based on the season. Therefore, in specific areas of the subtropical zone, tropopause folds occur, thus favoring the downward transport of ozone (O_3s). When there is an increased temperature gradient in the tropopause, indicating a significant difference, it intensifies the formation of tropopause folds, thereby enhancing this downward transport. Therefore, with a possible future increase in temperature, an enhancement of the tropopause fold is observed with the aim of enhancing STT transport. Consequently, it is logical that over time, namely until 2100, a greater increase in temperature is predicted, thus contributing to the increased vertical transport of stratospheric ozone towards the troposphere (O_3s). Tropopause folds will intensify more and more over time. More specifically, according to the figure 3.19 observed from 2080 to 2099, higher O_3s values, up to 2 units, are noted in subtropical regions due to the presence of jet streams and consequent tropopause folds in both the northern and southern hemispheres. Even higher values are observed in the Arctic region, up to 4 units, indicating the greater contribution of downward ozone transport from the stratosphere. The contribution of climate change, with its greater temperature increase, favors more intense tropopause fold and thus higher O_3s levels. This significant difference is reflected compared to the period from 2020 to 2039, where no significant temperature increase is observed to enhance the tropopause folds. There is a small increase of 1 unit in the Atlantic Ocean and the Arctic, therefore, there is no distinct increase in O_3s.

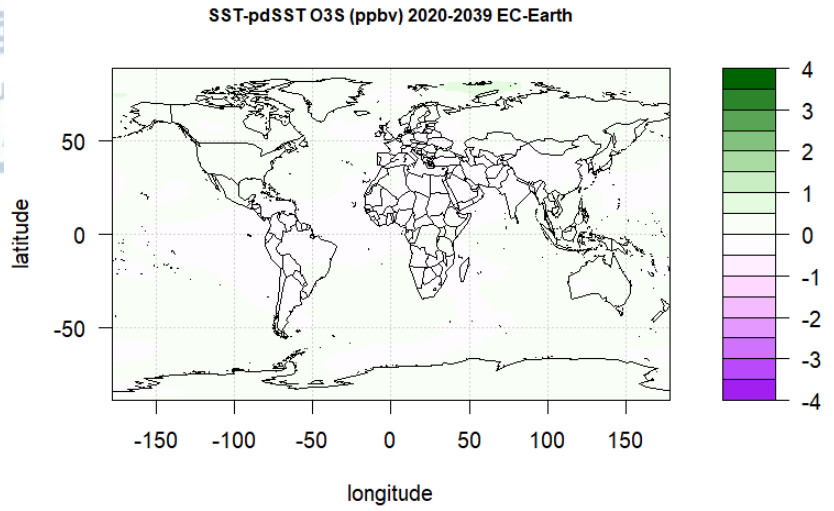

a)

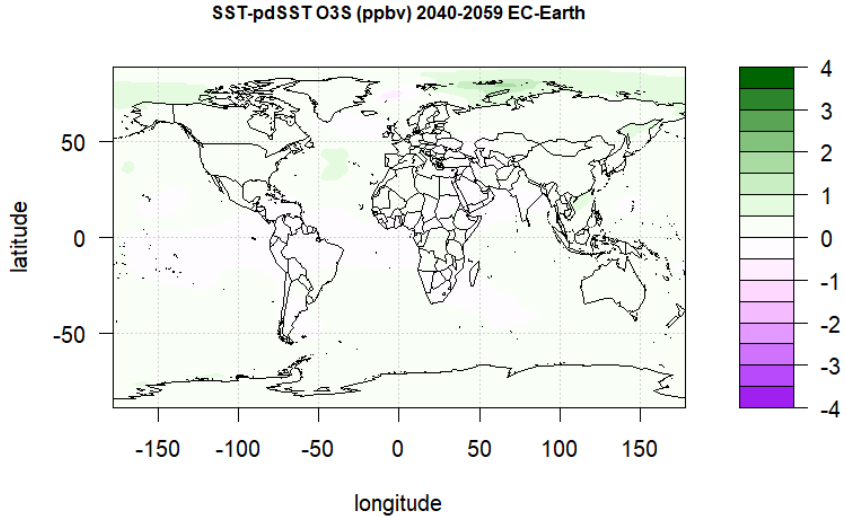

b)

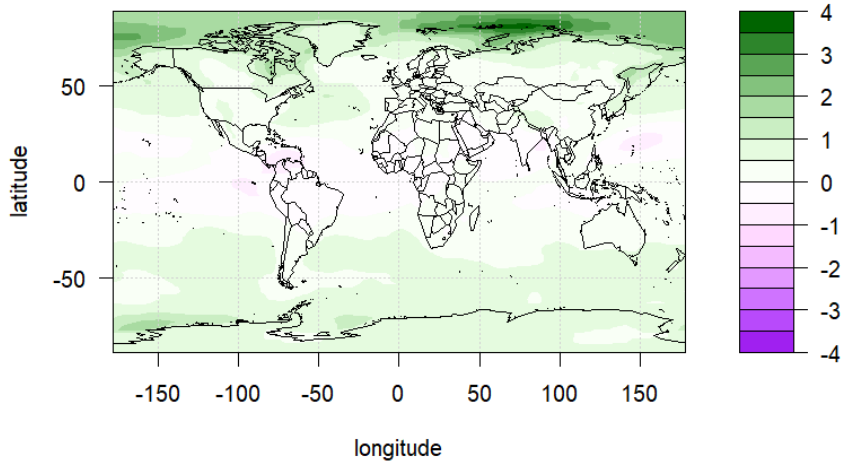

c)

Figure 3.19: Differences of ozone concentrations O_3s from CMIP6 model (EC-Earth3-AerChem) between the ssp370SST and ssp370pdSST experiments (shaded in ppbv) for the future period a) 2020-2039, b) 2040-2059, c) 2080-2099.

In figure 3.20, the vertical distribution of O_3s is observed according to simulations (a) ssp370SST and (b) ssp370pdSST during the upcoming future time periods. Higher ozone values up to 10 ppb are observed to approach and in some cases reach the surface level in the Northern Hemisphere, in comparison to the Southern Hemisphere, in both simulations across the three distinct time periods, respectively.

In the subtropical regions of both the northern and southern hemispheres, tropopause folds and jet streams occur, favoring the downward transport of ozone from the stratosphere to the troposphere, consequently leading to increased ozone concentrations. The most significant difference that can be addressed is that in the northern hemisphere's subtropical zone, ozone concentrations are higher due to the more intense circulation of the Brewer-Dobson Circulation (BDC), which interacts with Stratosphere-Troposphere Transport (STT) and favoring the formation of tropopause folds, thus enhancing ozone transport O_3s. Additionally, the lower O_3s values in the tropics are attributed to the absence of jet streams, making it difficult to form tropopause folds in the 0° to 30° latitude range.

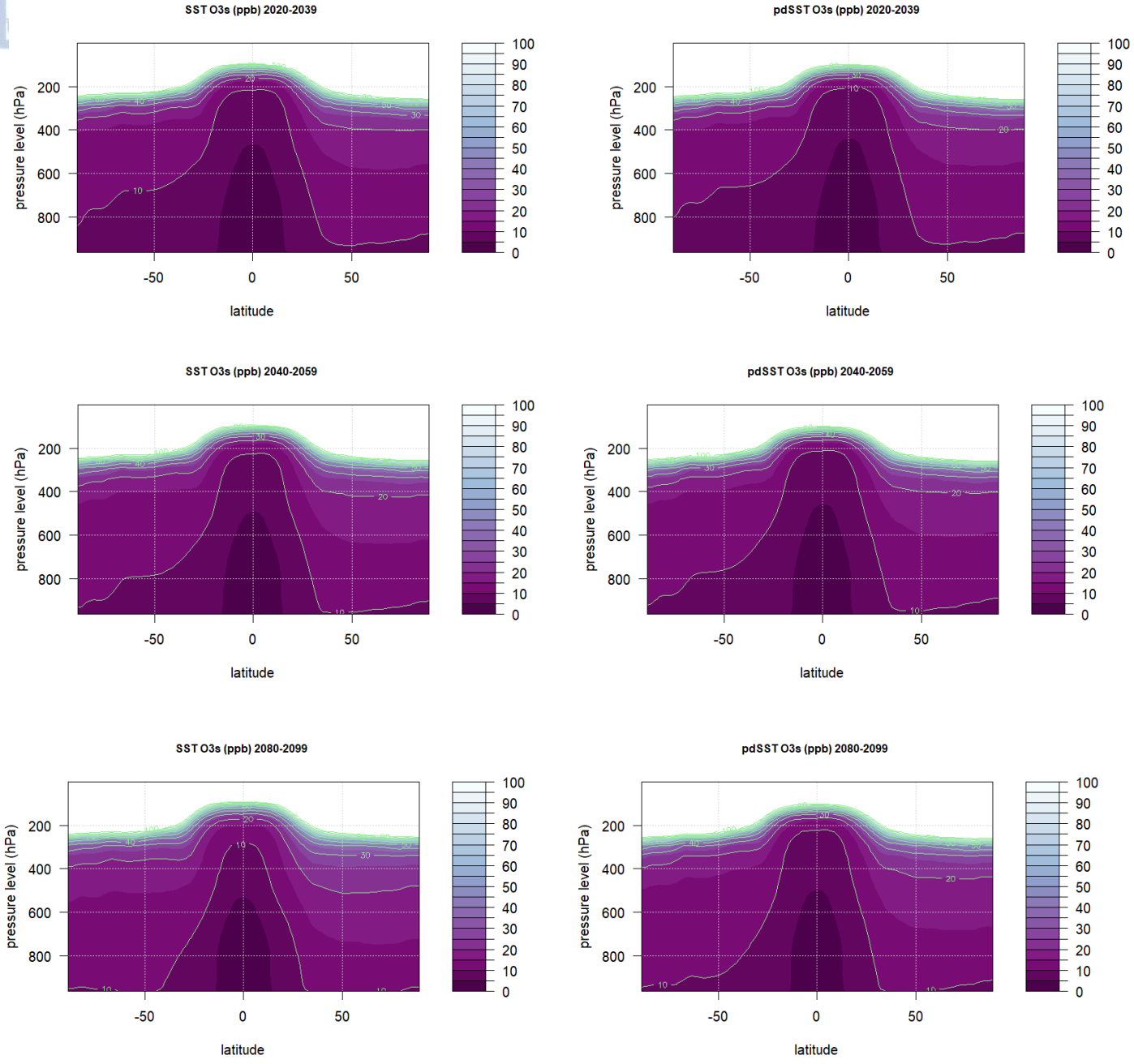

a) b)

Figure 3.20: Latitude-Pressure vertical cross section of ozone concentrations (shaded in ppbv) from CMIP6 model (EC-Earth3-AerChem) from two experiments a) ssp370SST and b) ssp370pdSST for the future period 2020-2039, 2040-2059, 2080-2099, respectively.

The following figure 3.21 illustrates the impact of climate change on the vertical transport of stratospheric ozone and, consequently, its effect on O_{3S} concentrations in the troposphere. Essentially the deviation of the O_{3S} values from the normal values is represented. It is observed that between 2020 and 2100, there is an increase in O_{3S} by 1 to 5 units mainly in the middle latitudes but also in the higher latitudes, in the upper troposphere. This phenomenon is due to the fact that tropopause folds occur in the subtropical regions near the jet streams at the isobaric level of 200 hPa during the summer months and at 300 hPa during the winter months. Specifically, climate change negatively affects O_{3S}, meaning that positive deviations above normal values prevail in these regions, as shown in Figure 3.21c, due to the more intense temperature increase during the period 2080-2099, the activity of these folds is intensified, which is why O_{3S} values are by 5 units higher in subtropical regions and by 2 units higher at higher latitudes. The strengthening of the Brewer-Dobson circulation (BDC), ultimately leading to the enhancement of tropopause fold and thus the increase in O_3s. Conversely, negative deviations below normal values, by -1 units, are observed in tropical regions during the period 2080-2099. This is because in the tropics the tropopause fold mechanism does not occur due to the absence of jet stream and so the O_{3S} values are below the normal values.

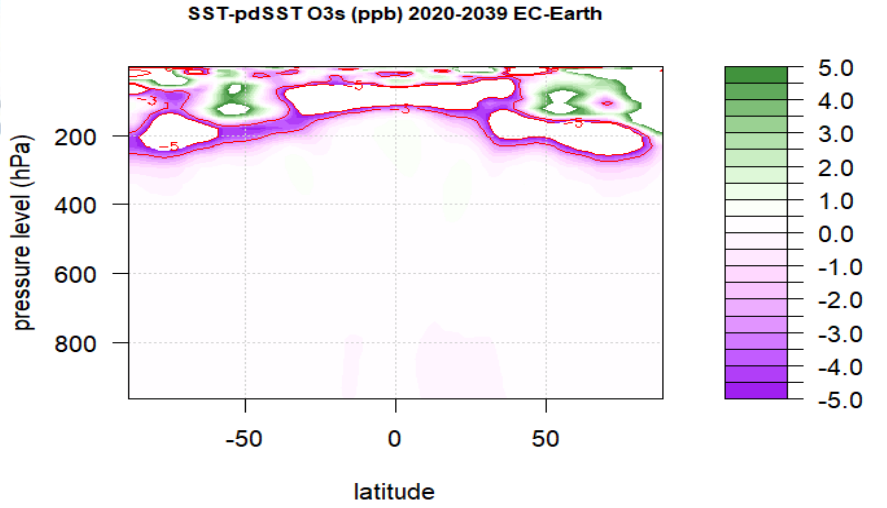

a)

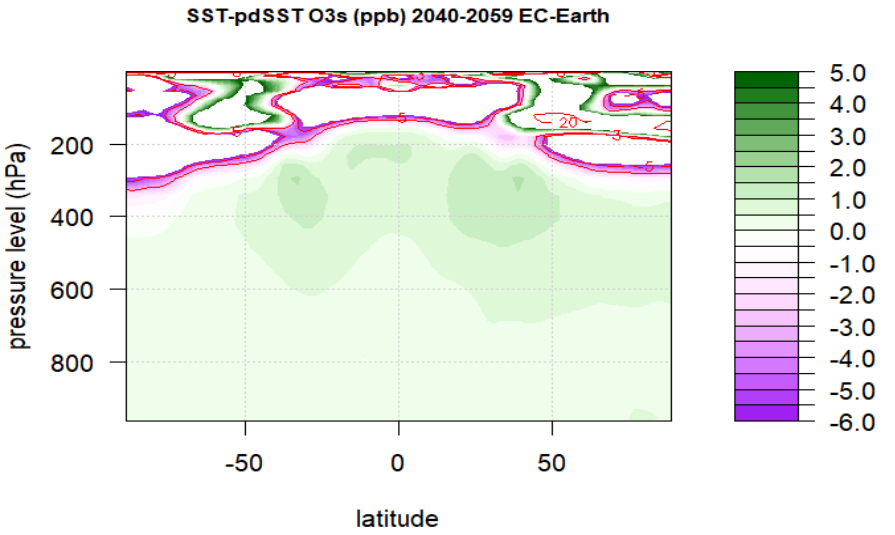

b)

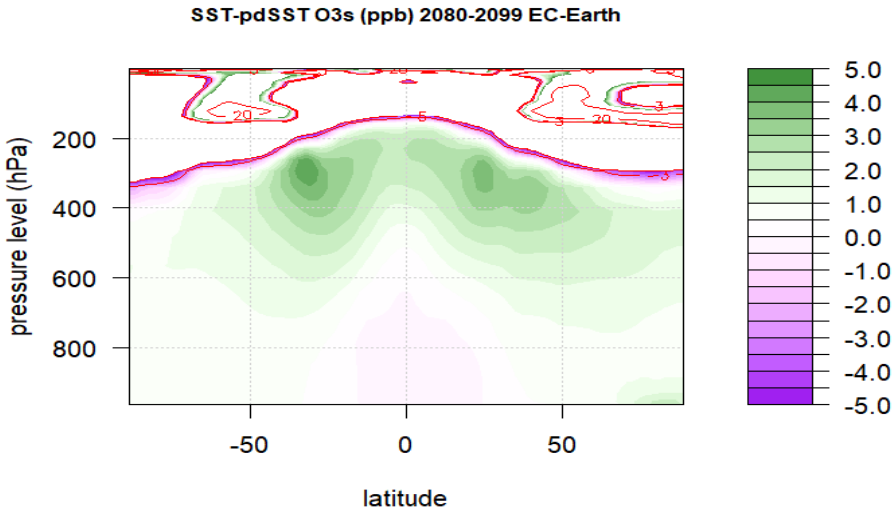

c)

Figure 3.21: Latitude-Pressure vertical cross section of differences of stratospheric ozone tracer (O3s) concentrations from CMIP6 model (EC-Earth3-AerChem) between the ssp370SST and ssp370pdSST experiments (shaded in ppbv) for the future period a) 2020-2039, b) 2040-2059, c) 2080-2099.

3.2 Future projected changes on tropospheric ozone

The future projections of tropospheric ozone were investigated using the CMIP6 model (EC-Earth3-AerChem), specifically simulations from two different experiments: ssp370SST and ssp370pdSST under the SSP3-7.0 scenario. The future period was divided into three distinct phases. To assess the impact of future climate change on tropospheric ozone under the SSP3-7.0 scenario, two different experiments were conducted: A) ssp370SST, which considers the effects of anthropogenic emissions and the combined influence of climate and B) ssp370pdSST, which only considers the effects of emission changes.

In Figure 3.22, the first column illustrates the future ozone changes according to the ssp370SST experiment for the periods 2020-2039, 2040-2059 and 2080-2099. Similarly, the second column depicts the future ozone changes according to the ssp370pdSST simulation for the corresponding time period. The comparison between the two simulations during the same time period and across different temporal phases does not exhibit significant variation. In the ssp370pdSST experiment, an increase in ozone up to 40 ppb is observed in the Southern hemisphere over time, mainly during the 2080-2099 period. Essentially, this implies that future anthropogenic emissions have a greater impact on ozone increase in the subtropical regions of the southern hemisphere compared to the impact of climate change on southern hemisphere ozone. A more substantial ozone increase from 2020 to 2099, ranging from 70 to 90 ppb, is globally observed in both experiments in the regions of North China and India, which are known for high emissions. In the regions of Africa, Northeast United States and Southeast United States, both experiments show high ozone values approaching 40 to 60 ppb from 2020 to 2099, indicating polluted areas. The critical threshold for which there is a risk if exceeded is 20 ppb annual. However, according to the results of this study, ozone values above 60 ppb are expected by 2100. These values are above the threshold under the pessimistic SSP3-7.0 scenario and are considered to need to be addressed.

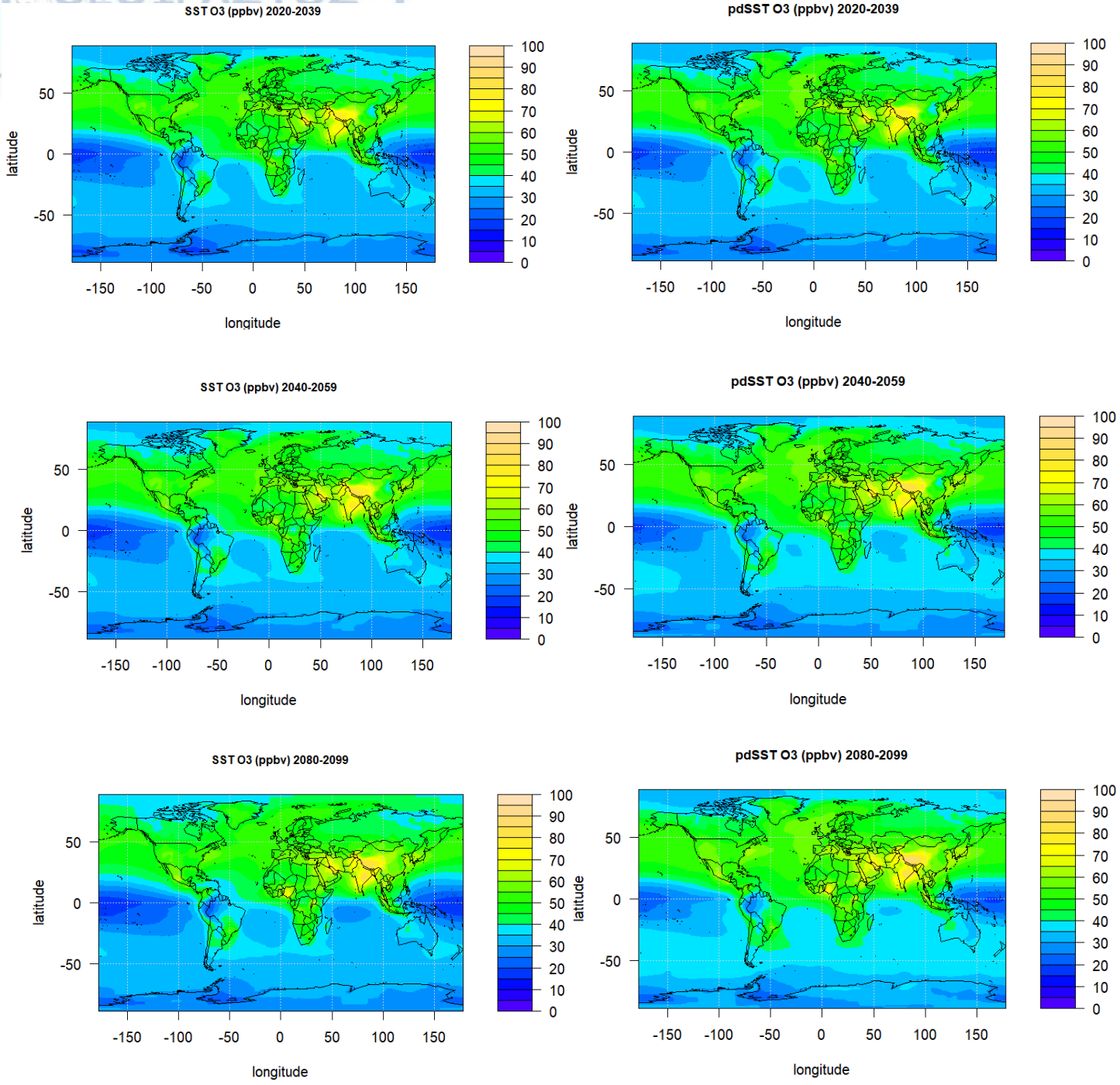

a) b)

Figure 3.22: Ozone concentrations (shaded in ppbv) from CMIP6 model (EC-Earth3-AerChem) from two experiments a) ssp370SST and b) ssp370pdSST for the future period 2020-2039, 2040-2059,2080-2099, respectively.

Therefore, the difference between the two experiments (fig.3.23) suggests that, in most regions, the impact of climate change contributes to ozone reduction, except in polluted regions like North China. However, the ssp370SST experiment, when considered independently, indicates an increase in ozone in most regions. This practically implies the dominant role of future emissions contributing to global ozone increase. This derives from the fact that when considering both climate change and emissions together, it indicates an increase in ozone concentrations in most regions. Conversely, when considering only climate change, it suggests a decrease in most areas. This implies that anthropogenic emissions primarily constitute a significant component of the global increase in ozone concentrations. In figure 3.23, the difference between the two experiments, ssp370SST and ssp370pdSST under the SSP3-7.0 scenario, is observed in conjunction with the anomaly. Essentially, this difference demonstrates the impact of climate change on ozone concentration. Thus, during the time period 2020-2039, higher ozone values are observed, by 4 units above the average, in China, Indonesia, Thailand, in polluted areas, while in most regions globally, a decrease prevails. That is, in the tropics there is a reduction up to -2 units of ozone from normal values. This is tangible evidence that climate change negatively impacts only the areas near polluted sources, which is why there is an increase in ozone levels there. In contrast, in the rest of the regions globally, lower values than the average are observed. This highlights that climate change primarily has adverse effects in proximity to polluted sources. Similarly, during the time period 2040-2059, the same higher ozone values are observed in China, Indonesia, Thailand, by 4 units. In the Arctic, higher values are also observed than normal due to stratospheric ozone transport to the troposphere. Larger negative values by -4 units than normal are observed in other regions, mainly near the equator in oceanic areas, a phenomenon easily explained by the abundance of water vapor destroying ozone due to global warming. Hence, in regions marked with a purple shades, a reduction in ozone is observed, indicating that climate change has a positive impact in these areas. During the time period 2080-2099, an even greater decrease by -8 units is observed in oceanic areas of the Northern and Southern Hemispheres due to the greater temperature increase and consequently global warming resulting in increased water vapor and greater ozone destruction. Furthermore, a greater increase in ozone is observed in the Arctic above 4 units during this decade, attributed to a higher occurrence of tropopause folds and consequently enhanced ozone transport. While an increase of 3 units is observed in Eastern China and India. Therefore, the signal of

climate change is stronger and moreover positive for ozone over time. Consequently, over the years, a more significant temperature increase is observed, particularly in oceanic regions, leading to ozone depletion.

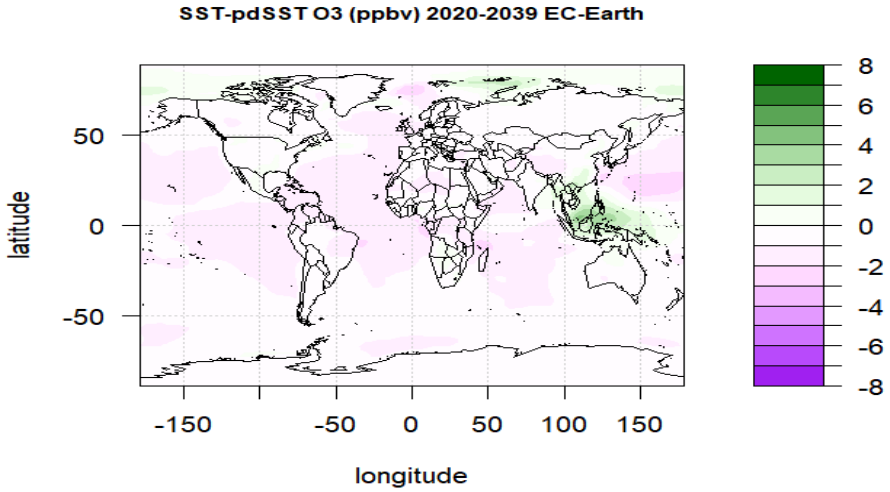

a)

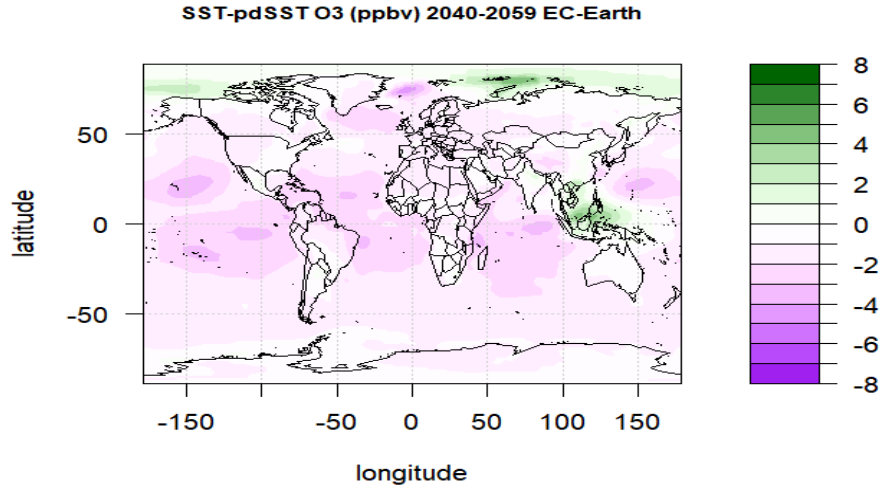

b)

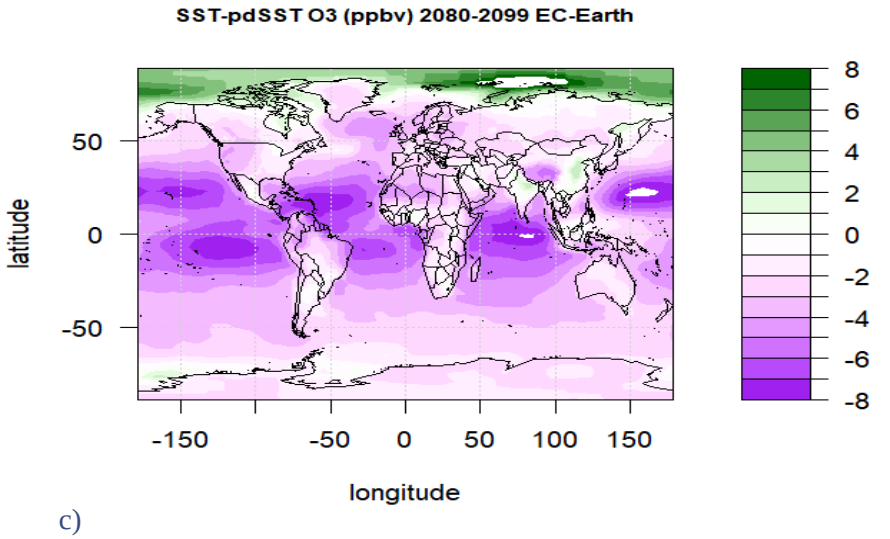

c)

Figure 3.23: Differences of ozone concentrations from CMIP6 model (EC-Earth3-AerChem) between the ssp370SST and ssp370pdSST experiments (shaded in ppbv) for the future period a) 2020-2039, b) 2040-2059, c) 2080-2099.

In figure 3.24, the vertical distribution of ozone concentration is observed according to simulations (a) ssp370SST and (b) ssp370pdSST during the upcoming future time periods. Higher ozone values exceeding 60ppb to 100ppb are observed to approach and in some cases reach the surface level in the Northern Hemisphere, in comparison to the Southern Hemisphere, in both simulations across the three distinct time periods, respectively. This evidence is observed due to the strengthening of the Brewer-Dobson Circulation (BDC), which, as hypothesized in the introduction, is more pronounced in the Northern Hemisphere, leading to the formation of tropopause folds and ozone enhancement. Additionally, the reduction in ozone in tropical regions is likely attributable to the strengthening of the BDC, explained by the increased ozone flux from tropical to polar regions, resulting in higher concentrations at mid and high latitudes (30^0-60^0). This essentially signifies that both the impact of climate change and emissions play a significant role in the increase of ozone in most regions, extending even to the lower layers of the atmosphere.

In addition, greater concentrations of ozone are observed in the Northern hemisphere than in the Southern hemisphere due to increased emissions of ozone precursors and greenhouse gases.

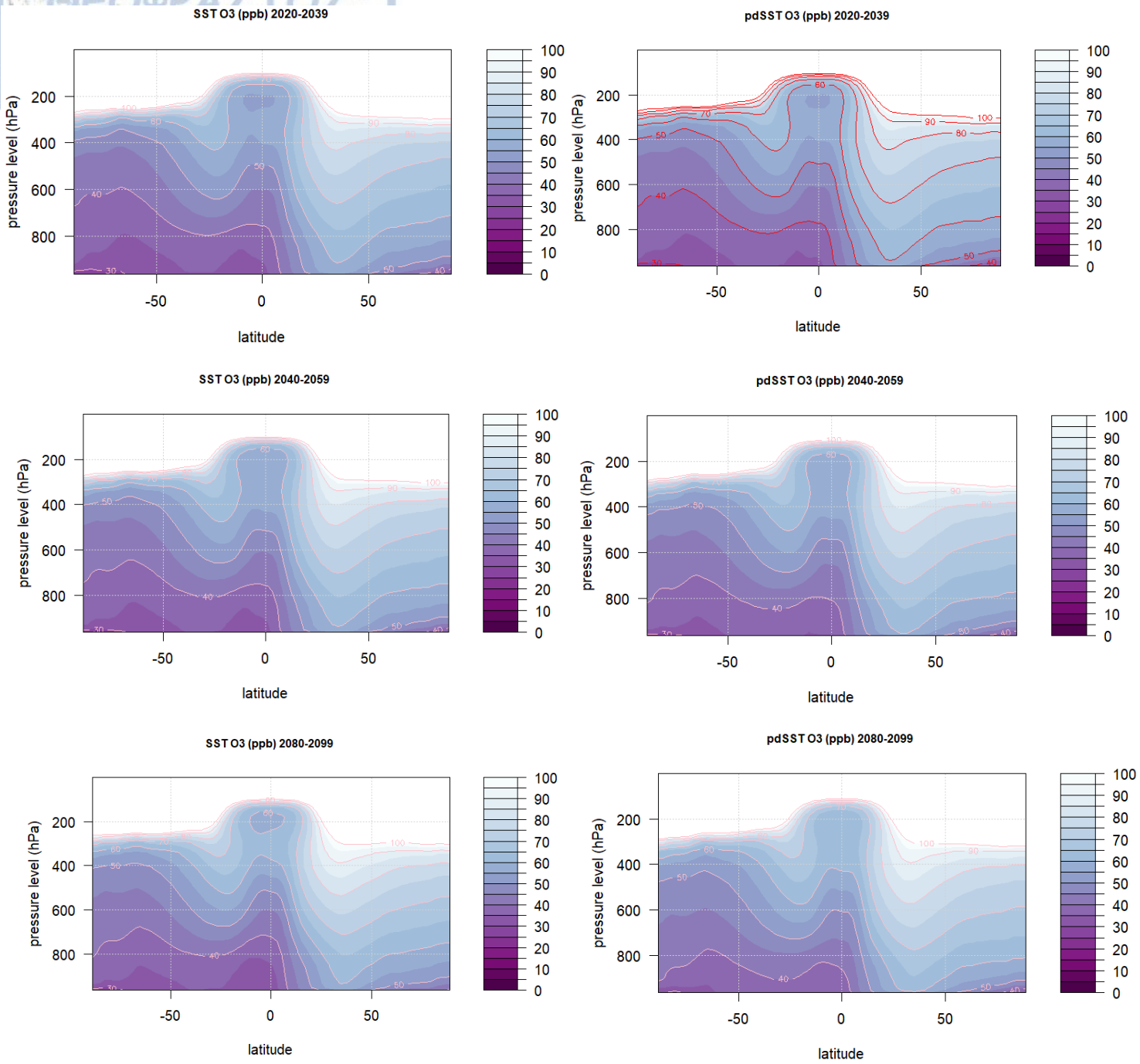

Figure 3.24: Latitude-Pressure vertical cross section of ozone concentrations (shaded in ppbv) from CMIP6 model (EC-Earth3-AerChem) from two experiments a) ssp370SST and b) ssp370pdSST for the future period 2020-2039, 2040-2059, 2080-2099, respectively.

The following figure 3.25 illustrates the impact of climate change on tropospheric ozone. It is observed that, mainly after the mid-21st century, there is an increase in O_3 by 2 units in the subtropical latitudes of the upper troposphere. As shown in Figure 3.25c, this phenomenon is due to the occurrence of tropopause folds in the subtropical regions near the jet streams. Specifically, during the period 2080-2099, climate change negatively affects O_3, meaning that positive deviations above normal values prevail in these regions. Additionally, this increase is attributed to the intense Brewer-Dobson circulation (BDC), which enhances the stratospheric transport of ozone and consequently the intensity of the folds. Moreover, the increase is also due to an increase in ozone precursor substances, such as NOx, until 2050, and from 2050 to 2100 due to the increase in greenhouse gases (GHG). As observed, ozone values are higher than normal in the period 2080-2099, which means that the increase in greenhouse gases is greater than the increase in NOx in the period 2020-2059. Conversely, negative deviations below normal values, by -5 units, are observed in tropical regions mainly during the period 2080-2099. This is due to the temperature increase and consequently the high abundance of water vapor, leading to reactions with ozone that result in its destruction at lower isobaric levels down to the surface.

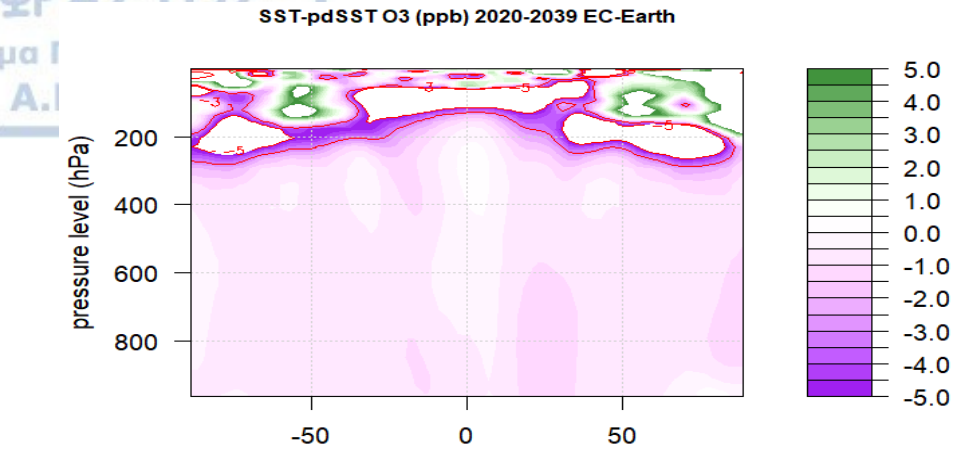

a)

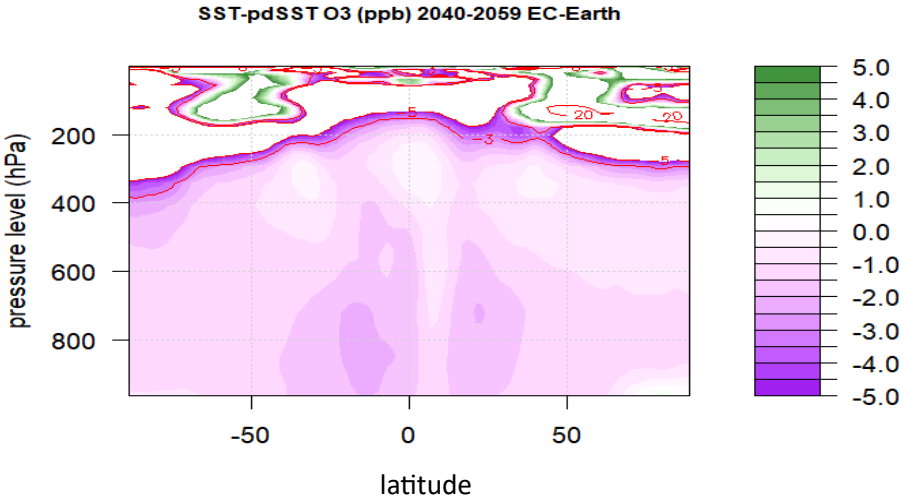

b)

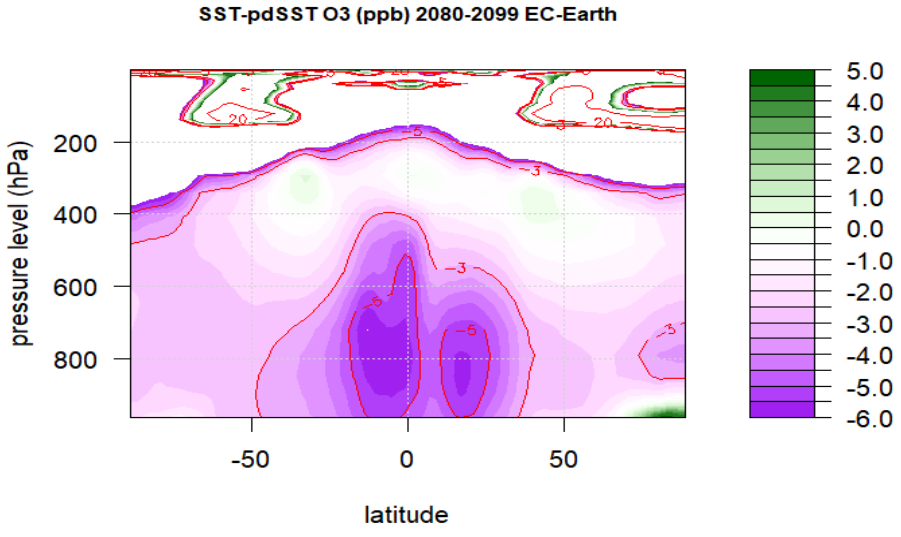

c)

Figure 3.25: Latitude-Pressure vertical cross section of differences of ozone concentrations from CMIP6 model (EC-Earth3-AerChem) between the ssp370SST and ssp370pdSST experiments (shaded in ppbv) for the future period a) 2020-2039, b) 2040-2059, c) 2080-2099.

Chapter 4. Conclusions

The tropopause folds have been a subject of significant research in recent years, with satellite meteorology playing a crucial role in identifying these events. In this study, a synoptic and thermodynamic analysis of the evolution of a stratospheric intrusion event that occurred on 26 January 2015 in the Hohenpeissenberg region was conducted. Additionally, this study investigates future projected changes in tropospheric ozone under the SSP3-7.0 emissions scenario, employing a transient simulation with CMIP6 models.

This study delves into a deep Stratosphere to Troposphere Transport (STT) event over Hohenpeissenberg during the time period from 23 to 28 January 2015, utilizing observational data from radiosondes, ozonesondes and CAMS reanalysis. The synoptic situation of this study was evaluated, which is described by the jet stream at the isobaric level of 300hPa, which is located on the west side of trough and presents maximum speeds. Because of ageostrophic wind in this area, vertical movements take place due to the abrupt change in wind speed, creating vertical motions under the tropopause fold and in combination with the baroclinicity.

The dynamic analysis reveals positive PV anomalies in the northern hemisphere, combined with the jet stream, leading to tropopause fold formation, depicted by a decrease in dynamic tropopause height at lower isobaric levels. Potential vorticity exhibits values equal to 1.5PVU in the study region, explaining the penetration of stratospheric air into the upper troposphere. This transport is evidenced by the cross section of the vertical velocity ω, where pronounced downward motions occur beneath the tropopause fold due to divergence on the surface and convergence in the region of the tropopause fold. Changes in the frequency of tropopause folds affect ozone concentrations. Additionally, it is coupled with cut-off lows in the upper atmosphere, resulting in intense surface weather events, which are intensified with the extent of stratospheric intrusion (shallow, medium, deep). A deep intrusion indicates extreme weather events supported by the baroclinic atmosphere. Furthermore, low values of relative humidity in this region indicate dry stratospheric intrusion in conjunction with water vapor images, confirming the dry intrusion with darker gray shades, indicating lower dynamic tropopause. Due to this mechanism, the transport of dry stratospheric

air to the upper troposphere is favored, leading to an increase in ozone concentration beyond normal levels. Essentially, the fields of potential vorticity, relative humidity, ozone and horizontal wind speed at the 300 hPa isobaric level were studied and analyzed. The same variables, excluding wind speed, were investigated at the 500 hPa isobaric level, where stratospheric intrusion occurs, with dynamic tropopause reaching up to the 500 hPa isobaric level and attaining a value of 1.5 pvu. Additionally, the vertical cross-section of ozone, potential vorticity and relative humidity is represented at a geographic longitude of 11.0° E. The most favorable regions for the formation of tropopause folds are primarily in Asia, especially during the winter when the jet stream is more pronounced, exhibiting the highest frequency of occurrence with shallow folds. Therefore, shallow folds play a crucial role in shaping the average climatology of tropopause folds. Shallow tropopause folds are situated at the mean climatological tropopause height, whereas medium and deep folds extend towards lower isobaric levels, below the mean climatological tropopause height.

The second part of this study explores the impact of climate change of STT on tropospheric ozone and the impact of climate change on tropospheric ozone, using simulations from CMIP6 models under the SSP3-7.0 scenario. Considering two simulations, ssp370SST and ssp370pdSST under the SSP3-7.0 scenario, it has been observed that the impact of anthropogenic emissions primarily constitutes the greatest impact on a global scale. This occurs due to the prevalent increase in tropospheric ozone in both polluted and unpolluted regions. In contrast, the signal of climate change on tropospheric ozone has different implications. The future temperature rise, referred to as climate change, positively influences tropospheric ozone in remote areas away from polluted sources, primarily in oceanic regions, as water vapors destroy ozone. However, in proximity to polluted areas, there is an increase in ozone levels. Changes in ozone quantity affect the climate, however, the climate change itself has a significant impact on ozone, both in its production and depletion. From the experiment ssp370SST alone, a greater increase in ozone concentration is observed, indicating that anthropogenic emissions have a larger impact on future ozone increases compared to the impact of climate change. Consequently, the future ozone concentration will depend on other greenhouse gases and anthropogenic emissions. Notably, the expected increases in ozone above the crucial threshold in the coming decades, according to SSP3-7.0 scenario, due to anthropogenic emissions. The findings highlight the urgent need for

strategic measures to stabilize or reduce these substances in the future. According to the literature and the results of this thesis, ozone values above 60 ppb are expected by 2100, this exceeds the critical threshold, which is 20 ppb annually.

It is noteworthy that according to the SSP3-7.0 scenario, tropospheric ozone concentrations increase by 10 ppb until 2050 due to the increase in ozone precursor substances. However, this increase continues by 16 ppb until 2100 due to other factors, despite the reduction in ozone precursor substances. The increase in greenhouse gases contributes to the elevation of the tropopause height and the strengthening of the Brewer-Dobson circulation (BDC), ultimately leading to the enhancement of tropopause fold and thus the increase in O_3s. In addition, climate change associated with jet stream activity contributes to this enhancement of tropopause fold due to more intense warming by the end of the 21st century in subtropical and polluted regions. In addition, Stratosphere-Troposphere Transport (STT) is observed even at higher latitudes.

The increase in premature deaths is projected to rise dramatically until 2100, attributed to ozone due to population growth and ageing to a greater percentage. Considering human health and air quality, it is necessary to implement adaptive policy measures and mitigation strategies for ozone precursor substances, but primarily for greenhouse gases, with the ultimate goal of mitigating climate change by 2100. Otherwise, health impacts will be detrimental, especially in North Asia until 2050 and Africa until 2100. The results of emission mitigation strategies will have an impact beyond the lifetime of each pollutant. Therefore, a more effective target is the mitigation of NTCFs. Utilizing satellite data and ground-based measurement stations is essential for quantifying climate change and its impacts.

The aforementioned results generally agree with the findings of other studies (*Akritidis et al., 2018; Akritidis et al., 2019; Akritidis et al., 2021; Zanis et al., 2003; Zanis et al.,2014; Zanis et al., 2022*), enhancing the reliability of the research. Despite minor quantitative discrepancies near the tropopause region between ozone observations ozonesondes and CAMS reanalyses, capturing sharp gradients around the tropopause remains difficult in global models. However, there is a good agreement at the vertical level of isobaric surfaces. The consequences arising from the tropopause fold event

include cyclogenesis at the surface and the occurrence of intense weather events in front of the trough.

In summary, the tropopause fold was examined in conjunction with stratospheric intrusion at Hohenpeissenberg on 26 January 2015, along with an investigation into the impact of climate change of STT on tropospheric ozone and the climate change on tropospheric ozone on a global scale. In conclusion, tropopause fold constitutes the primary mechanism for the exchange of air masses between the stratosphere and troposphere, ultimately aiming to modify the composition of tropospheric air by altering ozone concentrations.

BIBLIOGRAPHY

Abdel Basset, H., & Gahein, A. (2003). Diagnostic study on the relation between ozone and potential vorticity. Atmósfera, 16(2), 67-82.

Akritidis, D., Bacer, S., Zanis, P., Georgoulias, A. K., Chowdhury, S., Horowitz, L. W., ... & Pozzer, A. (2024). Strong increase in mortality attributable to ozone pollution under a climate change and demographic scenario. *Environmental Research Letters*, *19*(2), 024041.

Akritidis, D., Katragkou, E., Zanis, P., Pytharoulis, I., Melas, D., Flemming, J. & Eskes, H. (2018). A deep stratosphere-to-troposphere ozone transport event over Europe simulated in CAMS global and regional forecast systems: analysis and evaluation. Atmospheric Chemistry and Physics, 18(20), 15515-15534.

Akritidis, D., Pozzer, A., & Zanis, P. (2019). On the impact of future climate change on tropopause folds and tropospheric ozone. Atmospheric Chemistry and Physics, 19(22), 14387-14401.

Akritidis, D., Pozzer, A., Flemming, J., Inness, A., Nédélec, P., & Zanis, P. (2022). A process-oriented evaluation of CAMS reanalysis ozone during tropopause folds over Europe for the period 2003–2018. *Atmospheric Chemistry and Physics*, *22*(9), 6275-6289.

Akritidis, D., Pozzer, A., Flemming, J., Inness, A., & Zanis, P. (2021). A global climatology of tropopause folds in CAMS and MERRA-2 reanalyses. Journal of Geophysical Research: Atmospheres, 126, e2020JD034115. https://doi.org/10.1029/2020JD034115.

Ancellet, G., Beekmann, M., & Papayannis, A. (1994). Impact of a cutoff low development on downward transport of ozone in the troposphere. *Journal of Geophysical Research: Atmospheres*, *99*(D2), 3451-3468. doi:10.1029/93jd02551.

Bjerknes, J., and J. Holmboe (1944). On the theory of cyclones. J. Meteor., 1, 1–22.

Bithell, M., & Vaughan, G. (2000). Persistence of stratospheric ozone layers in the troposphere. ,34(16), 2563–2570. doi:10.1016/s1352-2310(99)00497-5.

Bönisch, H., Engel, A., Birner, T., Hoor, P., Tarasick, D. W., & Ray, E. A. (2010). On the structural changes in the Brewer-Dobson circulation after 2000. Atmos. Chem. Phys. Discuss, 10, 28399-28430.

Chen, J., & Hoek, G. (2020). Long-term exposure to PM and all-cause and cause-specific mortality: A systematic review and meta-analysis. Environment International, 143, 105974. https://doi.org/10.1016/J.ENVINT.2020.105974.

Conte, A., Otu-Larbi, F., Alivernini, A., Hoshika, Y., Paoletti, E., Ashworth, K., & Fares, S. (2021). Exploring new strategies for ozone-risk assessment: A dynamic-threshold case study. *Environmental Pollution*, *287*, 117620.

Danielsen, E. F. (1968). Stratosphere-troposphere exchange based on radioactivity, ozone and potential vorticity. *J. Atmos. Sci.*, *47*, 2013-2020.

Dafka, S., Akritidis, D., Zanis, P., Pozzer, A., Xoplaki, E., Luterbacher, J., & Zerefos, C. (2021). On the link between the Etesian winds, tropopause folds and tropospheric ozone over the Eastern Mediterranean during summer. *AtmosphericResearch*, *248*,105161.,doi:10.1016/j.atmosres.2020.105161.

De Marco, A., Garcia-Gomez, H., Collalti, A., Khaniabadi, Y. O., Feng, Z., Proietti, C., ... & Paoletti, E. (2022). Ozone modelling and mapping for risk assessment: An overview of different approaches for human and ecosystems health. *Environmental Research*, *211*, 113048.

Díaz, J., Ortiz, C., Falcón, I., Salvador, C., & Linares, C. (2018). Short-term effect of tropospheric ozone on daily mortality in Spain. *Atmospheric Environment*, *187*, 107-116.

Ertel, H. (1942). Ein neuer hydrodynamischer Wirbelsatz, Meteorol. Z., 59(9), 277–281.

Europe's, M. E. Europe's Environment. The Third Assessment. A summary.

Finlayson-Pitts, B. J., & Pitts Jr, J. N. (2000). *Chemistry of the upper and lower atmosphere: theory, experiments, and applications*. Elsevier.

Fiore, A. M., Naik, V., & Leibensperger, E. M. (2015). Air quality and climate connections. *Journal of the Air & Waste Management Association*, *65*(6), 645-685.

Georgiev, C., Santurette, P., & Maynard, K. (2016). Weather analysis and forecasting: Applying satellite water vapor imagery and potential vorticity analysis. Academic Press.

Gimeno, L., Trigo, R. M., Ribera, P., & Garcia, J. A. (2007). Special issue on cut-off low systems (COL). Meteorology and Atmospheric Physics, 96(1-2), 1.

Godoy, A. A., Possia, N. E., Campetella, C. M., & García Skabar, Y. (2011). A cut-off low in southern South America: dynamic and thermodynamic processes. Revista Brasileira de Meteorologia, 26, 503-514.

Gray, S. L. (2006). Mechanisms of midlatitude cross-tropopause transport using a potential vorticity budget approach. Journal of Geophysical Research: Atmospheres, 111(D17).

Griffiths, P. T., Murray, L. T., Zeng, G., Shin, Y. M., Abraham, N. L., Archibald, A. T., ... & Zanis, P. (2021). Tropospheric ozone in CMIP6 simulations. *Atmospheric Chemistry and Physics*, *21*(5), 4187-4218.

Hartmann, D. L., Tank, A. M. K., Rusticucci, M., Alexander, L. V., Brönnimann, S., Charabi, Y. A. R., & Zhai, P. (2013). Observations: atmosphere and surface. In *Climate change 2013 the physical science basis: Working group I contribution to the fifth assessment report of the intergovernmental panel on climate change* (pp. 159-254). Cambridge University Press.

Harvey, B., Methven, J., Sanchez, C. and Schaefler, A. (2020). Diabatic generation of negative potential vorticity and its impact on the North Atlantic jet stream. Quarterly Journal of the Royal Meteorological Society, 146 (728). pp. 1477-1497. ISSN 1477-870X doi: https://doi.org/10.1002/qj.3747.

Holton, J. R., Haynes, P. H., McIntyre, M. E., Douglass, A. R., Rood, R. B., & Pfister, L. (1995). Stratosphere-troposphere exchange. *Reviews of geophysics*, *33*(4), 403-439.

Hoskins, B. J., M. E. Mcintyre, and A. W. Robertson (1985). On the use and significance of isentropic potential vorticity maps, Q. J. R. Meteorol. Soc., 111,877-945.

J. D. Price; G. Vaughan (1993). The potential for stratosphere-troposphere exchange in cut-off-low systems.,119(510), 343–365. doi:10.1002/qj.49711951007.

Kanakidou, M., Mihalopoulos, N., Kindap, T., Im, U., Vrekoussis, M., Gerasopoulos, E., ... & Moubasher, H. (2011). Megacities as hot spots of air pollution in the East Mediterranean. *Atmospheric Environment*, *45*(6), 1223-1235.Kentarchos, A. S., & Davies, T. D. (1998). A climatology of cut-off lows at 200 hPa in the Northern Hemisphere, 1990–1994. *International Journal of Climatology: A Journal of the Royal Meteorological Society*, *18*(4), 379-390.

Keyser, D., and M.A. Shapiro (1986). A Review of the structure and dynamics of upper-level frontal zones, Mon. Weather Rev., 114, 452-499.

Kew, S. F., Sprenger, M., & Davies, H. C. (2010). Potential vorticity anomalies of the lowermost stratosphere: A 10-yr winter climatology. Monthly Weather Review, 138(4), 1234-1249.

Kunz, A.; Konopka, P.; Müller, R.; Pan, L. L. (2011). Dynamical tropopause based on isentropic potential vorticity gradients. Journal of Geophysical Research, 116(D1), D01110–. doi:10.1029/2010jd014343.

Lei, H., Wuebbles, D. J., & Liang, X. Z. (2012). Projected risk of high ozone episodes in 2050. *Atmospheric Environment*, *59*, 567-577.

Li, D., Bian, J., & Fan, Q. (2015). A deep stratospheric intrusion associated with an intense cut-off low event over East Asia. Science China Earth Sciences, 58, 116-128.

Lin, J. T., Wuebbles, D. J., & Liang, X. Z. (2008). Effects of intercontinental transport on surface ozone over the United States: Present and future assessment with a global model. *Geophysical Research Letters*, *35*(2).

Lorenz, D. J., and E. T. DeWeaver (2007). Tropopause height and zonal wind response to global warming in the IPCC scenario integrations, J. Geophys. Res., 112, D10119, doi:10.1029/2006JD008087.

McWilliams, J. C. (1980). An application of equivalent models to atmospheric blocking. Dyn. Atmos. Oceans., 5, 43- 66.

Miglietta M. M., Cerrai D., Laviola S., Cattani E. and Levizzani V. (2017). Potential vorticity patterns in Mediterranean “hurricanes”. Geophys. Res., 44, 2537–2545.

Morgenstern, O., Stone, K. A., Schofield, R., Akiyoshi, H., Yamashita, Y., Kinnison, D. E., Garcia, R. R., Sudo, K., Plummer, D. A., Scinocca, J., Oman, L. D., Manyin, M. E., Zeng, G., Rozanov, E., Stenke, A., Revell, L. E., Pitari, G., Mancini, E., Di Genova, G., Visioni, D., Dhomse, S. S., and Chipperfield, M. P. (2018). Ozone sensitivity to varying greenhouse gases and ozone-

depleting substances in CCMI-1 simulations, Atmos. Chem. Phys., 18, 1091–1114, https://doi.org/10.5194/acp18-1091-2018.

Neal, L. S., Dalvi, M., Folberth, G., McInnes, R. N., Agnew, P., O'Connor, F. M., Savage, N. H., and Tilbee, M. (2017). A description and evaluation of an air quality model nested within global and regional composition-climate models using MetUM, Geosci. Model Dev., 10, 3941–3962, https://doi.org/10.5194/gmd-10-3941-2017.

Nieto, R., Sprenger, M., Wernli, H., Trigo, R. M., & Gimeno, L. (2005). Identification and Climatology of Polar Lows over the Nordic Seas Based on ERA-40 Reanalysis. Monthly Weather Review, 133(9), 2438–2455. doi: 10.1175/mwr2982.1.

Oberländer-Hayn, S., Gerber, E. P., Abalichin, J., Akiyoshi, H., Kerschbaumer, A., Kubin, A., Kunze, M., Langematz, U., Meul, S., Michou, M., Morgenstern, O., and Oman, L. D. (2016). Is the Brewer-Dobson circulation increasing or moving upward, Geophys. Res. Lett., 43, 1772–1779, https://doi.org/10.1002/2015GL067545.

O'Neill, B. C., Kriegler, E., Riahi, K., Ebi, K. L., Hallegatte, S., Carter, T. R., Mathur, R., and van Vuuren, D. P.: A new scenario framework for climate change research: the concept of shared socioeconomic pathways, Clim. Change, 122, 387–400. (2014). https://doi.org/10.1007/s10584-013-0905-2.

Percy, K. E., Legge, A. H., & Krupa, S. V. (2003). Tropospheric ozone: a continuing threat to global forests. *Developments in Environmental Science*, *3*, 85-118.

Price, J. D., Vaughan, G., & Legras, B. (1994). Tropopause folds: Occurrence frequencies and three-dimensional structure. Journal of

Geophysical Research: Atmospheres, 99(D7), 12909–. doi:10.1029/94jd00393.

Rao, S., Klimont, Z., Smith, S. J., Dingenen, R. V., Dentener, F., Bouwman, L., et al. (2017). Future air pollution in the shared socio-economic pathways. Global Environmental Change, 42, 346–358. https://doi.org/10.1016/j.gloenvcha.2016.05.012.

Reed, R. J., M. Stoelinga, and Y- H. Kuo. (1992). A model-aided study of the origin and evolution of the anomalously high potential vorticity in the inner region of rapidly developing marine cyclone. Mon. Wea. Rev., 120, 893- 913.

Revell L E, Tummon F, Stenke A, Sukhodolov T, Coulon A, Rozanov E and Peter T. (2015). Drivers of the tropospheric ozone budget throughout the 21st century under the medium-high climate scenario RCP 6.0 Atmos. Chem. Phys. 15 5887–902.

Rind, D., D. Shindell, P. Lonergan, and N. K. Balachandran. (1998). Climate change and the middle atmosphere. part III: The doubled CO2 climate revisited, J. Clim., 11, 876 – 894.

Rondanelli, R., Gallardo, L., & Garreaud, R. D. (2002). Rapid changes in ozone mixing ratios at Cerro Tololo (30° 10′ S, 70° 48′ W, 2200 m) in connection with cutoff lows and deep troughs. *Journal of Geophysical Research: Atmospheres*, *107*(D23), ACL-6.

Roelofs, G. J. (2003). Intercomparison of tropospheric ozone models: Ozone transport in a complex tropopause folding event. Journal of Geophysical Research, 108(D12), 8529–. doi:10.1029/2003jd003462.

Russell, A., G. Vaughan, and E. G. Norton (2012). Large-scale potential vorticity anomalies and deep convection, Q. J. R. Meteorol. Soc., 138, 1627–1639, doi:10.1002/qj.1875.

Santer, B. D., Wehner, M. F., Wigley, T. M. L., Sausen, R., Meehl, G. A., Taylor, K. E. & Bruggemann, W. (2003). Contributions of anthropogenic and natural forcing to recent tropopause height changes. *science*, *301*(5632), 479-483.Shapiro, M. A. (1978). Further evidence of the mesoscale and turbulent structure of upper jet stream-frontal zone systems. Mon. Weather Rev., 106, 1100-1111.

Schönbein, C.F. (1840). Recherches sur la nature de l'odeur qui se manifeste dans certaines actions chimiques. C. R. Acad. Sci. Paris 10, 706–710.

Shaddick, G., Thomas, M. L., Mudu, P., Ruggeri, G., & Gumy, S. (2020). Half the world's population are exposed to increasing air pollution. Npj Climate and Atmospheric Science, 3(1), 1–5. https://doi.org/10.1038/s41612-020-0124-2.

Shapiro, M. A. (1980). Turbulent mixing within tropopause folds as a mechanism for the exchange of chemical constituents between stratosphere and troposphere. J. Atmos. Sci., 37, 994-1004.

Shepherd, T., Bodeker, G., Canziani, P., Dameris, M., Forster, P., Fioletov, V. & McFarland, M. (2005). Ozone and Climate: A Review of Interconnections. *Safeguarding the Ozone Layer and the Global Climate System: Special Report of the Intergovernmental Panel on Climate Change*, *1*, 83.

Sprenger, M., & Wernli, H. (2003). A Northern Hemispheric climatology of cross-tropopause exchange for the ERA15 time period (1979–1993). J. Geophys. Res., 108, 8521, doi:10.1029/ 2002JD002636.

Sprenger, M., Wernli, H., & Bourqui, M. (2007). Stratosphere–troposphere exchange and its relation to potential vorticity streamers and

cutoffs near the extratropical tropopause. Journal of the atmospheric sciences, 64(5), 1587-1602.

Škerlak, B., Sprenger, M., Pfahl, S., Tyrlis, E., & Wernli, H. (2015). Tropopause folds in ERA-Interim: Global climatology and relation to extreme weather events. Journal of Geophysical Research: Atmospheres, 120(10), 4860-4877.

Stohl, A., Bonasoni, P., Cristofanelli, P., Collins, W., Feichter, J., Frank, A., ... & Zerefos, C. (2003). Stratosphere-troposphere exchange: A review, and what we have learned from STACCATO. Journal of Geophysical Research: Atmospheres, 108(D12).

Stohl, A., et al. (2003b), Stratosphere-troposphere exchange: A review and what we have learned from STACCATO, J. Geophys. Res., 108(D12), 8516, doi:10.1029/2002JD002490.

Streets, D. G., Bond, T. C., Lee, T., & Jang, C. (2004). On the future of carbonaceous aerosol emissions. *Journal of Geophysical Research: Atmospheres*, *109*(D24).

Tang, Q., Prather, M. J., & Hsu, J. (2011). Stratosphere-troposphere exchange ozone flux related to deep convection. *Geophysical Research Letters*, *38*(3).

Turnock, S. T., Reddington, C. L., West, J. J., & O'Connor, F. M. (2023). The Air Pollution Human Health Burden in Different Future Scenarios That Involve the Mitigation of Near-Term Climate Forcers, Climate and Land-Use. *GeoHealth*, *7*(8), e2023GH000812.

Turnock, S. T., Allen, R. J., Andrews, M., Bauer, S. E., Deushi, M., Emmons, L., ... & Zhang, J. (2020). Historical and future changes in air

pollutants from CMIP6 models. *Atmospheric Chemistry and Physics*, *20*(23), 14547-14579.

Uccellini, D. Keyser, K. F. Brill, and C. H. Wash (1985). The Presidents' Day cyclone of 18–19 February 1979: Influence of upstream trough amplification and associated tropopause folding on rapid cyclogenesis. Mon. Wea. Rev., 113, 962–988.

Wandishin, M. S., Nielsen-Gammon, J. W., & Keyser, D. (2000). A potential vorticity diagnostic approach to upper-level frontogenesis within a developing baroclinic wave. Journal of the atmospheric sciences, 57(24), 3918-3938.

Wild, O., Fiore, A. M., Shindell, D. T., Doherty, R. M., Collins, W. J., Dentener, F. J., ... & Zuber, A. (2012). Modelling future changes in surface ozone: a parameterized approach. *Atmospheric Chemistry and Physics*, *12*(4), 2037-2054. https://doi.org/10.5194/acp-12-2037-2012.

Wimmers, Anthony J. (2003). Signatures of tropopause folding in satellite imagery. Journal of Geophysical Research, 108(D4), 8360–. doi:10.1029/2001jd001358.

World Health Organization. (2006). *Air quality guidelines: global update 2005: particulate matter, ozone, nitrogen dioxide, and sulfur dioxide*. World Health Organization.

World Meteorological Organization. (1986). Atmospheric ozone 1985. WMO Report No. 16, World Meteorological Organization, Case Postale No. 5, Geneva.

WMO. (1985). Atmospheric Ozone, Vol. I, Report No 16. WMO, Geneva.

Young, P. J., Archibald, A. T., Bowman, K. W., Lamarque, J.-F., Naik, V., Stevenson, D. S., Tilmes, S., Voulgarakis, A., Wild, O., Bergmann, D., Cameron-Smith, P., Cionni, I., Collins, W. J., Dalsøren, S. B., Doherty, R. M., Eyring, V., Faluvegi, G., Horowitz, L. W., Josse, B., Lee, Y. H., MacKenzie, I. A., Nagashima, T., Plummer, D. A., Righi, M., Rumbold, S. T., Skeie, R. B., Shindell, D. T., Strode, S. A., Sudo, K., Szopa, S., and Zeng, G. (2013). Preindustrial to end 21st century projections of tropospheric ozone from the Atmospheric Chemistry and Climate Model Intercomparison Project (ACCMIP), Atmos. Chem. Phys., 13, 2063– 2090, https://doi.org/10.5194/acp-13-2063-2013.

Zanis, P., Akritidis, D., Turnock, S., Naik, V., Szopa, S., Georgoulias, A. K., ... & van Noije, T. (2022). Climate change penalty and benefit on surface ozone: a global perspective based on CMIP6 earth system models. Environmental Research Letters, 17(2), 024014.

Zanis, P., Hadjinicolaou, P., Pozzer, A., Tyrlis, E., Dafka, S., Mihalopoulos, N., and Lelieveld, J. (2014). Summertime free–tropospheric ozone pool over the EM/Middle East. Atmospheric Chemistry and Physics. 14, 115–132. doi:10.5194/acp-14-115-2014.

Zanis, P., Trickl, T., Stohl, A., Wernli, H., Cooper, O., Zerefos, C., ... & Claude, H. (2003). Forecast, observation and modelling of a deep stratospheric intrusion event over Europe. *Atmospheric Chemistry and Physics*, *3*(3), 763-777.

Other sources

Zanis, (2014). Course notes on pollution and atmospheric chemistry. "MSc Meteorology, Climatology and Atmospheric Environment, Department of Geology, Aristotle University of Thessaloniki".

Karakostas, (2021). Dynamic Meteorology Course Notes. "MSc Meteorology, Climatology and Atmospheric Environment, Department of Geology, Aristotle University of Thessaloniki".

Katragkou, (2022). Course notes climate models. "MSc Meteorology, Climatology and Atmospheric Environment, Department of Geology, Aristotle University of Thessaloniki".

Makrogiannis and Sahsamanoglou, (2004). General Meteorology courses. Harris Publications. Thessaloniki.

Makrogiannis, (2007). Course notes on thermodynamics and statics of the atmosphere.

Pytharoulis, (2022). Synoptic Meteorology Course Notes. "MSc Meteorology, Climatology and Atmospheric Environment, Department of Geology, Aristotle University of Thessaloniki".

Feidas and Kartalis., (2003). Course Notes Satellite Meteorology Climatology. "MSc Meteorology, Climatology and Atmospheric Environment, Department of Geology, Aristotle University of Thessaloniki".

Stratospheric Ozone-An Electronic Textbook (http://www.ccpo.odu.edu/SEES/ozone/oz_class.htm).

APPENDIX A: Stratospheric intrusion event at 500 hpa

The following figures show the variables at the 500hpa isobaric level where the stratospheric intrusion occurs. Potential vorticity is depicted with contours (fig.A.1), while ozone concentrations are observed according to the color scale. From 25 January at 00Z, a distinctive flow with high ozone concentrations so-called “hook shaped” over the study area is noted. The synoptic situation on 25 January at 00Z is characterized by a deep upper-level trough at 500 hPa with a 1.5PVU isentropic surface, extending from Scandinavia to central Europe. This system moves eastward. Specifically, ozone concentrations exceed 40 ppb in the study area from 25 January at 00Z to 25 January at 12Z, coinciding with low relative humidity values and high PV values. On 25 January at 18Z, ozone concentrations approach 60 ppb, while on 26 January at 00Z, ozone concentrations approach 80 ppb, as evidenced by the cross section on 26 January at 00Z with the same ozone values. On 26 January at 12Z, ozone concentrations exceed 50 ppb, while on 27 January and later, the system has dissipated, moving southeastward. Consequently, over the study area, reduced ozone concentrations approaching 50 ppb are observed. In the region of high ozone concentrations approaching 90 ppb, potential vorticity values equal with 1.5 PVU are depicted.

Essentially, the synoptic situation at the 500 hPa level is studied because, from 26 January at 00Z, the tropopause fold appears and thus the stratospheric ozone intrusion from the stratosphere to the troposphere reaches up to the 500 hPa isobaric level. Certainly, lower ozone values are observed than those presented by the stratosphere, which is rich in ozone. Regarding the potential vorticity, it is equal to 1.5PVU. This value represents the dynamic tropopause at this isobaric level. The animation in the figure A.2 depicts the ozone flow at 500 hPa from 21 January at 00Z to 31 January at 18Z 2015, which appears to originate from west to east.

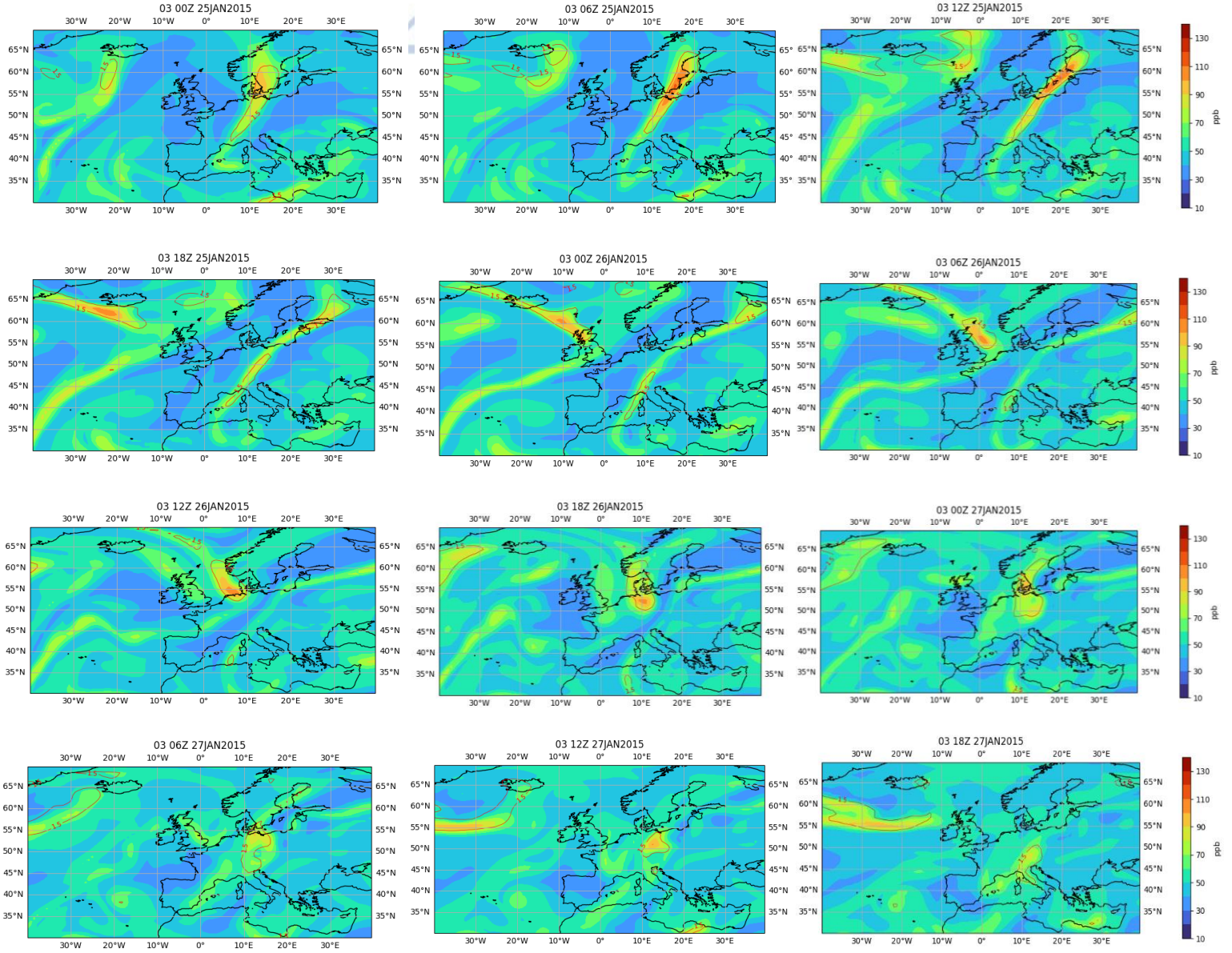

Figure A.1: Ozone mixing ratio (color shaded in ppb), Potential Vorticity (red contours in pvu) at 500 hPa during the period from 00Z on 25 January 2015 to 18Z on 27 January 2015 (6h interval).

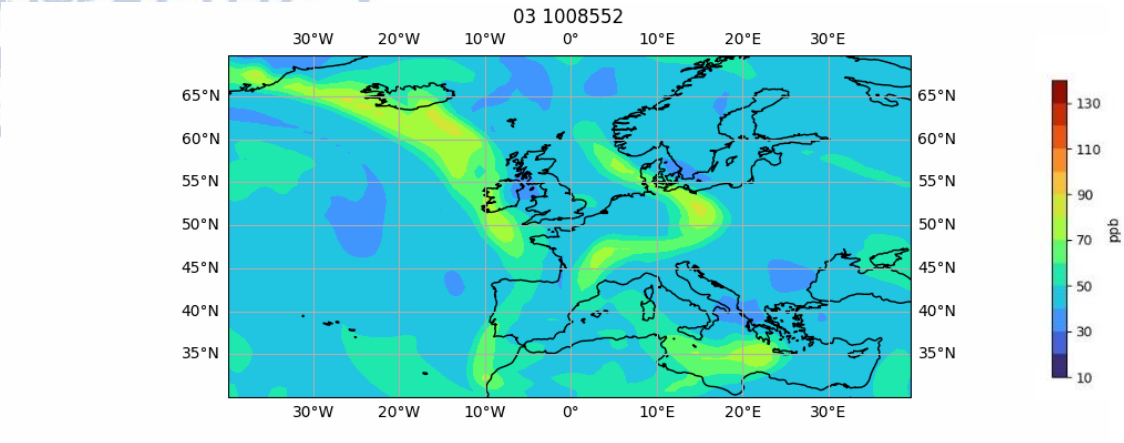

Figure A.2: Animation ozone mixing ratio (color shaded in ppb) at 500 hPa during the period from 00Z on 21 January 2015 to 18Z on 31 January 2015 (3h interval).

The monthly mean ozone values for January are observed over the time period from 2003 to 2022 at the 500 hPa isobaric level (fig.A.3). According to the color scale, over the European region and specifically above the study area, average monthly ozone values around 50 ppb are observed for the month of January. The highest monthly ozone values are discerned over the North Atlantic, exceeding 50 ppb. This observation represent good agreement with the mean climatology of tropopause folds as mentioned earlier. Specifically, in the North Atlantic, the highest frequency of tropopause folds is observed, leading to elevated ozone concentrations in this region. Consequently, the highest ozone concentrations prevail in this area.

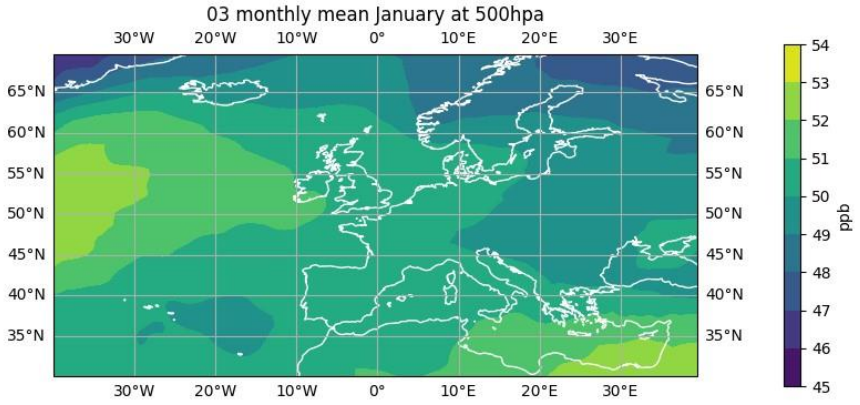

Figure A.3: Average monthly January ozone value (in ppb) for the period from 2003 to 2022 at 500 hPa.

By comparing daily ozone values to the mean climatology of ozone, insights can be derived regarding whether daily values exceed the climatological average. This can be achieved through the representation of deviation patterns. The deviation indicates the extent to which the observed variable exceeds or falls below the mean value for a specific time period. As a result, the occurrence of this tropopause fold mechanism is confirmed, justifying the higher ozone concentrations. In more detail, on 25 January 2015 at 00Z (fig.A.4), ozone concentrations in the study area approach values around 50 ppb, whereas in the study area's climatology, average ozone values are observed at 50 ppb. There is no distinct difference. Subsequently, on the following two dates on 25 January at 12Z and on 26 January at 00Z, there is an increase in ozone levels. Specifically, on 25 January at 12Z, ozone values are at 55 ppb, indicating an increase in ozone by 5 units from the climatological average. While on 26 January at 00Z, an even greater increase in ozone is observed, by 30 units, as ozone values on that specific date approach 80 ppb. This practically demonstrates the stratospheric intrusion due to elevated ozone values above the normal mean values.

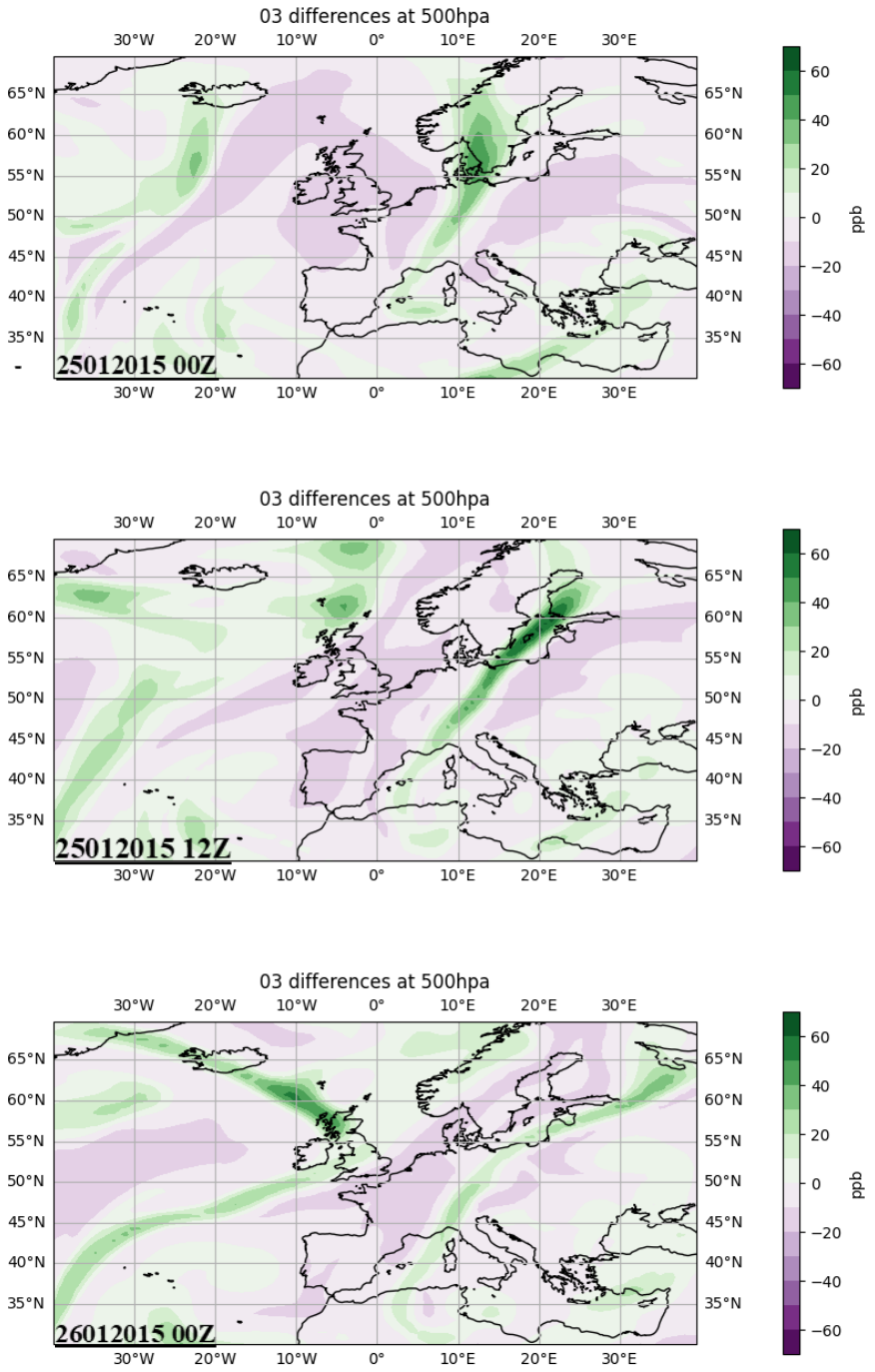

Figure A.4**:** Differences of ozone between average monthly January ozone value during 2003-2022 and a) at 00Z on 25 January 2015, b) at 12Z on 25 January 2015 and c) at 00Z on 26 January 2015 at 00Z at 500 hPa.

The evolution of meteorological conditions can also be illustrated by the appearance of a sequence of potential vorticity (PV) maps at the 500 hPa isobaric surface from 00UTC on 25 January to 18 UTC on 27 January (fig.A.5). The analysis of potential vorticity on

isentropic surfaces reveals a flow with high PV values, extending southeastward and exhibiting cyclonic curvature. The figure A.5 depicts the geopotential height field at the 500hPa isobaric level and the potential vorticity according to the color scale. Specifically, from 25 January at 06Z to 26 January at 06Z, potential vorticity (PV) equal to 1.5 PVU is observed over Hohenpeissenberg. In comparison to surrounding regions, a notable difference in the value of potential vorticity is observed, consequently influencing the extension of the dynamic tropopause to lower isobaric levels. Therefore, potential vorticity values equal to 1.5PVU indicate tropopause fold and essentially signify the indication of flow transport from the stratosphere to the troposphere through the tropopause. The intrusion of stratospheric air with high stability is observed to penetrate into the troposphere. On 27 January, the flow appears to be cut off from the main flow, indicating that the upper-level system has practically disconnected and the baroclinicity of the lower level has weakened. However, there is no apparent development of a cutoff low.

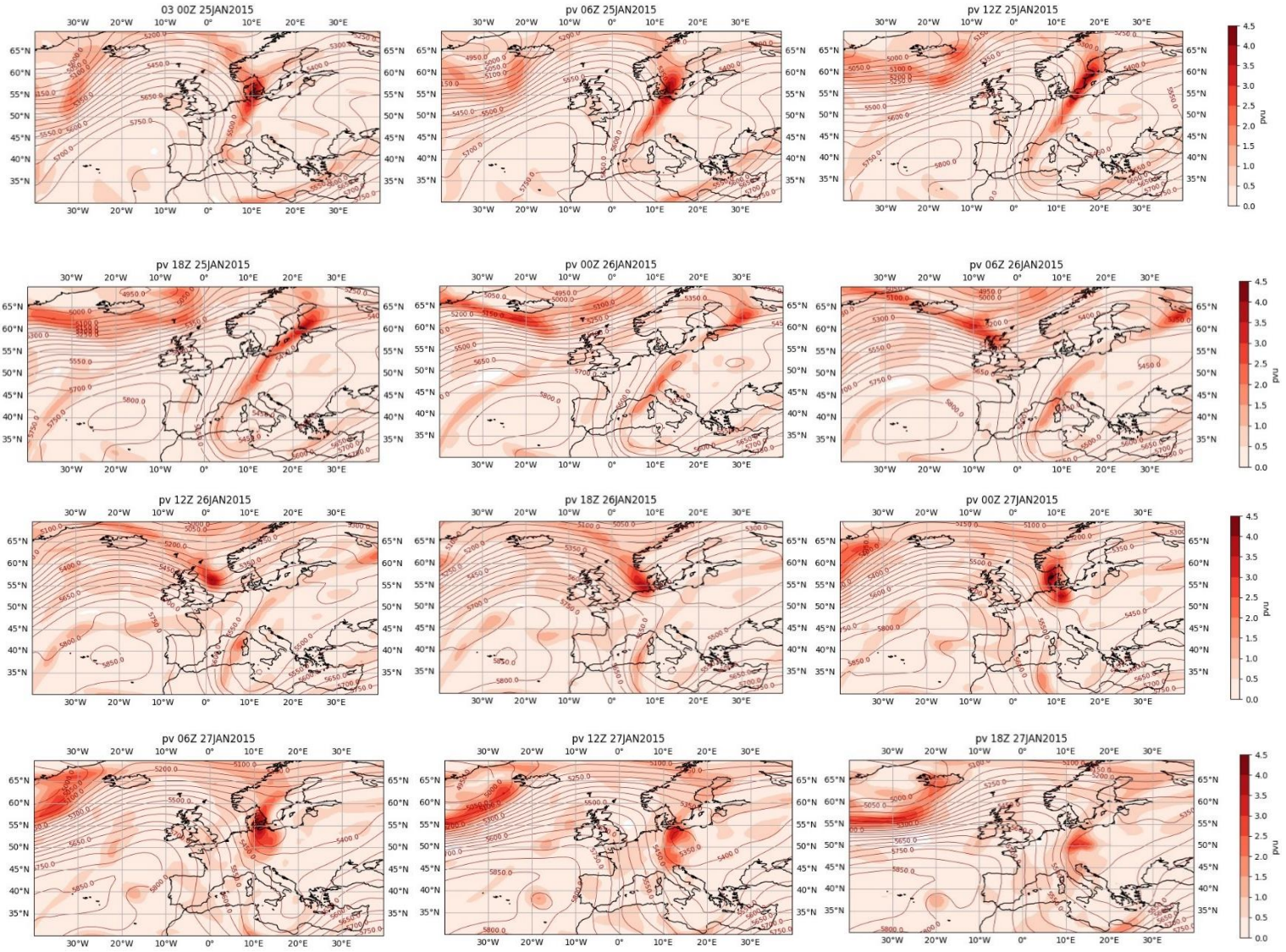

Figure A.5: Potential Vorticity (color shaded in pvu) and geopotential height (red contours in gpm) at 500 hPa, during the period from 00Z on 25 January 2015 to 18Z on 27 January 2015 (6 h interval).

Regarding relative humidity (fig.A.6), a characteristic flow is observed over the study area with very low relative humidity values below 0.30 on 26 January at 00Z. According to the previous parameters depicted in the figures, the low humidity values coincide with the presence of a dry intrusion into the troposphere. Contours represent the potential vorticity surface equal to 1.5PVU precisely over the study area with very low humidity, indicating the presence of dry air that has entered the troposphere from the stratosphere. Humidity values ranging up to 0.6 are observed at 00Z on 25 January over

Hohenpeissenberg and from 25 January at 18Z it starts to decrease, representing typical values of the corresponding high ozone and potential vorticity values.

Essentially, at the 500 hPa isobaric level where stratospheric intrusion reaches, the observed humidity originates from the stratosphere. Therefore, this distinct flow contains low humidity values, but slightly higher compared to the stratosphere. However, this flow is discernible with lower humidity values over the area of Hohenpeissenberg compared to the surrounding areas, which exhibit higher humidity values. In particular, on 26 January at 00Z, the relative humidity above the study area approaches 0.25. While on 27 January at 00Z, as the system begins to move away, it exhibits higher values approaching 0.8, which can be justified due to the absence of stratospheric intrusion. In other circumstances, stratospheric intrusion could result in lower relative humidity percentages.

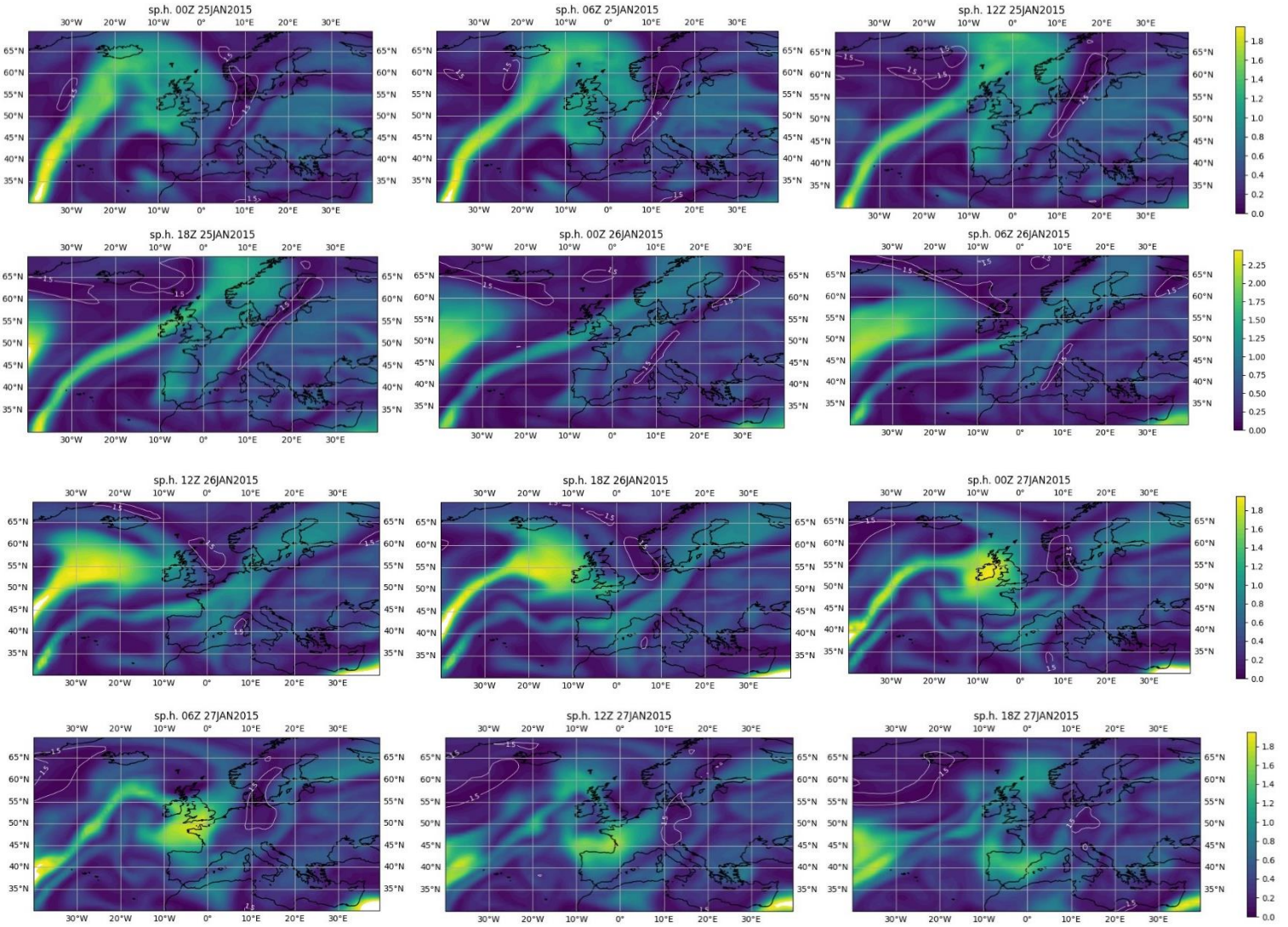

Figure A.6: Specific humidity (color shaded) and Potential Vorticity (white contours in pvu) at 500 hPa, during the period from 00Z on 25 January 2015 to 18Z on 27 January 2015 (6 h interval).